TECHNISCHE UNIVERSITÄT MÜNCHEN

Lehrstuhl für Experimentelle Genetik

Development of epigenomic signatures during intergenerational inheritance of diet-induced obesity and type 2 diabetes

Daniela Kaspar

Vollständiger Abdruck der von der TUM School of Life Sciences der Technischen Universität München zur Erlangung des akademischen Grades eines

Doktors der Naturwissenschaften

genehmigten Dissertation.

Vorsitzende: Prof. Dr. Angelika Schnieke
Prüfender der Dissertation: 1. Prof. Dr. Dr. h.c. Martin Hrabě de Angelis
                            2. Prof. Dr. Eckhard Wolf

I. TABLE OF CONTENTS

II.   TABLES AND FIGURES

Tables

Figures

III. ABBREVIATIONS

Abbreviation	Full name
5caC	5-carboxylcytosine
5fC	5-formylcytosine
5hmC	5-hydroxymethylcytosine
5mC	5-methylcytosine
ADP	Adenosine diphosphate
ALSPEC	Avon Longitudinal Study of Parents and Children
ATP	Adenosine triphosphate
AUC	Area under the curve
BAT	Brown adipose tissue
BMI	Body mass index
BPA	Bisphenol A
CGI	CpG island
ChIP-Seq	Chromatin immunoprecipitation-Sequencing
CpG	Cytosine-phosphate-Guanine
DEA	Differential expression analysis
DIO	Diet-induced obesity
DMR	Differentially methylated region
DNA	Deoxyribonucleic acid
DNMT	DNA methyltransferase
E	Embryonic day
EE	Environmental enrichment
ERK	Extracellular signal-regulated kinase
F0	Parental generation
F1/F2/...	1st/2nd/… filial generation
FC	Linear fold change
FDR	False discovery rate
GIP	Glucose-dependent insulinotropic peptide
GLM	Generalized linear model
GLP-1	Glucagonlike peptide-1
GLUT1	Glucose transporter 1
GLUT2	Glucose transporter 2
GO	GeneOntology
GR	Glucocorticoid receptor
GWAS	Genome-wide association studies
HAT	Histone acetyltransferase
hCG	Human Chorionic Gonadotropin
HDAC	Histone deacetylase
HFD	High-fat diet
HPA axis	Hypothalamic–pituitary–adrenal axis
ICM	Inner cell mass
IGF	Insulin-like growth factor
ipGTT	Intraperitoneal glucose tolerance test
IRS	Insulin-receptor substrate
IVF	*In vitro* fertilization

LFD	Low-fat control diet
LPD	Low-protein diet
MAPK	Mitogen-activated protein kinase
MeDIP-Seq	Methylated DNA immunoprecipitation Sequencing
MODY	Maturity Onset Diabetes of the Young
MZT	Maternal-to-zygotic transition
NEST	Newborn Epigenetics STudy
ORF	Open reading frame
padj	Adjusted p-value
PC	Principle component
PCA	Principle component analysis
PCR	Polymerase chain reaction
PGC	Primordial germ cell
PMSG	Pregnant mare serum gonadotropin
PTSD	Posttraumatic stress disorder
RIN	RNA integrity number
RISC	RNA-induced silencing complex
RNA	Ribonucleic acid
lncRNA	long non-coding RNA
miRNA	microRNA
mRNA	messenger RNA
ncRNA	non-coding RNA
piRNA	piwi-interacting RNA
rRNA	ribosomal RNA
siRNA	small-interfering RNA
sncRNA	small non-coding RNA
snoRNA	small nucleolar RNA
snRNA	small nuclear RNA
tRNA	transfer RNA
tsRNA	tRNA-derived small RNA
RNAa	RNA-based gene activation
RNAi	RNA interference
RNA-Seq	RNA sequencing
RT	Room temperature
SAT	Subcutaneous white adipose tissue
SSC	Spermatogonial stem cell
T2D	Type 2 Diabetes
TET	Ten eleven translocation
TS	Theiler stage
WAT	Visceral white adipose tissue
ZGA	Zygotic genome activation

IV.   SUMMARY & ZUSAMMENFASSUNG

Summary

For the past few years, there was a growing body of indications for the existence of intergenerational epigenetic inheritance in humans such as the transmission of an environmentally induced metabolic syndrome from parents to their children and maybe even grand-children. In animals, intergenerational and even transgenerational epigenetic inheritance has been shown already multiple times. Indeed, a previous study by our institute did prove the epigenetic inheritance of a metabolic phenotype via the parental gametes. The use of *in vitro* fertilization (IVF) and foster mothers for the production of examined offspring has proven crucial, in order to exclude confounding factors either in the seminal fluid or from the mother during gestation and lactation and to investigate the pure impact of gametes. The same method was applied in this project, to examine the phenotype of 3 weeks old offspring more closely. In addition, the transcriptome was analyzed at different stages of development to identify epigenetic signatures, which might be causative of the demonstrated intergenerational inheritance.

In our mouse model, parental generation was fed with either high-fat diet (HFD) or low-fat control diet (LFD). Afterwards, IVF was performed in order to obtain offspring of HFD-fed parents (F1 (HxH)) and LFD-fed parents (F1 (LxL)). Offspring was either harvested in early embryonic stage or organs were harvested during fetal organogenesis or at the age of 3 weeks. RNA was extracted from samples and RNA sequencing was performed.

3 weeks old F1 (HxH) show significantly higher body weight compared to F1 (LxL), which persists until the age of 15 weeks in males and females. Moreover, male F1 (HxH) develop impaired glucose tolerance at the age of 15 weeks. Remarkably, analyses of the transcriptomes reveal significant differences between HFD and LFD offspring at all examined developmental stages. These differences are sex-specific in the organs of 3 weeks old mice, meaning that different genes are altered by parental HFD in males and females. There is also barely any overlap in regulated genes between the analyzed organs. However, many of these differentially expressed genes are involved in metabolic processes such as the lipid and glucose metabolism. These alterations could be the underlying cause for current and prospective metabolic complications. Potential candidate genes including *Lep*, *Npr3*, *Tst*, *Retsat* and *Ddah* were identified. Parental HFD-induced alteration of gene expression in fetal liver tissue is sex-specific as well and not consistently regulated between the different stages. Highly dynamic changes during the time of organogenesis could be a reason for this. Nonetheless, various

regulated genes are involved in metabolic processes of energy homeostasis as well. In preimplantation embryos derived from HFD- and LFD-fed parents, significant differences in long and short transcripts were observed. Several regulated genes such as *Tet1*, *Lcmt2* and *Nsun2* act as methyltransferases and are therefore able to modify methylation marks on DNA and tRNAs, whereas *Drosha* can alter the content of miRNAs. Thus, these changes of epigenetic regulators could drastically affect the process of inheritance.

In summary, this work demonstrates that transcriptional and metabolic differences between HFD and LFD offspring are present already in fetal organs and at the age of 3 weeks. Moreover, they might be caused by epigenetic signatures such as small RNAs and DNA/tRNA methylation that are altered in preimplantation embryos of HFD-treated parents. Ultimately, this work suggests considerably more dynamic, versatile and complex mechanisms responsible for intergenerational epigenetic inheritance than postulated by other studies so far.

Zusammenfassung

Seit einigen Jahren mehren sich die Hinweise auf die Existenz von intergenerationaler epigenetischer Vererbung auch im Menschen, wie die Vererbung eines Umwelt-induzierten metabolischen Syndroms von Eltern an ihre Kinder und unter Umständen an ihre Enkel. Die Existenz von intergenerationaler und sogar transgenerationaler epigenetischer Vererbung in Tieren wurde dagegen schon vielfach gezeigt. In einer früheren Studie unseres Instituts wurde die epigenetische Vererbung eines metabolischen Phänotyps über die parentalen Gameten bewiesen. Ausschlaggebend hierbei war die Verwendung von *in vitro* Fertilisation (IVF) und Leihmutterschaft für die Produktion der zu untersuchenden Nachkommen. Dadurch konnten Störfaktoren in der Samenflüssigkeit sowie während der Gestations- und Laktationsphase ausgeschlossen werden und damit der reine Einfluss der Keimzellen untersucht werden. Dieselbe Methode wurde in dieser Arbeit verwendet, um den Phänotyp in 3 Wochen alten Nachkommen näher zu untersuchen. Zudem sollte das Transkriptom in verschiedenen Stadien der Entwicklung untersucht werden, um epigenetische Signaturen zu identifizieren, die möglicherweise verantwortlich für die gezeigte intergenerationale Vererbung sind.

In unserem Mausmodell wurde die Elterngeneration entweder mit HFD oder LFD gefüttert und anschließend eine IVF durchgeführt, um Nachkommen von HFD-gefütterten Eltern (F1 (HxH)) und LFD-gefütterten Eltern (F1 (LxL)) zu erhalten. Die Nachkommen wurden entweder im frühen Embryonalstadium gesammelt oder es wurden Organe im fötalen

Stadium während der Organentwicklung oder im Alter von 3 Wochen entnommen. Aus diesen Proben wurde RNA extrahiert und danach RNA-Sequenzierung durchgeführt.

3 Wochen alte Nachkommen von HFD-gefütterten Eltern zeigen signifikant höheres Körpergewicht als LFD-Nachkommen, das bis zum Alter von 15 Wochen in Männchen und Weibchen bestehen bleibt. Männliche HFD-Nachkommen entwickeln zudem eine verminderte Glukosetoleranz im Alter von 15 Wochen. Transkriptomanalysen zeigen signifikante Unterschiede zwischen HFD- und LFD-Nachkommen in allen untersuchten Entwicklungsstadien. Die Unterschiede sind in den Organen im Alter von 3 Wochen geschlechtsspezifisch. Das bedeutet, dass in Männchen und Weibchen verschiedene Gene durch die parentale HFD verändert sind und auch im Vergleich der untersuchten Organe finden sich wenig Überschneidungen in den regulierten Genen. Allerdings sind viele dieser differentiell exprimierten Gene in metabolische Prozesse wie den Lipidstoffwechsel und den Glukose-Metabolismus involviert. Diesen Genveränderungen könnten auch die bestehenden und zukünftigen metabolischen Komplikationen zugrunde liegen. Identifizierte Kandidatengene sind unter anderem *Lep*, *Npr3*, *Tst*, *Retsat* und *Ddah*. Im fötalen Lebergewebe sind die veränderten Gene ebenfalls geschlechtsspezifisch. Es sind jeweils unterschiedliche Gene in den verschiedenen Stadien reguliert. Dies kann unter anderem auch an den hochdynamischen Veränderungen zur Zeit der Organentwicklung liegen. Dennoch sind auch hier viele regulierte Gene in die metabolischen Prozesse zur Energie-Homöostase involviert. In Präimplantationsembryonen von HFD- und LFD-gefütterten Eltern wurden signifikante Unterschiede bei langen und kurzen Transkripten gefunden. Einige regulierte Gene wie *Tet1*, *Lcmt2* und *Nsun2* können als Methyltransferasen die Methylierungsmuster von DNA und tRNAs verändern, während *Drosha* den Gehalt an miRNAs modifizieren kann. Diese Veränderungen epigenetischer Regulatoren können folglich die Vererbung stark beeinflussen.

Zusammenfassend wurde in dieser Arbeit gezeigt, dass transkriptionelle und metabolische Unterschiede zwischen HFD- und LFD-Nachkommen bereits in fötalen Organen und im Alter von 3 Wochen existieren. Diese könnten durch epigenetische Signaturen wie small RNAs und DNA/tRNA Methylierung hervorgerufen werden, die in Präimplantationsembryonen von HFD-gefütterten Eltern verändert sind. Letztendlich zeigt diese Arbeit, dass die für intergenerationale epigenetische Vererbung verantwortlichen Mechanismen wesentlich dynamischer, vielfältiger und komplexer sind, als von anderen Studien bisher postuliert wurde.

1. INTRODUCTION

Parts of the introduction are based on two reviews from our group (*1, 2*).

1.1 Diabetes mellitus

Diabetes mellitus is one of the most prevalent metabolic disorders affecting over 425 million people worldwide in 2017 (*3*). This number is expected to further increase up to 629 million in 2045, especially in low- and middle-income countries (*3*). Basically, two main forms of diabetes mellitus have been described depending on the source of hyperglycemia, which is the hallmark of the disease. Type 1 diabetes mellitus is mainly an autoimmune disease in which β-cells are destroyed by the immune system leading to complete loss of insulin secretion. This renders patients dependent on lifelong exogenous insulin administration and accounts for 5-10% of all diabetes cases (*4*). Type 2 diabetes mellitus (T2D) on the other hand, is characterized by hyperglycemia and peripheral insulin resistance and accounts for 90-95% of the diabetes population (*4*). In addition to these two major types of diabetes, a variety of monogenic forms of diabetes mellitus such as neonatal diabetes and maturity onset diabetes of the young (MODY) exists with low prevalence of about 1-6% (*5*). Overall, T2D is a metabolic disorder which can cause serious macro- and microvascular complications such as diabetic nephropathy, diabetic retinopathy, diabetic neuropathy, ischemic heart disease and cerebrovascular disease. These various complications predominantly account for the increased mortality with T2D and the huge economic burden. The combination of different complications, high blood pressure, T2D and obesity is referred to as metabolic syndrome. Although drugs and therapies as treatment for T2D are available, the high prevalence prompts for more research on the reasons for this rapidly increasing T2D prevalence (*6, 7*).

1.1.1 Glucose homeostasis

Glucose is the fundamental energy source in the human body and therefore a constant supply is required. Disturbed glucose homeostasis by either a critical decrease in glucose availability (hypoglycemia) or constantly increased blood glucose levels (hyperglycemia) can result in coma and eventually death or long-term cardiovascular complications, respectively. Therefore, it is essential to maintain blood glucose levels within the euglycemic range of 70-140 mg/dL (3.9-7.8 mmol/L) in humans (*8*). Glucose homeostasis is critically controlled by a negative feedback loop that is comprised mainly of the pancreatic hormones insulin and glucagon but also other hormones such as the gut hormones GLP-1 and GIP play a role. After food intake, an increase in circulating glucose levels is sensed by pancreatic β-cells, which in

turn increase their insulin secretion into the blood. Insulin receptors at the main target tissues liver, skeletal muscle and adipose tissue recognize the insulin, thus leading to increased glucose uptake and inhibition of the endogenous glucose production in liver (*9*).

Sensing of an extracellular glucose molecule depends on the entry into the cell via passive glucose transporters (GLUT1 and GLUT2) and its conversion to glucose-6-phosphate by the enzyme glucokinase IV (*10*). High glucose concentration triggers adequate insulin secretion by β-cells. Release of insulin from pancreatic β-cells is mediated by glucose uptake and subsequently elevated ATP/ADP ratios resulting in closure of ATP-dependent potassium channels and therefore opening of voltage-gated calcium channels. Finally, enhanced intracellular calcium concentrations trigger release of insulin into the blood.

Although blood glucose concentration has the strongest impact on insulin secretion, other factors such as certain amino acids, free fatty acids and hormones can also modify the amount of secreted insulin. However, most of these factors act only in combination with high glucose concentrations. An important class of factors that increase the glucose-induced insulin secretion are the gastrointestinal hormones gastrin, secretin, cholecystokinin, glucagon-like peptide-1 (GLP-1) and glucose-dependent insulinotropic peptide (GIP) (*11*). The two most potent hormones GIP and GLP-1 are responsible for the so called "incretin effect". This effect was discovered when a much greater insulin response was observed after oral administration of glucose compared to intravenous injection of the same amount of glucose (*12*). Low blood glucose levels but also other factors such as the hormones somatostatin, noradrenaline and leptin decrease insulin secretion (*13, 14*).

Insulin sensing at target tissues such as liver, muscle and adipose tissue puts a multi-factorial response in action. Via the insulin signaling pathway both posttranslational and transcriptional responses are triggered. In more detail, insulin binds to the α-subunits of its receptor that is present in the cell membrane of target tissues and thereby autophosphorylates its β-subunits leading to an activation of tyrosine kinases. The tyrosine kinases phosphorylate various insulin-receptor substrates (IRS) that in turn activate or inhibit a variety of cellular enzymes. Overall in liver, this leads to increased glucose uptake, protein synthesis and glycogen synthesis on the one hand and transcriptional changes on the other hand, involving increase in glycolysis and lipogenesis and decrease in gluconeogenesis and fatty acid oxidation. In muscle, insulin binding to its receptor promotes rapid glucose uptake into the muscle cell and storage in the form of glycogen. In adipose tissue, insulin binding leads to a prompt transport of glucose into the fat cell. There, glucose is used to form fatty acids and α-glycerol phosphate as basic elements to synthesize triglycerides, the main storage form of fat (*11*). In contrast to the tissues mentioned before, insulin is not required for glucose uptake in the brain as most of the neurons are permeable for glucose (*15*). Nevertheless, insulin is

involved in the regulation of feeding behavior and monitoring energy stores in the brain. The impact of insulin action on glucose homeostasis was shown in mouse models with whole-body or tissue-specific knockout of the insulin receptor, resulting in diabetic ketoacidosis and early postnatal death or other more or less harmful diabetic phenotypes, respectively (*16*).

During periods of fasting and low blood glucose levels, insulin secretion is inhibited and all effects of insulin explained above are reversed. At the same time, pancreatic α-cells secrete glucagon, which stimulates target tissues to produce and/or release glucose into the blood. The secretion of glucagon prevents a critical drop in glucose availability and is amplified by neuro-endocrine factors such as adrenaline and noradrenaline via an increase in sympathetic nervous activity. Consequently, glucagon initiates breakdown of glycogen to glucose molecules as a first short-term source of glucose and at the same time causes stimulation of catabolic processes whereby endogenous glucose production in liver is enhanced. The glucagon signaling pathway, which eventually leads to enhanced glucose output, is initiated by binding of glucagon to its G-protein-coupled receptor and also puts in motion several posttranslational and transcriptional responses via a signaling cascade. Rapid posttranslational changes involve an increase in lipolysis and glycogenolysis as well as the decrease of lipogenesis and glycogen synthesis, whereas long-term changes in transcription involve increase of gluconeogenesis and fatty acid oxidation and decrease of glycolysis (*11*). The importance of glucagon was shown in a glucagon receptor knockout mouse model that appear normoglycemic despite streptozotocin-mediated destruction of β-cells. The diabetic phenotype could only be accomplished be re-expression of the hepatic glucagon receptor (*17*).

Hence, the pancreatic hormones insulin and glucagon play the central role in maintenance of balanced glucose levels.

1.1.2   Pathophysiology

Glucose homeostasis is impaired under the pathophysiological conditions of T2D and characterized by hyperglycemia and hyperinsulinemia. Development of T2D is usually a gradual process that starts with permanently elevated blood glucose concentrations, increasing insulin secretion and decreasing insulin sensitivity. With prolonged insulin resistance at peripheral tissues, however, compensatory increased insulin levels are no longer sufficient to maintain normal blood glucose levels. At later stages of T2D, pancreatic β-cells become dysfunctional and are unable to produce and release enough insulin to keep glucose concentrations within a healthy range. At the same time, peripheral insulin resistance causes increased glucose production in liver and decreased glucose uptake in adipose tissue and muscle at a certain insulin concentration (*11, 18*). Together, insulin resistance and β-cell

dysfunction result in abnormal blood glucose levels and impaired glucose tolerance thus marking the main characteristics of T2D (*19*). In Figure 1.1, risk factors that can lead to T2D and the pathophysiology of late stage T2D are shown.
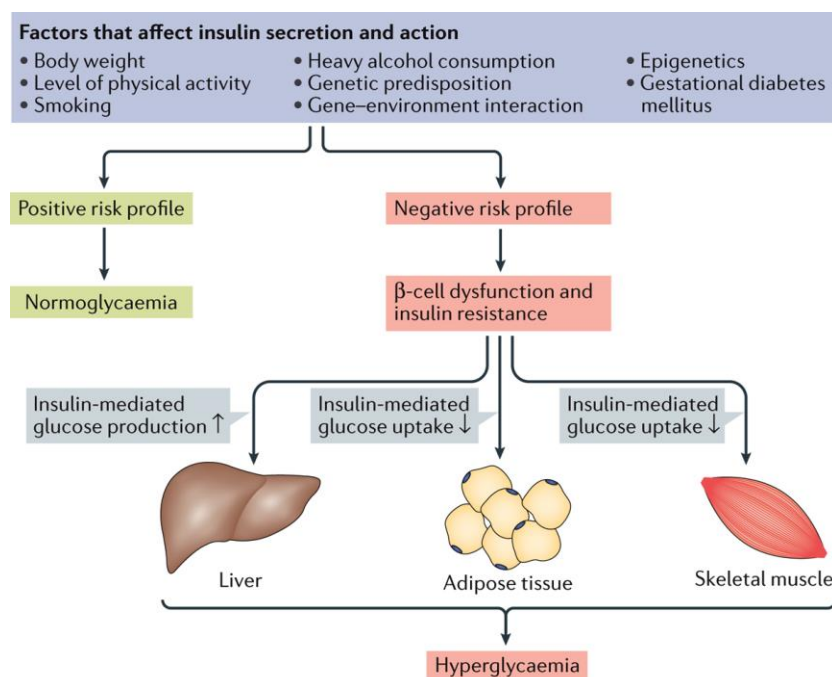
FIGURE 1.1 | RISK FACTORS AND PATHOPHYSIOLOGY OF HYPERGLYCEMIA IN T2D (*19*)

Various factors affect insulin secretion and action (listed at the top). Under normal conditions with a positive risk profile, insulin reduces glucose production by the liver and increases glucose uptake by skeletal muscle and adipose tissue to maintain normoglycemia. A negative risk profile can lead to β-cell dysfunction in the pancreas and insulin resistance in the liver, skeletal muscle or adipose tissue and subsequently hyperglycemia with strongly reduced insulin sensitivity. Reprinted with permission of Nature Publishing Group, a division of Macmillan Publishers Limited. Copyright © 2017 (License number 4947011092319)

1.1.3 Global pandemic – genetic versus environmental factors

The prevalence of T2D has been increasing tremendously within the last decades, reaching up to 8.8% in 2017 (*3*) and therefore, it became a major health and economic burden on a worldwide scale (reviewed in (*19, 20*)). Especially alarming is the increasing observation of T2D and prediabetes also among children and adolescents under the age of 20 years. There is a wide range for risk factors for developing T2D consisting of genetic, epigenetic and environmental factors. Although genetic factors play an important role in the predisposition to T2D, many cases of T2D can be prevented by a healthy lifestyle (*7*).

Nevertheless, there is clear evidence of a genetic basis in T2D from twin and family studies showing strong familial aggregation of T2D and 20-53% concordance in monozygotic twins compared to 0-29% concordance in dizygotic twins (*21, 22*). Dissection of these genetic factors

and identifying involved pathways have greatly contributed to our understanding of T2D. Genome-wide association studies (GWAS) have identified hundreds of genomic loci affecting T2D risk (*23*). Individually, these common variants only have mild effects on T2D risk and collectively can only explain a small fraction (around 15%) of the observed heritability. Accordingly, the term "missing heritability" was first introduced in 2008 spotlighting the inability to pinpoint the risk of diabetes and other complex diseases to distinct genetic elements (*24, 25*). Also lower-frequency variants could not explain the missing heritability as a large sequencing study recently demonstrated (*26*). There are several potential causes for the missing heritability such as microRNAs, undetected gene-gene or gene-environment interactions, epigenetic modifications or incorrect estimation of the heritability. On the other hand, already in 1962, James V. Neel published an explanation for the increasing incidence of diabetes in the western world (*27*). He proposed that possession of a "thrifty" genotype is an ancient trait that predisposes individuals to develop diabetes due to efficient fat storage that was advantageous during historical "feast-and-famine" conditions. Nowadays, under conditions of abundant supply of energy-dense food and less physical activity, this thrifty genotype is rather disadvantageous and predisposes individuals to both obesity and T2D (*28*). To date, although widely accepted, it is still not clear if the concept of the thrifty genotype is valid and what serves as the underlying molecular basis. However, considering the fast pace of increase in diabetes prevalence within a few decades from 4.7% in 1980 to 8.5% in 2014 (www.who.int/), genetic drift is very unlikely to be the reason for this pandemic.

On the other hand, environmental factors play a crucial role in the risk for T2D such as energy-dense diets, sedentary lifestyle, smoking and high consumption of alcohol (*29*). Also obesity and a high body mass index (BMI) are strongly associated with T2D risk. In accordance with the thrifty genotype hypothesis, Hales and Barker proposed the thrifty phenotype hypothesis in 1992 (*30*) implying that poor nutrition during fetal and early infant life increases risk for obesity and T2D in adulthood. Evidence for this hypothesis was provided by numerous human and rodent studies showing an increased risk of metabolic diseases in people born with low birth weight (*31-33*). However, pursuing a healthy lifestyle including balanced diet and exercise, is also very common nowadays.

An additional suspect that is more and more assumed to contribute to the diabetes pandemic is the epigenetic inheritance of acquired traits. Through transmission of experienced environmental cues such as malnutrition, a sedentary lifestyle and their resulting metabolic perturbations from parents to offspring, susceptibility to metabolic diseases might increase immensely over few generations (*34*). Recent discussion has also focused on the role of environmental chemicals such as endocrine disruptors and the microbiome in the pandemic of obesity and T2D (*35, 36*).

1.2 Epigenetics

1.2.1 Epigenetic regulators

The term "epigenetics" was first established by Conrad Waddington in 1942 (*37*) in the context of developmental processes but since then various definitions have emerged. Generally, epigenetics is the study of heritable changes of gene expression through chemical alterations of DNA or associated histone proteins without altering the DNA sequence itself. Remarkably, these changes can be stably transmitted through mitosis and meiosis and are reversible. Compared to the static genome, the epigenome is highly dynamic and varies significantly among different cell types within a given individual but also among individuals due to exogenous influences, which can induce epigenetic modifications. The major epigenetic regulators include DNA methylation, posttranslational histone modifications, X chromosome inactivation and genomic imprinting and more recently, several classes of non-coding RNAs as posttranscriptional regulators (Figure 1.2) (*38-40*).
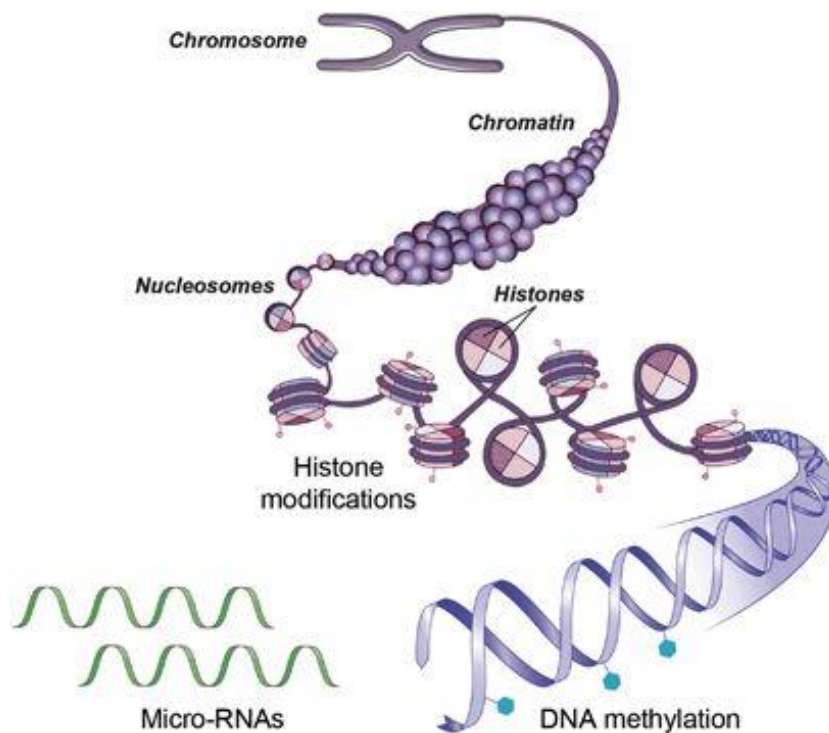
FIGURE 1.2 | EPIGENETIC REGULATORS (*41*)

Schematic representation of the three major epigenetic regulators. Chromatin is a DNA-protein complex in which DNA is wrapped around a core of histone proteins. The chromatin structure is determined by histone modifications and important for activation or inhibition of gene expression. DNA methylation of cytosine residues is another important epigenetic mark that can influence gene expression. Finally, microRNAs (miRNAs) and other classes of small non-coding RNAs can control target gene expression post-transcriptionally. Reprinted with permission by the Creative Commons CC BY license.

1.2.1.1   Histone modification

Histones are proteins that package DNA into structural units called nucleosomes. Five major classes of histones exist with H2A, H2B, H3, and H4 as core histones and H1 as linker histone. Each core histone forms a dimer and the resulting four dimers assemble to one octameric nucleosome core (*42*). 146 bp of DNA are wrapped around the nucleosome core and held in place by the linker histone. The assembly of nucleosomes into higher-order chromatin structures can achieve a further organization. The protein structure of core histones contains tails that extend from the nucleosome and can undergo post-translational modification at several residues. These histone modifications such as methylation, acetylation, phosphorylation, ubiquitination, and citrullination can alter chromatin structure by directly affecting histone-histone and histone-DNA interactions. Acetylation and methylation of lysine residues at the histone tails are the two most common posttranslational modifications of histones. Methylation at lysine residues can exist in three different states, namely mono-, di- and trimethylation. Alterations in chromatin structure can influence gene expression. For example, methylation (especially di- and trimethylation) at lysines 9, 27, and 36 on histone H3 causes reduced gene expression, while methylation (especially di- and trimethylation) of lysines 4 and 79 on histone H3 and lysine 20 on histone H4 leads to increased gene expression (*43, 44*). Acetylation by histone acetyltransferases (HATs) opens the condensed chromatin structure allowing transcription of the DNA, whereas deacetylation by histone deacetylases (HDACs) forms the closed chromatin structure that is inaccessible to transcription factors (*45, 46*). In general, tightly folded and condensed chromatin (heterochromatin) is associated with inactive genes, while more open chromatin (euchromatin) contains actively transcribed genes (*47*). This way, histone modifications are epigenetic regulators that can influence gene expression.

1.2.1.2   DNA methylation

DNA methylation describes the chemical addition of a methyl group to a DNA base. In mammals, this occurs predominantly at cytosine residues of CpG dinucleotides resulting in 5-methylcytosine (5mC). Gene promoters often contain CpG-rich regions known as CpG islands (CGIs) so that methylation and demethylation of CpGs can switch gene expression off and on, respectively (*48*). High levels of 5mC in a certain genomic region are therefore associated with gene silencing. DNA methylation patterns are established very early during embryonic development and are then transmitted during somatic cell division by a maintenance mechanism. These mechanisms involve two classes of DNA methyltransferases (DNMTs) for active DNA methylation (*49*) and additionally ten eleven translocation (TET) enzymes catalyzing the conversion of 5mCs back to normal cytosines for active demethylation. DNMT3A and DNMT3B are responsible for the *de novo* establishment of DNA methylation

whereas DNMT1 recognizes hemi-methylated DNA and methylates the newly replicated DNA strand thereby maintaining the methylation status of the mother cell in the daughter cells (reviewed in (*50, 51*)). In mice, a deletion of the *Dnmt1* gene resulted in reduced methylation levels compared to wildtype mice and embryonic lethality before mid-gestation (*52*). However, more recent observations suggest that *de novo* methylation also during cell division by DNMT3A and DNMT3B is required, otherwise DNA sequences will eventually lose their methylation (*53, 54*). DNA demethylation can be achieved either passively by dilution of 5mC during DNA replication or actively with TET enzymes mediating the oxidation of 5mC to 5-hydroxymethylcytosine (5hmC), 5-formylcytosine (5fC) and 5-carboxylcytosine (5caC). These oxidized forms of 5mC will be diluted with every DNA replication or excised by thymine DNA glycosylase and repaired by the base excision repair mechanism resulting in the reconversion to a normal cytosine (*55*).

Taken together, the DNA methylation status, particularly in promoters or other regulatory regions, has a profound effect on the expression level of a given gene and is therefore a pivotal epigenetic regulator within cells to transmit information to daughter cells during cell division and potentially even to the next filial generation.

1.2.1.3 Non-coding RNAs

Non-coding RNAs (ncRNAs) are defined as RNAs that are not translated into a protein, nevertheless, they can have a functional relevance for the cell. Depending on their length, long non-coding RNAs (lncRNAs) containing for example transfer RNAs (tRNAs) and ribosomal RNAs (rRNAs), and small non-coding RNAs including for example microRNAs (miRNAs), small-interfering RNAs (siRNAs), piwi-interacting RNAs (piRNAs), and tRNA-derived small RNAs (tsRNAs) can be distinguished (*56, 57*).

With the discovery of RNA interference (RNAi) in 1998 (*58*), small RNA molecules were found to function as regulators of gene expression and translation by targeting messenger RNA (mRNA) molecules. The most common and well-studied mode of action of small RNAs is gene silencing via RNAi, in which endogenous miRNAs or siRNAs induce the degradation of complementary mRNAs. Primary miRNAs are transcribed in the nucleus and trimmed to form 60-70 bp hairpin pre-miRNAs, which are then transported to the cytoplasm and further trimmed to approximately 22 bp double-stranded miRNAs by the Dicer enzyme. After binding to the RNA-induced silencing complex (RISC), the strands are separated and only the guide-strand is retained. The active components of the RISC are endonucleases called Argonaute proteins, which cleave the target mRNA that is complementary to their bound miRNA (*59, 60*). siRNAs act in a very similar way, but compared to miRNAs, they derive from longer regions of double-stranded RNA. piRNAs represent the largest class of small non-coding RNAs

and differ in size from miRNAs (26-31 bp compared to 21-24 bp, respectively). They interact with PIWI proteins, a subclass of the Argonaute protein family, to form RNA-protein complexes, which mostly act in the post-transcriptional silencing of transposons in the genome (*61*). Interestingly, evidence for miRNA-based gene activation (RNAa) was found as well recently (*62*). Other non-coding RNAs such as rRNAs and tRNAs as well as their fragments are also presumed to play a role in the regulation of gene expression. Indeed, there is increasing evidence that fragmented tRNAs and rRNAs can act as epigenetic regulators across generations (*63*).

1.2.2 Reprogramming

1.2.2.1 Oogenesis and spermatogenesis

Gametogenesis is the process of gamete formation from the primordial germ cells (PGCs). In males and females, PGCs develop to spermatozoa through spermatogenesis and to oocytes through oogenesis, respectively (Figure 1.3).

Spermatogenesis is a continuous process that takes place in the seminiferous tubules of the testis and is initiated after onset of puberty. It consists of three main stages: spermato-cytogenesis (mitotic phase), spermatidogenesis (meiotic phase), and spermiogenesis (maturation). During spermatocytogenesis, the spermatogonium undergoes mitotic division to produce two types of diploid spermatogonia, the primary spermatocyte and the spermatogonial stem cell (SSC), which maintains the SSC population. In meiosis I, the primary spermatocyte divides into two secondary spermatocytes. During spermatidogenesis, the secondary spermatocyte undergoes meiosis II and forms two haploid spermatids. Finally, during spermiogenesis, spermatids differentiate into mature spermatozoa that are capable of fertilizing an oocyte (*64*).

Oogenesis takes place in the ovaries and differs considerably from spermiogenesis. It is initiated during early embryogenesis and completed after onset of puberty with a months/years-lasting meiotic arrest phase in between. Oogonia enter the first meiotic division late during embryonic development (oocytogenesis) and the resulting primary oocytes progress further through the first meiotic prophase until the diplotene stage, at which point they are maintained until puberty. With the onset of adolescence, groups of oocytes periodically resume meiosis and form the haploid secondary oocyte containing most of the cytoplasm and the first polar body containing hardly any cytoplasm. During the following meiosis II, the mature ovum and a second polar body are established. Due to another unequal cytokinesis, the oocyte's cytoplasm volume is conserved in one single cell rather than splitting

it equally among four cells (*65*). These meiotic divisions are called ootidogenesis and are followed by the maturation phase.

Folliculogenesis is a separate important process that accompanies and supports oogenesis. It produces the follicle surrounding the developing ovum and is controlled by endocrine signals. At the stage of meiosis I, primary oocytes are surrounded by a thin layer of follicular cells. In the course of ootidogenesis, they secrete a layer of glycoproteins (forming the zona pellucida) and grow larger to form the outer granulosa cells. Subsequently, the follicle is growing larger in size and matures. During each menstrual cycle, several follicles mature but typically only one reaches full maturity resulting in ovulation whereas the rest undergoes apoptosis. At this point, the mature ovum within the surrounding follicle is ready to be fertilized.
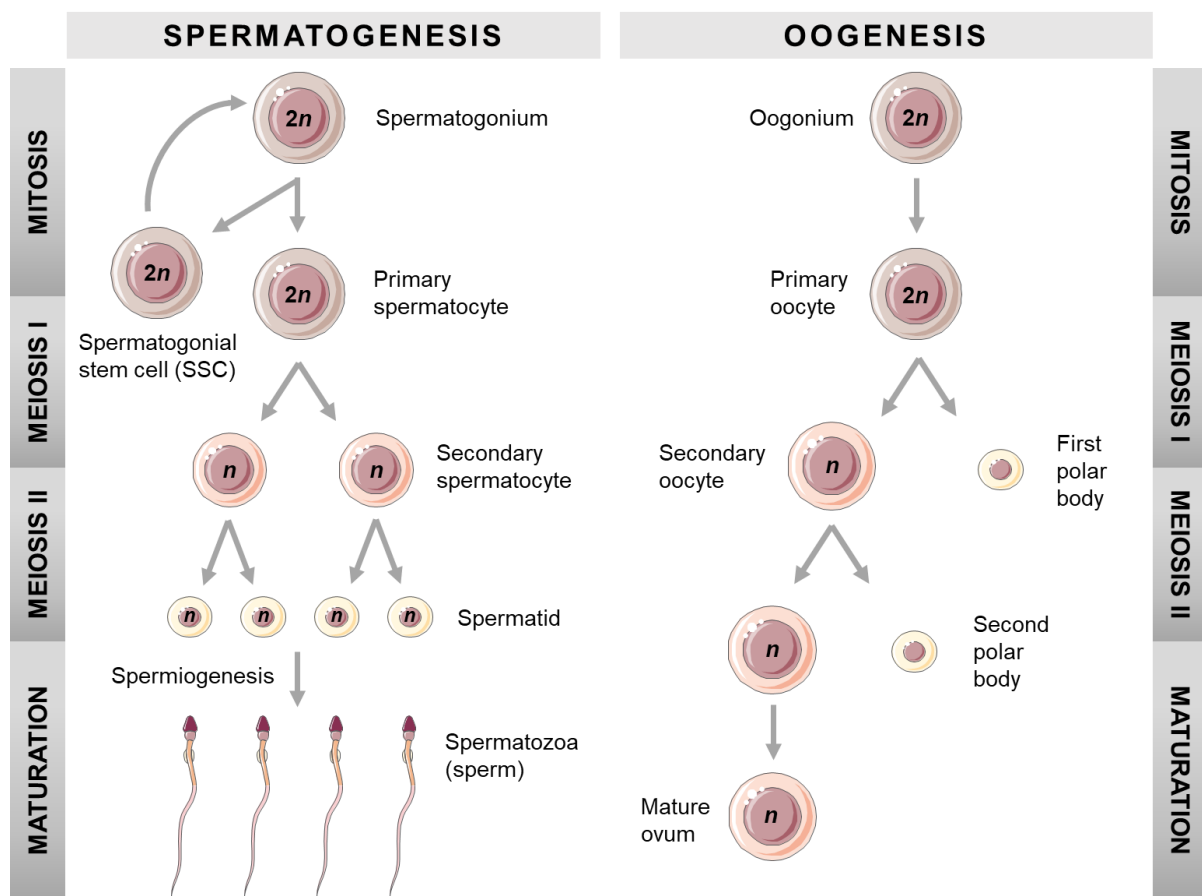
FIGURE 1.3 | GAMETOGENESIS IN MAMMALS

Gametogenesis is the development of spermatozoa in males (spermatogenesis) and mature oocytes in females (oogenesis) from primordial germ cells. Both undergo mitotic divisions followed by two meiotic divisions thereby reducing their chromosome sets to a haploid form. This figure was created using Servier Medical Art templates, which are licensed under a Creative Commons Attribution 3.0 Unported License; https://smart.servier.com.

It is worth mentioning that in mammalian sperm histones are widely replaced by protamines in order to package the DNA even tighter (*66*). Immediately after fertilization, protamines are

replaced with maternally derived histones that are strongly acetylated leading to asymmetric gene expression between maternal and paternal genome (*67*). Due to the exchange of histones with protamines in sperm, epigenetic information encoded within histone modifications might be lost. However, there are indications that a small fraction (10-15% in humans and 1-8% in mice) of nucleosomes in the sperm genome and histone modifications are retained, predominantly at genetic loci that function during embryogenesis (*68, 69*).

1.2.2.2   Two hits of demethylation

The epigenetic signatures and mechanisms elucidated in Chapter 1.2.1 have important functions in mammalian somatic cells in the regulation and fine-tuning of gene expression depending on developmental needs and in reaction to external stimuli (*70*). This epigenetic memory can be transmitted from mother to daughter cells during mitotic cell division to preserve the information in daughter cells. In order to reset epigenetic memory and to establish totipotency, epigenetic reprogramming in parental germ cells is crucial (*71*). In case of DNA methylation there are two major developmental periods of reprogramming: during germ cell development and during preimplantation embryo development (Figure 1.4) (*72*).
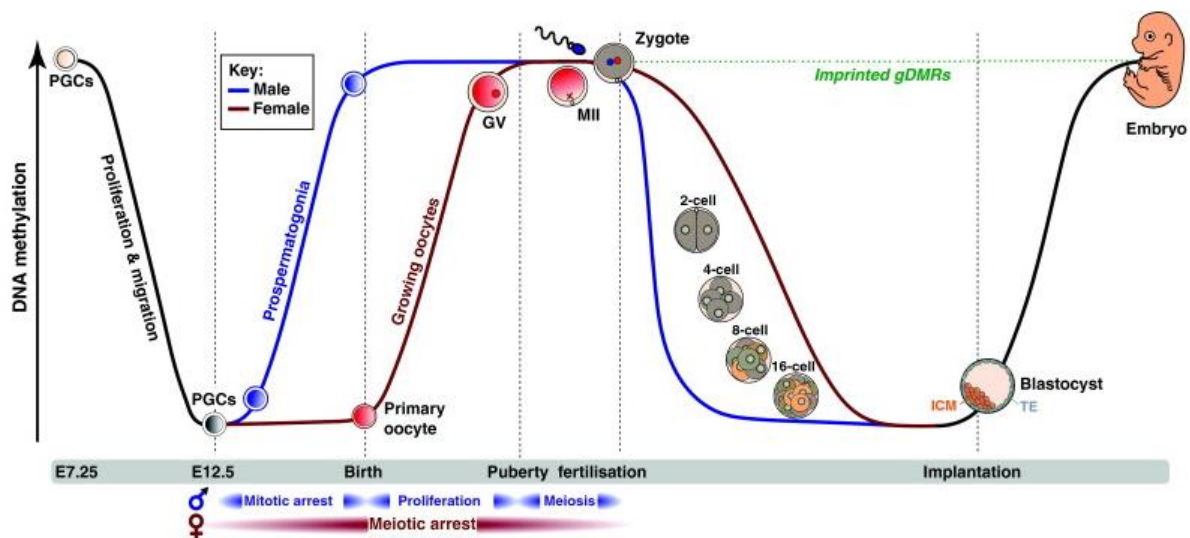
FIGURE 1.4 | DNA METHYLATION LEVELS DURING DEVELOPMENT (*73*)

Dynamic changes in DNA methylation during mammalian development are displayed. Two waves of global DNA demethylation and remethylation occur during development. First, during gametogenesis, primordial germ cells (PGCs) are completely demethylated (E7.25-E12.5) and then remethylated (after E12.5) in a sex-specific manner, including imprinting. Second, during embryogenesis, active demethylation in the male (blue) and passive demethylation in the female (red) pronucleus starts directly after fertilization followed by a wave of *de novo* methylation after implantation. This way, parental epigenetic memory is erased and totipotency is established at certain developmental stages. However, several imprinted loci (green) and some retrotransposons maintain their methylation pattern throughout embryogenesis. Reprinted with permission of Elsevier Ltd. Copyright © 2011 (License number 4947020414138)

The first hit of genome-wide demethylation occurs early in the development of PGCs between embryonic days E6.5 and E13.5 in mice and between 8-16 weeks of gestation in humans (*74, 75*). The proliferation and migration of PGCs and the genome-wide changes of DNA methylation were studied extensively in the mouse before they were examined also in humans (*76*). Progenitors of the PGCs originate from the posterior mesoderm of the epiblast and originally, PGCs inherit the methylation patterns of somatic cells during their specification in the epiblast. In mice, PGCs migrate from the epiblast to the extraembryonic mesoderm, passing through the developing hindgut endoderm and eventually colonizing the embryonic gonads. At this time, sex-specific differentiation starts (*77*). Around E13.5, when the group of PGCs has reached approximately 26.000 cells, proliferation stops and male and female germ cells enter mitotic and meiotic arrest, respectively. At this stage, genome-wide DNA methylation reaches its minimum and methylation of imprinted genes is completely erased (*78*). However, recent insights indicate that several loci and imprinted genes are able to escape this global demethylation. Nevertheless, following complete demethylation, sex-specific re-establishment of DNA methylation patterns occurs in the developing sperm and oocyte in order to reset imprints. Remethylation appears to occur earlier in the male germline, at the prospermatogonia stage during embryonic development whereas in the female germline it takes place only after birth during the growth of oocytes (*79*).

The second global demethylation takes place after fertilization to induce totipotency in the forming zygote (*80, 81*). Interestingly, a remarkable asymmetric loss of DNA methylation between male and female pronucleus is observed after fertilization. Paternal DNA undergoes active demethylation within 6 h after fertilization whereas the maternal pronucleus is only passively demethylated during multiple cell divisions until the blastocyst stage. 5mC levels reach their lowest point during the blastocyst stage, after which a wave of *de novo* methylation occurs in the epiblast to establish the new methylation pattern. In mouse embryos, genome-wide analysis from blastocyst to post-implantation stages reveals that DNA methylation is re-established within two days of implantation between E4.5 and E6.5 (*82*).

1.2.2.3   Imprinting

Interestingly, within these two waves of global demethylation, imprinting is only erased once, namely during gametogenesis in the developing PGCs. This way, epigenetic changes in imprinted genes in the parental germ cells can be retained in the developing next generation. Genomic imprinting is an important genetic mechanism in mammals that takes place during development in order to limit the expression of distinct genes to only one of the two parental chromosomes (*83*). It is based on differential DNA methylation between the parental alleles of the same gene. The importance of genomic imprinting and both parental genomes for normal development was shown by microsurgical transplantation experiments, in which male

and female pronuclei were exchanged in murine zygotes resulting in incomplete embryogenesis (*84, 85*). Around 150 genes in the murine genome and less in the human genome display imprinting characterized by mono-allelic parent-of-origin specific expression, most of which are organized in distinct clusters across the genome. The first three imprinted genes identified in mice were *Igf2* (insulin-like growth factor 2), *Igf2r* (IGF2 receptor) and H19 (maternally expressed non-coding transcript) (*86-88*). In humans, various diseases can be attributed to loss or gain of expression at imprinted genes such as Angelman syndrome and Prader-Willi syndrome. Patients with Angelman syndrome present with intellectual disability, developmental delay and prominent happy demeanor resulting from the loss of maternal ubiquitin protein ligase E3A (*UBE3A*) gene expression. Prader-Willi syndrome is a separate condition with patients displaying developmental delay, hyperphagia and often obesity and T2D caused by a similar loss of the paternal *UBE3A* gene expression (*83, 89*). These examples show the importance of imprinted genes and that regular embryogenesis requires both, maternal and paternal genome and their interplay.

1.2.2.4　Zygotic genome activation

Reprogramming of the terminally differentiated oocyte and sperm into a totipotent embryo after fertilization requires major changes at the transcription level. During a period called the maternal-to-zygotic transition (MZT), the fertilized oocyte has to transform into the zygote. This MZT comprises two major molecular events: First, the destabilization and degradation of maternal mRNAs and proteins. However, it is not clear yet, if the elimination of a significant fraction of all maternal mRNAs prevents abnormal mRNA dosage in the embryo, or rather the elimination of a specific set of maternal mRNAs is required for further embryonic development (*90*). Second, two waves of zygotic genome activation (ZGA) during which zygotic gene expression is initiated (*91*). Maternal clearance is completed before the first cell division. The minor ZGA starts during zygotic stage whereas the major ZGA starts only at the 2-cell stage. In mice, first cleavage takes place about 22 h after fertilization but inhibition or delay of ZGA is associated with an arrest in development at the 2-cell stage, referred to as the 2-cell block (*92, 93*).

Similar to some histone modifications, some genomic regions can escape the erasure of DNA methylation including retrotransposons and the germline differentially methylated regions (gDMRs) of imprinted genes. These escapees from embryonic reprogramming hint to a potential contribution of constituents of chromatin and their modifications to epigenetic inheritance across generations. However, as shown above, major alterations in the expression of imprinted genes can also have detrimental effects on development.

1.3 Epigenetic inheritance across generations

There is no doubt regarding the transmission of epigenetic marks between mother and daughter cells during mitosis, but the inheritance of epigenetic signatures across generations has long been under controversial discussion. However, more and more evidence is emerging showing epigenetic inheritance of acquired phenotypes from parents to their progeny in human cohorts and animal studies.

1.3.1 *In utero* exposure versus inter- and transgenerational transmission

As proposed in the thrifty phenotype hypothesis, *in utero* and early childhood exposures and experiences can strongly affect the phenotype in adulthood (*94-96*). However, the impact of maternal environment during gestation and lactation on the offspring's phenotype does not represent epigenetic inheritance from the mother to her child because the embryo and/or the newborn itself is directly exposed to these conditions. Moreover, these conditions, often referred to as confounding factors, seem to have an even greater impact on the offspring during these early stages of development than they would have in adulthood. Real epigenetic inheritance is defined as the inheritance of a parentally (F0) acquired phenotype that causes a distinct phenotypic change also in the next generation(s) (F1, F2, F3, …), even when the environmental factor that triggered the phenotype in the parental generation is absent in the following generations. In order to classify as epigenetic inheritance, the phenotype must be transmitted via any type of epimutation (DNA methylation, RNAs, histone modification or similar) in maternal and/or paternal gametes and the epimutation (or the resulting epiallele) is not encoded within the sequence of the genomic DNA.

Furthermore, it is necessary to distinguish inter- from transgenerational epigenetic inheritance, which is illustrated with dark and light gray background in Figure 1.5. Of note, environmental exposure of the parental F0 generation does also directly affect sperm and/or oocytes (F1) within the F0 generation and in case of a pregnant female also the developing F1 embryo including F2 PGCs within the F1 embryo. Intergenerational inheritance occurs if epimutations are only transmitted from the parental F0 generation to the F1 generation in the case of F0 pre-conceptional exposure, or to the F1 and F2 generation for F0 *in utero* exposure and not further. Transgenerational inheritance, on the other hand, occurs if the environmental information is transmitted from the F0 generation to the F2 generation and beyond in the case of pre-conceptional exposure or from the F0 to the F3 generation and beyond in case of *in utero* exposure. Consequently, intergenerational epigenetic inheritance implies that causative epimutations only persist through the second wave of reprogramming that strikes the

preimplantation embryo after fertilization, whereas for transgenerational inheritance to occur, epimutations have to resist both waves of epigenetic reprogramming (see Figure 1.4).
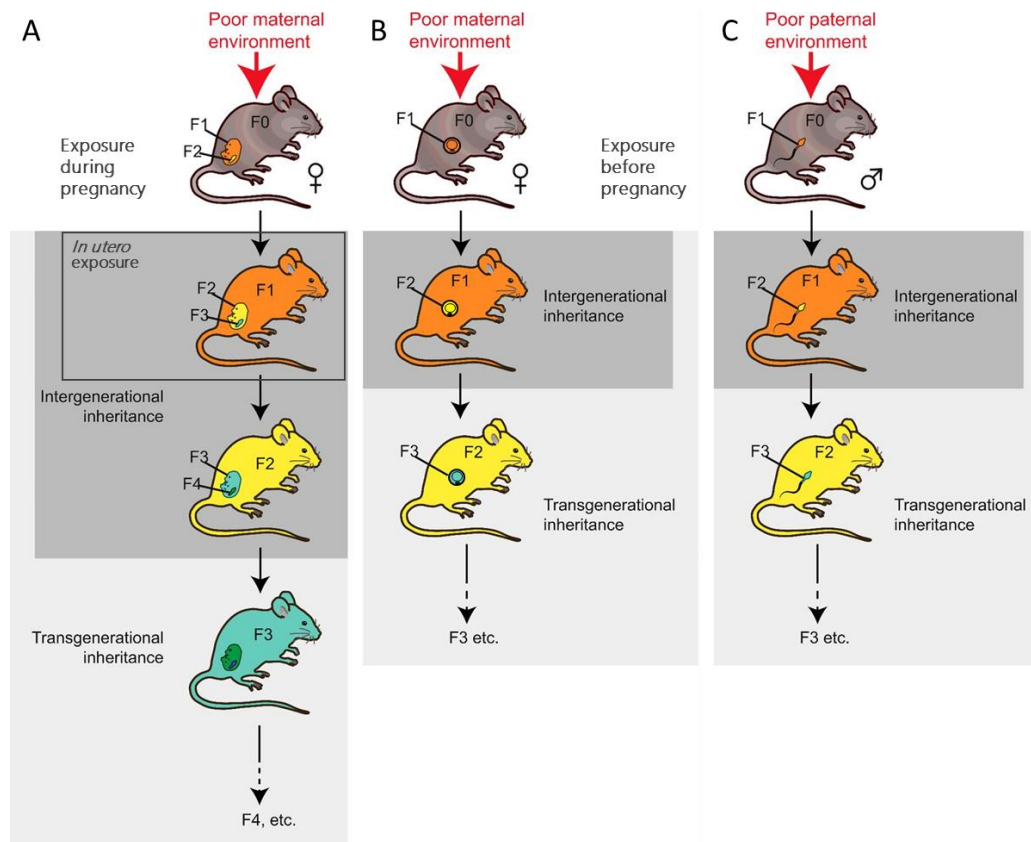
FIGURE 1.5 | INTER- AND TRANSGENERATIONAL INHERITANCE (MODIFIED FROM (*97*))

Exposure to an altered parental environment during (A) or before (B, C) pregnancy can lead to inter- or transgenerational inheritance of a distinct phenotype to the offspring. Maternal exposure to a poor environment during pregnancy exposes both her developing fetus *in utero* (F1, orange) as well as the PGCs in the fetus which later give rise to the F2 generation (yellow), both of which are present at the time of environmental exposure. This is referred to as intergenerational inheritance. Cells, which form the F3 generation (green) are not present at the time of environmental exposure, meaning that a phenotype in the F3 is transmitted by transgenerational inheritance. For pre-conceptual maternal and/or paternal exposure to poor environment, only oocytes and/or sperm cells which form the F1 generation are present and directly exposed to the poor environment (intergenerational inheritance), whereas phenotypes which persist into F2 and beyond are referred to as transgenerational inheritance.

As previously reviewed in (*98, 99*), research of the last decades has provided compelling evidence that epigenetic inheritance of acquired traits across generations is probably more pervasive in animals than previously perceived. Epidemiological studies in humans and experimental studies in animals and especially in rodents are very helpful in deciphering the role of epigenetic inheritance in human health and the pending T2D pandemic. Nutrition, stress, trauma, and enriched environments were found to be among the factors that can affect metabolic health, anxiety and cognitive plasticity across generations.

1.3.2 Epidemiological studies support epigenetic inheritance across generations

Famines and wars are not predictable disasters during history that can give a lot of insights into the human handling of stressful situations and also the impact these experiences may have on their progeny. Epidemiological studies in humans are another excellent opportunity to study effects of nutrition on health parameters over generations. An overview on epigenetics in human obesity and T2D is given in this review (*100*).

One of the first documented examples of intergenerational inheritance of a metabolic disorder in humans is the Dutch hunger winter famine in 1944/45. Thereby, a well-nourished population within a certain area underwent a brief period of intense caloric deprivation. Due to extensive documentation of maternal and offspring's health after the famine, poor prenatal nutrition could be associated with development of the metabolic syndrome in later life (*96, 101*). Offspring's birth weight and fertility were reduced compared to well-nourished siblings (*102, 103*) whereas glucose levels were elevated, glucose tolerance decreased and rates of cardiovascular disease increased in adulthood (*32, 101, 104*). However, these are cases of *in utero* exposure to undernutrition supporting the thrifty phenotype hypothesis but they cannot be considered as epigenetic inheritance. Nevertheless, also the offspring of prenatally undernourished fathers, but not mothers, displayed higher rates of obesity than offspring of prenatally well-nourished parents indicating intergenerational inheritance (*105*). Co-occurring DNA methylation changes of several genes involved in pathways related to growth and metabolism, in blood samples of adult prenatally undernourished fathers could be a hint for a mechanism involved in human intergenerational inheritance (*106-108*). Another very severe famine with millions of casualties was the Great Chinese famine (1959-1961). Various studies have been conducted analyzing effects of prenatal undernutrition on metabolic health in adulthood. Many of these find overweight, T2D, hyperglycemia, the metabolic syndrome, and schizophrenia more common among adults born during the famine years compared to controls born after the famine. However, these findings might be dependent on the age difference of the analyzed siblings (*109*) and represent effects of *in utero* exposure. First indication of intergenerational transmission of these parental experiences is given by a study from Li et al. showing that parental prenatal exposure to famine also increases the risk for hyperglycemia in offspring (*110*).

Other severe health problems such as anxiety disorders and posttraumatic stress disorder (PTSD) can be caused by traumatic events and transmitted to the offspring. For example, survivors of the Holocaust that developed PTSD afterwards, passed increased PTSD risk and low cortisol levels on to their offspring (*111, 112*). Later studies showed that maternal, but not

paternal, PTSD was associated with increased glucocorticoid sensitivity in offspring (*113, 114*) concomitant with lower methylation at the promoter region of the glucocorticoid receptor gene (*115*). Also, DNA methylation patterns were significantly altered in sperm of trauma-exposed Vietnam war veterans suggesting possible candidates for intergenerational inheritance (*116*). Although these findings are in agreement with a hypothetical role of epigenetic inheritance of anxiety related behavior in humans to the next generation, they only represent correlations and no causal relationship. In particular, progeny of Holocaust survivors was exposed to many confounding factors such as parental PTSD and altered behavior putting these correlations in questionable perspective.

In large human cohort studies, epigenetic inheritance of acquired phenotypes especially related to metabolic health across generations is further investigated. The Överkalix study utilizes historical records on food supply to determine mortality rates and causes. Nutrition during the slow growth period of childhood was found to have a profound effect on cardiovascular and diabetes-related deaths in offspring and grand-offspring through the male lineage indicating inter- and transgenerational inheritance (*94*). Intergenerational effects of parental smoking were analyzed in the Avon Longitudinal Study of Parents and Children (ALSPEC) demonstrating higher BMI in 9-year-old sons the earlier the father started smoking. Despite no significant association with BMI, daughters displayed a reduction in total lean mass due to paternal smoking (*117, 118*). Grandmaternal smoking during pregnancy on the other hand, resulted in increased birthweight, birth length and BMI in grandsons but not granddaughters (*119*). A study in Norwegian men found that risk of obesity increased with higher paternal, but not maternal age at birth (*120*). Moreover, as shown in the Newborn Epigenetics STudy (NEST) cohort, paternal obesity altered epigenetic profiles such as modification in small RNA content and DNA methylation in human spermatozoa (*121*) as well as DNA methylation patterns in offspring of these obese fathers (*122*). Furthermore, also parental exercise can have a strong impact on the offspring as reviewed in (*123*). For example, pyruvate dehydrogenase kinase 4 (*PDK4*) expression in skeletal muscle is decreased following exercise training (*124*), but also different circulating miRNAs are controlled by exercise (*125-127*) and genome-wide DNA methylation changes are detectable in human spermatozoa (*128*). Maternal exercise during pregnancy on the other hand was linked to a reduced obesity risk (*95*) and differentially methylated regions in imprinted genes in offspring (*129*). These changes in epigenetic marks even in the germline hint to a probable epigenetic transmission to the offspring, however, to date, no studies are available substantiating intergenerational inheritance of parental exercise beyond *in utero* effects. Nevertheless, a plethora of studies show that a multitude of environmental factors influence our progeny and can induce a multitude of potential effects.

Unfortunately, it is very difficult to dissect correlation from causality in epidemiological human studies. Data are often evaluated and reported by the subjects themselves or their relatives and other relevant data or biological samples are not available. Furthermore, full adjustment for potential confounding factors such as genetic and non-genetic family history, physical activity, dietary patterns and energy intake, culture, and behavior is not possible.

1.3.3 Animal studies demonstrate epigenetic inheritance across generations

Considering the limitations of human epidemiological studies, animal studies especially in rodents have been utilized to specifically determine the causal relations between parental environment and health parameters in offspring. Using animal models enables the exclusion of most confounding factors and limitations of human studies. Within the last ten years, many studies have been conducted showing that parental nutrients, stress and trauma as well as other environmental factors can have profound effects on cognitive plasticity, fertility, anxiety, and metabolic health across generations.

Recent reviews highlight the impact of environmental factors and epigenetic processes on mammalian brain development and memory function (*130, 131*). Especially environmental enrichment (EE) has a major influence on cognitive plasticity and learning ability. EE refers to animal housing conditions, in which rodents are exposed to novel and stimulatory objects that support cognitive training, have enhanced social interactions, and have access to devices for physical activity, such as running wheels. An early study in 1987 already found that rat progeny showed enhanced learning ability when the dams had been exposed to EE before pregnancy (*132*) and in mice, strengthening of hippocampal synapses was detected in females exposed to EE at a juvenile age as well as their offspring (*133*). In contrast, exposure of male mice to EE during adulthood increased hippocampal activity and memory function in their male and female offspring, but not in their grand-offspring (*134*). Strikingly, injection of isolated sperm RNA from either EE exposed or non-exposed fathers into zygotes from naïve parents provided evidence that overexpression of miR-212/132 in sperm is sufficient to confer enhanced hippocampal activity on the offspring, but did not suffice to provide a cognitive benefit (*134*). In addition, alterations in dietary nutrients such as a paternal diet enriched in methyl donors, are able to negatively influence cognitive and neural functions in the offspring generation (*135*). In contrast to this association, depletion of dietary methyl donors exacerbates anxiety- and depression-like behaviors in male rats (*136*) and their male offspring (*137*). Additionally, grandmaternal exposure to high-fat diet (HFD) during pregnancy increased anxiety- and depression-like behavior in granddaughters through the maternal germline (*138*).

Many commonly used chemicals act as endocrine disruptors in mammals and are therefore suspected to have adverse effects. A well-known example is bisphenol A (BPA), which is used in many daily-use plastics and therefore detectable in most humans (*139*). It is believed to reduce fertility and increase risk of T2D, obesity and several other diseases. In rodents, exposure to BPA increases anxiety and reduces fertility in males and females for at least three generations (*140, 141*). Altered gene expression and loss of imprinting was also detected in brain tissues of F_3 juveniles from prenatally BPA exposed versus control lineages indicating robust transgenerational inheritance (*142*). For another environmental endocrine disruptor called vinclozolin (used as fungicide in some countries), transgenerational effects on male fertility have been demonstrated in rats that correlate with altered DNA methylation patterns in the germline (*143, 144*).

Not only nutrients and chemicals but also stress or trauma represent environmental factors that can have transgenerationally inherited effects on anxiety and behavioral traits (*145*). In rats, early postnatal stress through impairment of maternal care (measurable as reduced licking and grooming of pups and arched-back nursing) resulted in different anxiety-like behaviors later in adulthood. Concomitantly, hypermethylation of specific CpG sites of the *Nr3c1* promoter causes reduced expression of the glucocorticoid receptor (GR) in the hippocampus and enhanced activation of the hypothalamic–pituitary–adrenal (HPA) axis under stress (*146-148*). Intriguingly, these maternal care-related phenotypes could be reversed by cross-fostering offspring with a control female, but also by treatment with an HDAC inhibitor (*148*). Conversely, anxiety related phenotypes could be established by infusion of a methyl donor to the hippocampus of control rats (*147*). These studies support the hypothesis of a causal correlation between DNA methylation and an anxiety phenotype. Similarly, repeated random separation of mouse pups from their mother result in depression-like behavior and affected the behavioral response to aversive stimuli in adult life (*149*). Interestingly, these traits were transgenerationally inherited in a complex and sex-specific fashion through the paternal lineage with some traits present in the F_3 generation. At the same time, altered DNA methylation of several candidate genes in sperm of stressed males was observed and partly maintained in sperm of male offspring as well as in brains of female offspring (*149*). Furthermore, it was shown that individual miRNAs were altered in sperm of mice that passed an acquired anxiety phenotype (paternal trauma by unpredictable maternal separation and maternal stress) to the next generation (*150*), indicating a role of small non-coding RNAs as potential mediators of epigenetic inheritance (*151*). Behavioral changes were also associated with decreased methylation of the GR promoter and increased expression of the GR. Even so, the transgenerational transmission of such behavioral symptoms could be prevented by EE (*152*). Chronic social defeat stress also in adult male mice resulted in anxiety- and depression-like behavior in both male and female offspring as well as in increased levels

of corticosterone in plasma and decreased levels of vascular endothelial growth factor (VEGF) in male offspring. Importantly, offspring that was generated through *in vitro* fertilization (IVF) did not display most of these behavioral changes pointing towards modes of intergenerational inheritance that were not associated with information transmitted via germ cells. Instead, mechanisms such as learning of behaviors from parents appeared to dominate the inheritance (*153*). In contrast to this, a much-noticed study could demonstrate transgenerational inheritance of odor-induced fear by using IVF to produce offspring (*154*). In this experiment, paternal mice were subjected to odor fear conditioning using acetophenone before conception, which activates the known odorant receptor *Olfr151*. The F1 and F2 generation showed increased behavioral sensitivity and enhanced neuroanatomical representation of the *Olfr151* pathway. In addition, sperm of F0 and unexposed F1 males were characterized by hypomethylation of CpG sites in the *Olfr151* gene. In line with the definition of epigenetics, this behavioral phenotype and over-representation of *Olfr151* in the F1 generation could be reversed by extinction-based behavioral strategies (*155*).

Regardless of the kind of stress or chemical compound that led to an altered behavioral phenotype, there is evidence for resulting epimutations for example in sperm as well as tissues in offspring and therefore clear indication of intergenerational and in some cases even transgenerational epigenetic inheritance.

Nutrition is a major environmental factor leading to acquired metabolic phenotypes that can be inherited across generations. Even in non-mammalian animals such as Drosophila, a paternal high-sugar diet caused obesity in offspring through changes in the chromatin structure in sperm (*156*). In rodents, there is overwhelming evidence that parental HFD can increase susceptibility to develop obesity and glucose intolerance in offspring generated via natural fecundation (*157-160*). Streptozotocin-induced prediabetes in male mice affected DNA methylation patterns in their sperm cells as well as in pancreatic islets of the F1 and F2 generation (*161*). Additionally, intergenerational inheritance was evident when offspring was produced via IVF from gametes of parents fed from HFD and when healthy foster mothers were used to carry out the progeny. In this case, the use of IVF excluded that confounding factors during gestation and lactation, or transfer of parental microbiomes, or behavior acquired from parents could contribute to the observed epigenetic inheritance (*162*). Similarly, low-protein diet (LPD) (*163*) and over- (*164*) as well as undernutrition (*165*) were shown to have an impact on offspring's hedonistic behavior and metabolism. On the one hand, phenotypic changes caused by the nutritional environment of the mother can be epigenetically transmitted either via the oocytes (*162, 166*) or during intrauterine exposure of the embryo and during lactation (*160, 165, 167-169*). On the other hand, they may be transmitted by the father via sperm cells or factors such as hormones that are present in seminal fluids (*170-173*).

Considering the possibility that epimutations in DNA methylation patterns could be causative of this epigenetic inheritance, changes in the sperm methylome were not found accountable by several studies. For example, paternal LPD and paternal HFD did influence the metabolic phenotype in offspring, but sperm methylomes were not consistently affected (*174*). Another study showed that maternal HFD affected female body weights in the F3 generation via the paternal lineage. However, DNA methylation in F1 and F2 sperm was not significantly different comparing HFD and control diet progeny (*160*). Furthermore, maternal HFD during gestation had no effect on offspring's DNA methylation patterns in the liver (*175*). Intriguingly, several studies identified sperm-derived small RNAs as potential mediators of epigenetic inheritance. By injecting either specific miRNAs or isolated fractions of sperm RNAs into naïve zygotes, metabolic phenotypes of specific dietary interventions could be reproduced in the offspring (*63, 171, 173*). Although these experiments provided the proof that specific small RNAs are sufficient to reproduce the respective phenotypes, they did not demonstrate that the examined small RNAs represent the causative epimutation also *in vivo*. Interestingly, recent work could demonstrate the mechanistical importance of tRNA aspartic acid methyltransferase 1 (*Trdmt1/Dnmt2*) for intergenerational inheritance via sperm sncRNAs. Here, the deletion of *Dnmt2* in mice abolished the transmission of HFD-induced metabolic disorders to the offspring by preventing modifications to sperm sncRNAs (*176*).

Taken together, there is abundant proof that parentally acquired diet-induced metabolic phenotypes and behavior-related disorders can be inter- and transgenerationally inherited in mammals. In most of the studies provided above, offspring was procreated via natural fecundation allowing a number of confounding factors to potentially impact the inherited phenotype through *in utero* interactions between mother and fetus. However, there is also clear evidence, in particular from IVF-based approaches, that such inheritance can be epigenetically transmitted via maternal and paternal germ cells. And finally, while there is only very limited evidence for DNA methylation as source for epimutations, current observations provide substantial evidence that small RNAs, including miRNAs and fragmented tRNAs, may represent the causative epimutations (*177, 178*).

Evidence from this growing number of animal studies clearly demonstrates the existence of epigenetic inheritance across generations in mammals and may help to understand the human situation, in which observations already support this phenomenon.

1.4 Aim of this thesis

In the last decades, the missing heritability of T2D has been investigated in various studies. Additional to genetic and environmental risk factors for T2D, emerging evidence points towards epigenetic factors as potential contribution to the missing heritability. In rodent animal models, the parental environment like the nutritional status could alter the phenotypic outcome in offspring. Information about the parental environment was thereby transmitted to the progeny through intergenerational and transgenerational epigenetic inheritance. Although definite proof for intergenerational and transgenerational epigenetic inheritance is still missing in humans, it has been suggested by various retrospective and prospective epidemiological studies. Thus, epigenetic inheritance of the parental nutritional status to the offspring could contribute to the tremendous increase in obesity and T2D prevalence, which cannot be explained by genetic risk factors (common and rare alleles found in GWAS) and altered environmental factors (high-caloric processed food and sedentary lifestyle) alone. In our group, we are addressing the question if epigenetic inheritance through gametes in an environment that is rich in high-caloric diets could contribute to this pandemic.

In a previous study, we have shown that 6 weeks of parental HFD increases offspring's susceptibility to develop overweight and glucose intolerance in adulthood in a sex-specific and parent-of-origin specific manner. By using IVF and embryo transfer into healthy foster mothers we could exclude potential confounding factors and prove intergenerational epigenetic inheritance of an acquired metabolic phenotype (*162*). Preliminary data also suggest alterations in epigenetic marks such as DNA methylation and short and long RNA transcripts in the parental gametes that could be mediators of this epigenetic inheritance (*P. Huypens et al, unpublished*).

In order to examine if and how these parental epigenetic signatures can persist throughout development and influence the metabolic phenotype in adult offspring, we aim to analyze the epigenetic differences between offspring derived from HFD- or LFD-treated parents at different stages during development. As shown in Figure 1.6, these examined stages include the preimplantation phase with zygote, 2-cell embryo and blastocyst, different Theiler stages during fetal organogenesis such as TS20, TS22 and TS23 as well as juvenile mice at the age of 3 weeks. The focus of this thesis is on transcriptomic differences between HFD- and LFD-derived offspring (Figure 1.6). In preimplantation embryos, sequencing of long and small coding and non-coding RNAs should provide insights into the impact of parental HFD during early development and discover epigenetic marks and mechanisms potentially involved in epigenetic inheritance. Additionally, by sequencing long coding and non-coding RNAs in relevant organs during fetal development and in young mice common regulated transcripts

and altered pathways should be discovered and linked to the metabolic phenotype in HFD-derived F1 generation. Furthermore, regulatory molecules such as small RNAs in early embryos might be linked to regulated transcripts during later development. Changes in DNA methylation patterns and histone modifications were disregarded in this thesis due to limited availability of sample material.

	Oocyte	Sperm	Fertilization	Zygote	2-cell embryo	Blastocyst	Fetus	Juvenile mouse	Adult mouse
Age				E0.5	E1.0	E4.0	E11 - E15	3 weeks	15 weeks
Phase	Gametogenesis			Embryogenesis			Organogenesis	Growth	
Tissue	Previously analyzed			Pool of approx. 50 zygotes	Pool of approx. 30 2-cell embryos	Pool of approx. 15 blastocysts	Liver (TS 20, 22, 23)	Liver, WAT, SAT	Previously analyzed
Transcriptome				Long RNA + sncRNA	Long RNA + sncRNA	Long RNA + sncRNA	Long RNA	Long RNA	

FIGURE 1.6 | EXPERIMENTAL STRATEGY

Murine development is examined from fertilization to adulthood at different developmental stages in the F1 generation.

In more detail, three stages during the preimplantation phase were examined: zygotes at approximately 4-6 h after fertilization (E0.5), 2-cell embryos at 24±2 h after fertilization (E1.0) and blastocysts at approximately 4 days after fertilization (E4.0). At these stages of embryogenesis, a number of single embryos - all derived from the same sperm donor and the same IVF event - were pooled in order to enable the extraction of sufficient amounts of total RNA. From these samples, long and small RNA-Seq data were obtained and analyzed. During organogenesis, only developing liver tissue was analyzed at three different Theiler stages (*179*), specifically TS20 (E12), TS22 (E14) and TS23 (E15). After birth, at the age of 3 weeks, three different tissues that are heavily involved in the metabolism were analyzed, namely liver tissue, visceral white adipose tissue (WAT) and subcutaneous white adipose tissue (SAT). Long RNA-Seq data were obtained and analyzed from these different tissues at the different developmental stages. Parental gametes and various tissues of adult F1 mice at the age of 15 weeks have been analyzed previously and will not be addressed within the scope of this thesis.

Overall, with this comprehensive transcriptome analysis covering important developmental stages of the F1 generation we aim to find common regulated transcripts or regulatory elements as well as altered biological processes that could hint to a mechanism or involved epigenetic regulators for the intergenerational epigenetic inheritance of diet-induced obesity and T2D.

2. MATERIAL AND METHODS

2.1 Material

2.1.1 Mouse equipment

Mouse equipment	Company	Catalogue #
C57BL/6NTac Mice	Taconic	
CO2 Incubator CB 53	Binder GmbH	
Contour next Glucose meter	Bayer	
Dissection needle	Fine Science Tools (F.S.T.)	
Dumont Forcep	Fine Science Tools (F.S.T.)	
Forceps	Fine Science Tools (F.S.T.)	
HFD (DIO – 60 kJ% fat)	ssniff Spezialdiäten	E15741
Holder for Retransfer- and Handlingpipettes	BioMedical Instruments	
Illuminator for Microscopy KL 1500 LCD	Leica	
LFD (LF Control – 21% protein, 11 kJ% fat)	ssniff Spezialdiäten	E15000
Microscope Stage HT 300	Minitüb	
Normal chow diet	Altromin	1314
Retransfer Pipette Ø 108-114 µm	BioMedical Instruments	
Scissors	Fine Science Tools (F.S.T.)	
SealsafePlus AERO IVC Greenline	Tecniplast	
Spring scissor	Fine Science Tools (F.S.T.)	
Stereomicroscope Leica MZ9.5	Leica	

2.1.2 Consumables

Consumables	Company
8 microTUBE strip	Covaris
Cell culture dishes 35x10 mm; with 4 inner rings	Greiner Bio-One GmbH
Combitips advanced ® 10 mL; 25 mL; 50 mL	Eppendorf
Contour next Sensoren	Bayer
Cryotube Vials 1.0 mL	Thermo Fisher Scientific
Filter Unit 0.22 µm	Merck Millipore
IVF Petri dishes 35x10 mm	Thermo Fisher Scientific
IVF Petri dishes 60x15 mm	Thermo Fisher Scientific
Microplate 96 well, U-bottom	Greiner Bio-One GmbH
Needle 20G; 23G	B Braun
Non-Stick RNase-free Microfuge Tubes 1.5 mL	Ambion
Omnican ® F 0.01 mL - 1.0 mL (with integrated needle)	B Braun
Omnifix ® F 1.0 mL; 10 mL; 50 mL (without integrated needle)	B Braun
PCR 8er CapStrips	Biozym Scientific GmbH
PCR 8er SoftStrips 0.2 mL	Biozym Scientific GmbH
Pipettes 10 mL; 25 mL	Greiner Bio-One GmbH
Reaction tubes 1.5 mL; 2.0 mL	Eppendorf

Reaction tubes 1.5 mL; 2.0 mL	Sarstedt
SurPhob ® Filter tips 10 µL; 20 µL; 100 µL; 200 µL; 1000 µL	Biozym Scientific GmbH
Tubes 15 mL; 50 mL	Sarstedt

2.1.3   Solutions, reagents and media

Solutions, reagents and media	Company/Recipe
0.9% NaCl	Fresenius Kabi
Agarose	Biozym Scientific GmbH
β-Mercaptoethanol	Sigma
EmbryoMax® HTF	Merck Millipore
EmbryoMax® KSOM+AA with D-Glucose	Merck Millipore
EmbryoMax® M2 medium with phenol red	Merck Millipore
Ethanol, absolute	Millipore Corp.
Human Chorionic Gonadotropin (hCG)	
Mineral oil (light)	Sigma
One*Taq*® Hot Start 2X MM w/Std Buffer	New England Biolabs
PBS (10x)	80 g NaCl 2 g KCl 17.8 g Na_2HPO_4 x $2H_2O$ 2.72 g KH_2PO_4 Dissolved in ddH_2O and adjusted to pH 7.3 ddH_2O added to a final volume of 1 L
Pregnant Mare Serum Gonadotropin (PMSG)	
Preincubation (PI) medium	697.6 mg NaCl 35.6 mg KCl 29.3 mg $MgSO_4$ x $7H_2O$ 16.2 mg KH_2PO_4 210.6 mg $NaHCO_3$ 5.5 mg Sodium pyruvate 100.0 mg Glucose 25.1 mg $CaCl_2$ x $2H_2O$ 98.3 mg Methyl-β-cyclodextrin 7.5 mg Penicillin G 5.0 mg Streptomycin 100 mg Polyvinyl alcohol Dissolved in ddH_2O ddH_2O added to a final volume of 100 mL Sterile-filtered through a 0.22 µm filter unit
RnaseZAP ®	Sigma
SYBR Green I	Thermo Fisher Scientific
TAE (50x)	242.2 g Tris base Dissolved in ddH_2O 57.1 mL Acetic acid 100 mL 0.5 M EDTA, pH 8.0 ddH_2O added to a final volume of 1 L
Water for molecular biology	Millipore Corp.

2.1.4 Kits

Kit	Company	Catalogue #
Agencourt AMPure XP Magnetic Beads	Beckman Coulter	A63881
Agilent DNA High Sensitivity Kit	Agilent Technologies	5067-4626
Agilent RNA 6000 Pico Kit	Agilent Technologies	5067-1513
Encore Biotin Module	Nugen	4200-60
GenElute Mammalian Genomic DNA Miniprep Kit	Sigma	G1N70
HiSeq PE Cluster Kit v4 cBot	Illumina	PE-401-4001
HiSeq PE Rapid Cluster Kit v2	Illumina	PE-402-4002
HiSeq Rapid SBS Kit v2 (200 cycles)	Illumina	FC-402-4021
HiSeq Rapid SBS Kit v2 (50 cycles)	Illumina	FC-402-4022
HiSeq Rapid SR Cluster Kit v2	Illumina	GD-402-4002
HiSeq SBS Kit v4 (250 cycles)	Illumina	FC-401-4003
HiSeq SBS Kit v4 (50 cycles)	Illumina	FC-401-4002
HiSeq SR Cluster Kit v4 cBot	Illumina	GD-401-4001
Hybridization Wash and Stain Kit	Affymetrix	900720
MinElute Reaction Cleanup Kit	Qiagen	28204
miRNeasy® Mini Kit	Qiagen	217004
NEBNext Multiplex Oligos for Illumina (Primer Sets 1,2,3,4)	New England Biolabs	E7335S, E7500S, E7710S, E7730S
NEBNext Ultra DNA Library Prep Kit for Illumina	New England Biolabs	E7370S
NucleoSpin Gel and PCR Clean-Up kit	Macherey-Nagel	740971
Ovation Pico WTA System V2	Nugen	3302-60
Ovation RNA-Seq System V2	Nugen	7102-32
Ovation SoLo RNA-Seq System	Nugen	0501-96
Qubit™ dsDNA BR Assay Kit	Thermo Fisher Scientific	Q32853
Qubit™ dsDNA HS Assay Kit	Thermo Fisher Scientific	Q32854
RNase-Free DNase I Kit	Norgen	25710
RNase-Free DNase Set	Qiagen	79254
RNeasy MinElute Cleanup Kit	Qiagen	74204
Single Cell RNA Purification Kit	Norgen	51800
SMARTer smRNA-Seq Kit	Takara/Clonetech	635031

2.1.5 Laboratory equipment

Laboratory equipment	Company
96-Well Aluminum Heating/Cooling Block	Sigma/Light Labs
accu-jet Pipettierhelfer	Brand
Agilent 2100 Bioanalyzer	Agilent Technologies
Centrifuge 5415 R	Eppendorf
Centrifuge 5418	Eppendorf
E220 Focused Ultrasonicator	Covaris
Electrophoresis power supply	Micro-Bio-Tec Brand
Gel documentation	Vilber Lourmat

Gel electrophoresis system	Thermo EC
GeneChip Fluidics Station 450	Affymetrix
GeneChip Hybridization Oven 645	Affymetrix
GeneChip Scanner	Affymetrix
Homogenizer Ultra-Turrax T8	IKA
Magnetic Stand -96	Ambion
Multipette Xstream	Eppendorf
Qubit Fluorometer	Thermo Fisher Scientific
Spectrophotometer ND-1000	Nanodrop
Thermal Cycler T100	Bio-Rad
Vortex mixer	Vortex
Water bath	B Braun

2.2 Methods

2.2.1 Metabolic physiological methods

2.2.1.1 Mouse maintenance

Mice were kept in a specific-pathogen-free environment in compliance with the Federation of European Laboratory Animal Science Associations Protocols (FELASA) and all experimental procedures were performed in accordance with German and European Union guidelines.

Male and female C57BL/6NTac mice were housed in ventilated cages (SealsafePlus AERO IVC Greenline, Tecniplast) on a 12-h light/12-h dark cycle at constant temperature (22 ± 1 °C) and under controlled humidity. Mice had *ad libitum* access to water and food.

2.2.1.2 Dietary challenge

Mice were fed a normal chow diet (Altromin 1314) from birth to the age of 9 weeks und pregnant females during gestation and lactation. Starting at the age of 9 week for a period of 6 weeks, mice received either low-fat control diet (LFD) or high-fat diet (HFD). The energy content of the HFD (DIO – 60 kJ% fat, ssniff Spezialdiäten) is 21.6 MJ/kg, with 60% of the metabolizable energy derived from fat. The energy content of the LFD (LF Control – 21% protein, 11 kJ% fat, ssniff Spezialdiäten) is 15.2 MJ/kg, with 11% of the metabolizable energy derived from fat.

2.2.1.3 Body weight and metabolic studies

Body weight and blood glucose levels were measured on a weekly basis. Glucose tolerance was determined at 15 weeks of age by an intraperitoneal glucose tolerance test (ipGTT). Mice were fasted for 4 to 6 hours in the morning, prior to an intraperitoneal injection of 2 g/kg of glucose (20% solution, Braun). Glucose concentration was measured using Contour next glucose meter (Bayer) from tail blood at time points 0, 15, 30, 60 and 120 minutes.

2.2.1.4 *In vitro* fertilization

In vitro fertilization (IVF) was conducted with gametes of C57BL/6NTac mice at the age of 15-16 weeks. Female oocyte donors were stimulated with 7.5 U of pregnant mare serum gonadotropin (PMSG) and 7.5 U of human chorionic gonadotropin (hCG) 64 and 14 hours prior to oocyte collection, respectively. Fresh sperm was obtained from the *cauda epididymis* and cultured in preincubation medium for 1 hour to allow capacitation. Oocytes were collected from the ampulla and co-cultured with 5 µL of capacitated sperm in HTF medium at 37 °C and 5% CO_2. After incubation for 4-6 hours, fertilized oocytes were washed in HTF to remove

sperm and cumulus cells, transferred into KSOM medium and incubated overnight at 37 °C and 5% CO_2. In the morning, 2-cell embryos were selected, washed und cultured in KSOM medium for 3 days until blastocyst stage.

Preimplantation embryos at these different developmental stages (zygote, 2-cell embryo and blastocyst) were washed three times in PBS and snap-frozen in liquid nitrogen for further analyses. In order to obtain RNA of high quality and a sufficient yield, 10-60 embryos were pooled in a minimal volume of PBS.

In order to obtain living offspring, zygotes were cultivated overnight and 2-cell embryos were used for embryo transfer (see 2.2.1.5).

2.2.1.5   Embryo transfer

Oocytes were fertilized *in vitro* and cultivated overnight until the 2-cell stage. 2-cell embryos were transferred into pseudopregnant foster mothers of the CD-1 strain that have been mated with vasectomized males on the previous day and displayed a vaginal plug. CD-1 females were anaesthetized with a mixture of ketamin (100 mg/kg) and xylazin (16 mg/kg) before surgery and embryos were transferred bilaterally into the oviducts through two minor incisions. Postsurgical pain management was ensured by subcutaneous injection of metamizol (200 mg/kg) before and for three days after surgery.

2.2.1.6   Organ dissection

In order to collect organs for transcriptome analyses, mice were fasted for 4 to 6 hours prior to dissection. Mice were anesthetized with an overdose of isoflurane leading to respiratory arrest due to its repressive effects on cardiovascular system and respiration. Only after absence of agonal respiration and the toe reflex, the abdomen was opened and blood was drawn from *Vena cava caudalis* leading to the definite death of the animal. Whole blood was centrifuged for 10 min at 1,700 xg at 12 °C to obtain blood plasma samples for further analyses. Plasma samples were snap-frozen in liquid nitrogen and stored at -80 °C. Then all organs of interest i.e. liver, visceral and subcutaneous adipose tissue, pancreas, muscle and hypothalamus were collected promptly, snap-frozen in liquid nitrogen and stored at -80 °C.

2.2.2   Molecular methods

2.2.2.1   DNA extraction

Genomic DNA was extracted from mouse tissues using the GenElute Mammalian Genomic DNA Miniprep Kit (Sigma) following the manufacturer's instructions. In short, tissue was digested by incubating at 55 °C overnight in a mixture of 180 μL Lysis Solution and 20 μL

Proteinase K. After digestion, cells were lysed in Lysis Solution C by vortexing and 100% ethanol was added. DNA-binding columns were prepared and the lysate was loaded onto the column. After two washing steps and complete drying of the column, DNA was eluted in 50 µL Elution solution.

2.2.2.2   Sex genotyping

To determine the sex of embryos collected between embryonic days E11 and E15, the male-specific sequence *Sry* was amplified by PCR and detected by gel electrophoresis as shown by Lambert et al. (*180*). PCR components were added to the reaction according to Table 2.1 containing two sets of primers specific for *Sry* gene (chromosome Y) and *Il3* gene (chromosome 11) and embryonic DNA. Amplification was carried out following the PCR program shown in

Table 2.2 with 33 cycles.

TABLE 2.1 | PCR REACTION MIX

Component	Amount
One*Taq*® Hot Start 2X MM w/Std Buffer	25 µL
Primer Mix Sry (10 µM)	2 µL
Forward Sequence:	5'-TGGGAGTGGTGACAATTGTC-3'
Reverse Sequence:	5'-GAGTACAGGTGTGCAGCTCT-3'
Primer Mix IL3 (6 µM)	2 µL
Forward Sequence:	5'-GGGACTCCAAGCTTCAATCA-3'
Reverse Sequence:	5'-TGGAGGAGGAGGAAAAGCAA-3'
DNA (50 ng/µL)	3 µL
Nuclease-free water	18 µL
Total Volume	**50 µL**

TABLE 2.2 | PCR PROGRAM FOR SEX GENOTYPING

Temperature	Duration	
95 °C	4.5 min	
95 °C	35 sec	
50 °C	1 min	} 33x
72 °C	1 min	
72 °C	5 min	

The assessment of the results was done by gel electrophoresis in 2% agarose run at 100 V. DNA is visualized by binding of SYBR Green I (Thermo Fisher Scientific) and emission of green light

under UV light (Vilber Lourmat). Male embryos show the band for *Sry* at 402 bp and the 544 bp product of *Il3* as positive control. Female embryos only show the *Il3* band.

2.2.2.3   RNA extraction

Total RNA was extracted from murine tissues and preimplantation embryos using two different protocols.

Murine tissues were stored at -80 °C since collection and RNA was extracted using the miRNeasy Mini Kit (Qiagen). 700 µL QIAzol Lysis Reagent were added to approximately 10 mg of pestled liver tissue, 30 mg of adipose tissue or an entire fetal liver after which the tissue was homogenized for approximately 10-30 seconds with the T8 Ultra Turrax Homogenizer (IKA). After incubation at room temperature (RT) for 15 min 140 µL chloroform were added to induce phase separation. Samples were mixed vigorously for 15 seconds and incubated for 3 min at RT. After centrifugation for 15 min at 12,000 xg at 4 °C, the upper aqueous phase was carefully transferred to a new tube and 1.5 volumes of 100% ethanol were added and thoroughly mixed. The samples were loaded onto the RNeasy Mini column to allow binding of the RNA to the column and centrifuged at 8,000 xg for 15 seconds at RT. After discarding the flow-through the column was washed with 350 µL RWT buffer. For the DNA digest a mix of 70 µL RNase-free DNase digestion buffer and 10 µL RNase-free DNase was added directly onto the column and incubated for 15-20 min at RT. Afterwards, column was washed again with 350 µL RWT buffer and twice with 500 µL RPE buffer and always centrifuged at 8,000 xg for 15 seconds at RT. In order to remove all traces of ethanol, the column was centrifuged for 2 min at 12,000 xg and transferred to a new collection tube. Elution of the sample was conducted by adding 30-50 µL RNase-free water directly onto the membrane and centrifuging for 1 min at 8,000 xg at RT.

Pools of preimplantation embryos in PBS were stored at -80 °C and total RNA was extracted using the Single Cell RNA Purification Kit (Norgen). Cells were thawed and lysed by adding 100 µL of Buffer RL (supplemented with 1 µL β-mercaptoethanol) and careful mixing. 100 µL of 70% Ethanol were added to the lysate and mixed by vortexing. Lysate was applied to the spin-column and centrifuged for 1 min at 3,500 xg and an additional 1 min at 14.000 g. Column was washed by applying 400 µL Wash Solution A and centrifuging for 2 min at 14,000 xg. For on-column DNase digest a mix of 15 µL DNase I and 100 µL Enzyme Incubation Buffer was prepared for every reaction. 100 µL of the DNase I Solution was applied directly onto the column and centrifuged for 1 min at 14,000 xg. Flow-through was re-applied onto the column and incubated for 15 min at RT. Afterwards, column was washed twice with 400 µL Wash Solution A and centrifuged for 1 min at 14,000 xg. In order to dry the membrane column was centrifuged for another 2 min at 14,000 xg. Column was placed into a new elution

tube, 10 µL of Elution Solution A were added directly onto the membrane and column was centrifuged for 1 min at 200 xg followed by 2 min at 14,000 xg.

2.2.2.4   Quantity and quality measurement

Yield of RNA extraction was measured with NanoDrop™ 1000 Spectrophotometer (Thermo Fisher Scientific) or if higher sensitivity was required with the Qubit 4 Fluorometer (Thermo Fisher Scientific).

The NanoDrop measures the concentration and purity of nucleic acids in a 1 µL sample by photometry.

In order to measure the concentration with the Qubit system, a Working Solution was prepared by diluting the Qubit reagent 1:200 in Qubit buffer. Two standards were prepared by mixing 10 µL Standard with 190 µL Working Solution. For every sample 2 µL were mixed with 198 µL Working Solution in thin-wall, clear 0.5 ml PCR tubes. All sample and standard tubes were vortexed for a few seconds and incubated for 2 min at RT. First, the two standards were measured to generate a standard curve and then the samples were measured.

To assess the quality of extracted RNA the 2100 Bioanalyzer Instrument (Agilent Technologies) with the RNA 6000 Pico Kit (Agilent) was used according to manufacturer's instructions. Briefly, the chip priming station was set up by adjusting the syringe to a volume of 1 ml and the Bioanalyzer was washed with RNase-free water. Also, all reagents were first equilibrated to RT for at least 30 min. Gel was prepared by applying 550 µL of RNA 6000 Pico gel matrix to a spin filter and centrifuging at 1,500 xg for 10 min. RNA 6000 Pico dye was vortexed and span down. Then 1 µL was added to a 65 µL aliquot of filtered gel, vortexed and centrifuged at 13,000 xg for 10 min. 9 µL of gel-dye mix was added to a RNA Pico Chip, that was located on the Chip priming station. The plunger of the syringe at the priming station was pushed down and released after 30 seconds. Next, 9 µL of gel-dye mix, 9 µL of RNA 6000 Pico conditioning solution, 5 µL of RNA 6000 Pico marker and 1 µL of denatured RNA 6000 ladder was added according to marking on the chip. 1 µL of each sample was added to according sample well. The chip was vortexed for 1 min at 2,400 rpm (IKA MS 3 Vortex Mixer) and inserted in the receptacle of the Bioanalyzer to start chip run.

2.2.3   Microarrays

2.2.3.1   Amplification and hybridization

Preparation of labeled cDNA fragments for hybridization on Microarrays was performed in three different consecutive steps followed by hybridization, washing and scanning of arrays. For synthesis and amplification of cDNA from total RNA, the Ovation Pico WTA System V2

(Nugen) was used followed by purification of the cDNA with the MinElute Reaction Cleanup Kit (Qiagen). Then, fragmentation and labeling was conducted using the Encore Biotin Module (Nugen) and hybridization cocktails were prepared. Amplified cDNA was hybridized on Affymetrix Mouse Gene 2.0 ST arrays. As input, 30 ng total RNA were used and all protocols were performed as recommended by the manufacturers. To each sample, a polyA control was added and at different stages during the protocol, yield and quality were checked by NanoDrop or Bioanalyzer measurement (see 2.2.2.4). Staining (Fluidics script FS450_0002) and scanning was performed according to the Affymetrix expression protocol including minor modifications as suggested in the Encore Biotin protocol.

2.2.3.2   Data analysis

Analysis of microarray data was performed using the expression console (v.1.3.0.187, Affymetrix) for quality control and to obtain normalized RMA gene-level data (standard settings including median polish and sketch-quantile normalization). Annotation was downloaded manually from Affymetrix (NetAffx, October 2016). Statistical analyses were performed by utilizing the statistical programming environment R. Differential expression analysis was conducted employing the limma t-test and Benjamini-Hochberg multiple testing correction (FDR < 10%). Heat maps were generated with CARMAweb (*181*) and principle component analysis (PCA) with an R script kindly provided by Dr. Martin Irmler. Gene set enrichment analysis including GeneOntology terms was performed with a set of significantly regulated genes using the GeneRanker tool from http://www.genomatix.de/.

2.2.4   Next Generation Sequencing

2.2.4.1   Library Preparation from total RNA (Tissue)

Library preparation for total RNA sequencing from murine tissues was performed in three different consecutive steps. First, cDNA was synthesized, amplified and purified using the Ovation RNA-Seq System V2 (Nugen). This kit uses the Single Primer Isothermal Amplification (Ribo-SPIA) technology enabling amplification from total RNA without prior ribosomal RNA depletion. Second, amplified cDNA was fragmented using the Covaris system to a size of 200 bp. Third, libraries were constructed using the NEBNext Ultra DNA Library Prep Kit for Illumina (New England Biolabs). Thereby, adapters were ligated and barcodes were incorporated during PCR amplification to enable multiplexing during sequencing. All protocols were performed according to manufacturer's recommendations.

Approximately, 50 ng total RNA in 5 µL were used as input material, mixed with 2 µL First Strand DNA/RNA chimeric Primer Mix and incubated at 65 °C for 5 min. This way, the DNA

portion of the primer hybridizes either to the 5' portion of the poly(A) sequence or randomly across the transcript. Next, 3.5 µL First Strand Buffer Mix was mixed with 0.5 µL First Strand Enzyme Mix, added to the sample-primer mix and incubated in the thermal cycler with the following program: 4 °C for 1 min, 25 °C for 10 min, 42 °C for 10 min, 70 °C for 15 min and 4 °C until further proceeding. The included reverse transcriptase extends the 3' DNA end of each primer generating first strand cDNA. The resulting cDNA/mRNA hybrid molecule contains a unique RNA sequence at the 5' end of the cDNA strand. For generation of the second strand, 9.7 µL Second Strand Buffer Mix and 0.3 µL Second Strand Enzyme Mix were mixed and added to the reaction tube. The following program was run: 4 °C for 1 min, 25 °C for 10 min, 50 °C for 30 min, 80 °C for 20 min and 4 °C until further proceeding. Fragmentation of the mRNA within the cDNA/mRNA complex creates priming sites for DNA polymerase to synthesize a second strand, which includes DNA complementary to the 5' unique sequence of the first strand chimeric primers. The result is a double-stranded cDNA with a unique DNA/RNA heteroduplex at one end. The resulting cDNA was purified using magnetic Agencourt AMPure XP beads (Beckman Coulter) that are able to bind DNA. Beads must have completely reached RT before proceeding. Then, 32 µL beads (1.6 volumes) were added to 20 µL second strand cDNA, mixed and incubated together at RT for 10 min to let cDNA bind to the magnetic beads. After binding, tubes were transferred to the magnet and kept for at least 5 min until the solution was completely cleared of beads. The clear supernatant was discarded and beads washed three times by adding 200 µL freshly prepared 70% ethanol and incubating for 30 seconds. After the final wash, as much ethanol as possible was removed and beads were air-dried on the magnet for 15-20 min to ensure that all the ethanol has evaporated. The purification was immediately followed by SPIA amplification by adding 40 µL SPIA Master Mix directly to the cDNA bound to the dried beads with the SPIA Master Mix consisting of 20 µL SPIA Buffer Mix, 10 µL SPIA Primer Mix and 10 µL SPIA Enzyme Mix. The following program was used for the amplification: 4 °C for 1 min, 47 °C for 60 min, 80 °C for 20 min and 4 °C until further proceeding. Afterwards, tubes were transferred to the magnet and kept there for 5 min to completely clear the solution of beads. 40 µL cleared supernatant containing the SPIA cDNA were transferred to a fresh tube. SPIA cDNA was then purified using the MinElute Reaction Cleanup Kit (Qiagen) following manufacturer's recommendations. In brief, the entire volume of the SPIA reaction was added to 300 µL Buffer ERC and vortexed. The sample/buffer mixture was loaded onto the MinElute column and centrifuged for 1 min at maximum speed. After discarding the flow-through, 750 µL Buffer PE were added and centrifuged for 1 min at maximum speed. Flow-through was removed and column was centrifuged for an additional 2 min at maximum speed. In order to elute cDNA, 22 µL Buffer EB were added directly to the center of the column, incubated at RT for 1 min and centrifuged for 1 min at maximum speed.

Yield and purity of cDNA was measured using the Nanodrop or Qubit and Bioanalyzer as described in 2.2.2.4 and 2.2.4.4.

In the next step, 3 µg purified cDNA was sheared into 200 bp fragments. Therefore, 3 µg cDNA were diluted in 130 µL and loaded to the 8 microTUBE Strip (Covaris) through the aluminum seal. The tubes were re-sealed with aluminum seal for further processing, placed in the designated rack and tightly closed. Samples were processed in the E220 Focused-ultrasonicator (Covaris) at 7 °C with the following settings: Peak Incident Power 175 W, Duty Factor 10%, Cycles per Burst 200, Treatment Time 180 sec. After fragmentation, samples were immediately taken out of the 8 microTUBE Strip and purified using magnetic Agencourt AMPure XP beads (Beckman Coulter). In short, magnetic beads were allowed to reach RT, then 170 µL resuspended beads (1.4 volumes) were added to 120 µL fragmented cDNA, mixed and incubated for 10 min at RT. Beads were separated on the magnet for 5 min and washed twice with 400 µL freshly prepared 80% ethanol. After removing all residual ethanol, beads were air-dried for 3-5 min while making sure not to over-dry them. Fragmented cDNA was eluted in 30 µL nuclease-free water after incubation for 5 min. Yield of purified fragmented cDNA was measured by Nanodrop or Qubit.

800 ng of fragmented cDNA were used as input material for final library preparation in the NEBNext Ultra Library Prep Kit for Illumina (New England Biolabs). Because DNA fragmentation does not result in homogeneous, blunt-ended fragments, end repair is needed to ensure that each molecule is free of overhangs, and contains 5′ phosphate and 3′ hydroxyl groups. Therefore, 3 µL End Prep Enzyme Mix and 6.5 µL End Repair Reaction Buffer (10x) were mixed with 55.5 µL fragmented DNA and incubated at 20 °C for 30 min and at 65 °C for 30 min. In the next step, adaptors were ligated by adding a mixture of 15 µL Blunt/TA Ligase Master Mix, 2.5 µL NEBNext Adaptor for Illumina and 1 µL Ligation Enhancer to the sample and incubating at 20 °C for 15 min. Then, due to the hairpin structure of the ligated Adaptor, an incorporated uracil has to be excised by adding 3 µL USER enzyme to the ligation mixture and incubating at 37 °C for 15 min to obtain double-stranded DNA fragments with adaptors. Next, a cleanup of adaptor-ligated DNA using magnetic Agencourt AMPure XP beads (Beckman Coulter) was performed. 86.5 µL of resuspended magnetic beads (1.0 volumes) were added to the Adaptor Ligation reaction and incubated at RT for 5 min. After collecting the beads on the magnet, supernatant was discarded and the beads were washed twice with 200 µL of freshly prepared 80% ethanol. Remaining ethanol was removed and beads were air-dried for up to 5 min, while making sure not to over-dry the beads. The DNA was then eluted from the beads in 15 µL of 0.1X TE buffer. Next, DNA was amplified by PCR allowing the addition of index sequences at the same time. Therefore, 15 µL of purified Adaptor Ligated DNA Fragments were mixed with 25 µL of NEBNext Q5 Hot Start HiFi PCR Master Mix, 5 µL

Index Primer and 5 µL Universal PCR Primer and the following program was run: 98 °C for 30 sec, [98 °C for 10 sec, 65 °C for 75 sec] x 4 cycles, 65 °C for 5 min and 4 °C until further proceeding. After PCR amplification, a final cleanup was performed with magnetic Agencourt AMPure XP beads (Beckman Coulter). 45 µL magnetic beads (0.9 volumes) were mixed with 50 µL of the PCR reaction and incubated for 5 min at RT. After collecting the beads on the magnet, supernatant was discarded and beads were washed twice with 200 µL of freshly prepared 80% ethanol. Remaining ethanol was removed and beads were air-dried for up to 5 min, while making sure not to over-dry the beads. The DNA was then eluted from the beads in 30 µL of 0.1X TE buffer and yield and quality of the final libraries was measured using the Nanodrop or Qubit and Bioanalyzer as described in 2.2.2.4 and 2.2.4.4.

2.2.4.2 Library Preparation from total RNA (Embryos)

RNA extraction from pools of preimplantation embryos yields only very small amounts of total RNA. In order to prepare sequencing libraries from these RNA samples, the Ovation SoLo RNA-Seq System (Nugen) was used according to the manufacturer's recommendations. An overview of all reactions and incubation programs is shown in Table 2.3. A Thermal Cycler (BioRad) with heated lid at 105 °C was used for all incubation steps. All steps were carried out on ice. Master mixes were prepared shortly before usage, mixed well and added to the samples. Samples and master mix were mixed well and shortly span down before incubation. A negative control containing water instead of RNA was used for every library preparation batch.

TABLE 2.3 | TOTAL RNA LIBRARY PREPARATION WORKFLOW

DNase TREATMENT AND PRIMER ANNEALING		
Master Mix		
	DNase Buffer	1 µL
	First Strand Primer Mix	2.6 µL
	DTT Solution	1.7 µL
	Nuclease-free Water	0.7 µL
	HL-dsDNase	2 µL
Program		
	37 °C	10 min
	65 °C	5 min
	4 °C	Hold

FIRST STRAND cDNA SYNTHESIS		
Master Mix		
	First Strand Buffer Mix	1 µL
	First Strand Enzyme Mix	1 µL
Program		
	25 °C	5 min
	40 °C	30 min
	70 °C	10 min
	4 °C	Hold

cDNA PROCESSING

Master Mix

	cDNA Processing Enzyme I	0.5 µL
	cDNA Processing Enzyme II	0.5 µL

Program

	37 °C	30 min
	4 °C	Hold

Master Mix

	cDNA Processing Reagent I	2 µL

Program

	90 °C	20 min
	4 °C	Hold

Master Mix

	cDNA Processing Reagent II	2 µL

Program

	4 °C	Hold

Master Mix

	cDNA Processing Reagent III	1 µL
	cDNA Processing Enzyme III	1 µL

Program

	37 °C	30 min
	70 °C	10 min
	4 °C	Hold

Master Mix

	cDNA Processing Reagent IV	7 µL
	cDNA Processing Enzyme IV	1 µL

Program

	37 °C	30 min
	75 °C	20 min
	4 °C	Hold

SECOND STRAND SYNTHESIS

Master Mix

	Second Strand Buffer Mix	3.5 µL
	Second Strand Primer Mix	3.5 µL
	Second Strand Enzyme Mix	1 µL

Program

	25 °C	15 min
	37 °C	15 min
	70 °C	10 min
	4 °C	Hold

END REPAIR

Master Mix

	End Repair Enzyme Mix I	1 µL
	End Repair Enzyme Mix II	1 µL

Program

	25 °C	30 min
	70 °C	10 min
	4 °C	Hold

ADAPTOR LIGATION

Add	Barcoded Adaptor Mix	3.25 µL
Master Mix		
	Ligation Buffer Mix	13 µL
	Ligation Enzyme Mix	2 µL
	Nuclease-free Water	1.75 µL
Program		
	25 °C	30 min
	70 °C	10 min
	4 °C	Hold

ADAPTOR LIGATION PURIFICATION

DNA Binding		
	Agencourt AMPure XP beads	100 µL (1.0 volumes)
Bead Washing		
	70% ethanol (freshly prepared)	2x 200 µL
DNA Elution		
	DNA Resuspension Buffer Mix	30 µL

LIBRARY AMPLIFICATION I

Master Mix		
	Amplification Buffer Mix	10 µL
	Amplification Primer Mix I	9.5 µL
	Amplification Enzyme Mix	0.5 µL
Program		
	70 °C	10 min
	94 °C	30 sec
	60 °C	30 sec	12 cycles
	72 °C	1 min
	72 °C	5 min
	4 °C	Hold

LIBRARY AMPLIFICATION I PURIFICATION

DNA Binding		
	Agencourt AMPure XP beads	40 µL (0.8 volumes)
Bead Washing		
	70% ethanol (freshly prepared)	2x 200 µL
DNA Elution		
	DNA Resuspension Buffer Mix	50 µL
DNA Binding		
	Agencourt AMPure XP beads	40 µL (0.8 volumes)
Bead Washing		
	70% ethanol (freshly prepared)	2x 200 µL
DNA Elution		
	DNA Resuspension Buffer Mix	25 µL

InDA-C/AnyDEPLETE

Aliquot	10 ng Library	8.5 µL in Nuclease-free Water
Master Mix		
	Amplification Buffer Mix	5 µL
	InDA-C Primer Mix	10 µL
	InDA-C Enzyme Mix	0.5 µL
	Amplification Enzyme Mix	1 µL

Program

	37 °C	10 min
	95 °C	2 min
	50 °C	1 min
	65 °C	10 min
	4 °C	Hold

Master Mix

	Amplification Buffer Mix	5 µL
	Adaptor Cleavage Enzyme Mix	2.5 µL
	Nuclease-free Water	17.5 µL

Program

	55 °C	30 min
	95 °C	5 min
	4 °	Hold

LIBRARY AMPLIFICATION II

Master Mix

	Amplification Buffer Mix	10 µL
	Amplification Primer Mix II	39.5 µL
	Amplification Enzyme Mix	0.5 µL

Program

	95 °C	2 min
	95 °C	30 sec
	60 °C	90 sec	2x
	95 °C	30 sec
	65 °C	90 sec	6x
	65 °C	5 min
	4 °C	Hold

LIBRARY AMPLIFICATION II PURIFICATION

DNA Binding

	Agencourt AMPure XP beads	100 µL (1.0 volumes)

Bead Washing

	70% ethanol (freshly prepared)	2x 200 µL

DNA Elution

	DNA Resuspension Buffer Mix	50 µL

DNA Binding

	Agencourt AMPure XP beads	50 µL (1.0 volumes)

Bead Washing

	70% ethanol (freshly prepared)	2x 200 µL

DNA Elution

	DNA Resuspension Buffer Mix	25 µL

QUANTITATIVE AND QUALITATIVE ASSESSMENT OF THE LIBRARY

The number of cycles required for an input of 1-5 ng total RNA in Library Amplification I was determined empirically by considering the manufacturers recommendations. For the input of approx. 2 ng total RNA, 12 cycles were found to yield sufficient amounts of library for sequencing.

2.2.4.3   Library preparation from small RNA

In order to prepare small RNA-Sequencing libraries from these samples, the SMARTer smRNA-Seq Kit for Illumina (Takara) was used according to the manufacturer's recommendations. An overview of all reactions and incubation programs is shown in Table 2.4. A Thermal Cycler (BioRad) with heated lid at 105 °C was used for all incubation steps. All steps were carried out on ice. Master mixes were prepared shortly before usage, mixed well and added to the samples. Samples and master mix were mixed well and shortly span down before incubation. In addition to the samples, a negative control with water instead of RNA and miR163s (provided in the kit: 5' Phos-GAAGAGGACUUGGAACUCGAUC) as positive control were used throughout the whole library preparation procedure.

TABLE 2.4 | SMALL RNA LIBRARY PREPARATION WORKFLOW

POLYADENYLATION		
RNA Input		
	Total RNA (approx. 2 ng)	7 µL
Master Mix		
	Poly(A) Polymerase (2 U/µL)	0.25 µL
	RNase Inhibitor (40 U/µL)	0.25 µL
	smRNA Mix1	2.5 µL
Program		
	16 °C	5 min
	4 °C	1-5 min
cDNA SYNTHESIS		
Master Mix		
	3'smRNA dT Primer	1 µL
Program		
	72 °C	3 min
	4 °C	2 min
Master Mix		
	smRNA Mix2	6.5 µL
	RNase Inhibitor (40 U/µL)	0.5 µL
	PrimeScript RT (200 U/µL)	2 µL
Program		
	42 °C	60 min
	70 °C	10 min
	4 °C	Hold
LIBRARY AMPLIFICATION		
Master Mix		
	Nuclease-free H2O	24 µL
	2X SeqAmp PCR Buffer	50 µL
	SeqAmp DNA Polymerase	2 µL
Primer		
	Forward Primer	2 µL
	Reverse Primer	2 µL

Program

98 °C	1 min	
98 °C	10 sec	
60 °C	5 sec	⟳ 18 cycles
68 °C	10 sec	
4 °C	Hold	

PCR PURIFICATION (NucleoSpin Kit)

DNA Binding

PCR product	100 µL
Buffer NTI	200 µL

Washing

Wash Buffer NT3	2x 600 µL

DNA Elution

Elution Buffer NE	30 µL

SIZE SELECTION

DNA Binding

Purified PCR product	30 µL
Nuclease-free H2O	20 µL
Agencourt AMPure XP beads	40 µL
Agencourt AMPure XP beads	60 µL

Bead Washing

80% ethanol (freshly prepared)	2x 200 µL

DNA Elution

Tris Buffer	50 µL

DNA Binding

Agencourt AMPure XP beads	40 µL
Agencourt AMPure XP beads	60 µL

Bead Washing

80% ethanol (freshly prepared)	2x 200 µL

DNA Elution

Tris Buffer	20 µL

QUANTITATIVE AND QUALITATIVE ASSESSMENT OF THE LIBRARY

2.2.4.4 Quantity and quality control during and after library preparation

Yield of DNA fragments of prepared libraries was measured with the Qubit 4 Fluorometer (Thermo Fisher Scientific).

In order to measure the concentration with the Qubit system, a Working Solution was prepared by diluting the Qubit reagent 1:200 in Qubit buffer. Two standards were prepared by mixing 10 µL Standard with 190 µL Working Solution. For every sample 2 µL were mixed with 198 µL Working Solution in thin-wall, clear 0.5 ml PCR tubes. All sample and standard tubes were vortexed for a few seconds and incubated for 2 min at RT. First, the two standards were measured to generate a standard curve and then the samples were measured.

To assess the fragment sizes of DNA libraries the 2100 Bioanalyzer Instrument (Agilent Technologies) with the High Sensitivity DNA Kit (Agilent) was used according to manufacturer's instructions. Briefly, the chip priming station was set up by adjusting the syringe to a volume of 1 ml and the Bioanalyzer was washed with RNase-free water. Also, all reagents were first equilibrated to RT for at least 30 min. 15 µL of High Sensitivity DNA dye concentrate was added to a High Sensitivity DNA gel matrix vial, vortexed, transferred to spin filter and centrifuged at 2,300 xg for 10 min. 9 µL of gel-dye mix was added to a High Sensitivity DNA Chip, located on the Chip priming station. The plunger of the syringe at the priming station was pushed down and released after 60 seconds. Next, 9 µL of gel-dye mix, 5 µL of High Sensitivity DNA marker and 1 µL of High Sensitivity DNA ladder was added according to marking on the chip. Chip was vortexed for 1 min at 2,400 rpm (IKA MS 3 Vortex Mixer) and inserted in the receptacle of the Bioanalyzer to start chip run.

2.2.4.5   RNA sequencing

Sequencing of long and small RNA libraries was performed in collaboration with Dr. Christine Wurmser (Chair of animal breeding, TUM).

Libraries of long and small RNAs of the same experiment were normalized to 2 nM with EB buffer (Qiagen), pooled according to Protocol A (page 9) in the Illumina User Guide (http://emea.support.illumina.com/content/dam/illumina-support/documents/documentation/system_documentation/hiseqkits/hiseq-ga-denaturing-diluting-libraries-reference-guide-15050107-06.pdf) and diluted to a final concentration of approximately 12 pM for clustering. Libraries were then sequenced on a HiSeq2500 (Illumina) using appropriate Cluster and SBS Kits and generating 125 bp of paired-end (PE) reads or 50 bp single reads (SR). HiSeq Control Software (versions 2.2.58 and 2.2.70) was used for sequencing and Real-Time Analysis (RTA) Software (versions 1.18.64 and 1.18.66.4) were used for image analysis and base calling. For generation of fastq-files the CASAVA BCL2FASTQ Conversion Software (versions 1.8.3 and 2.20) was applied and obtained fastq-files were then processed in further analyses.

2.2.4.6   Preprocessing of sequencing data

Bioinformatic preprocessing of long RNA-Seq data was performed in collaboration with Karolina Worf (Institute of computational biology, Helmholtz Zentrum München). FastQC version 0.11.9 was used for quality control of raw reads. Then, the wrapper tool TrimGalore! version 0.6.5 was applied to trim Illumina adapters from paired-end reads using cutadapt (*182*) version 2.8 with a subsequent quality control of the trimmed reads using FastQC. Following the recommendation of the Ovation SoLo RNA-Seq System, the first 5 bp from the 5' end of the forward reads were additionally trimmed in the case of all zygote, 2-cell embryo

and blastocyst samples. Reads were mapped to the Ensembl mouse reference genome GRCm38 release 99 and its annotated transcripts (GTF file) using STAR (*183*) version 2.7.3a. The index generation was performed using the fasta and GTF file of GRCm38 and setting the parameters of the length of the genomic sequence around the annotated junction to 124 bp (Read length – 1 bp), the number of threads to 64 and the run mode to "genomeGenerate". Afterwards, following STAR parameters were applied for the mapping step: reading gzipped files, a maximum of 150 alignments per read, a maximum of 5 million collapsed junctions and output of a coordinate sorted BAM file of mapped paired-end reads for each sample. STAR also produces log output files including detailed information about the run, job progress and summary mapping statistics as well as a tab delimited file including high confidence collapsed splice junctions for every sample.

A summary of all preprocessing and QC steps was generated using MultiQC (*184*) version 1.8 for all samples of a stage. The MultiQC output includes general statistics, feature counts (e.g. reads lying on exons or promoter regions), STAR alignment scores, length of trimmed sequences, sequence counts (e.g. # duplicated and unique sequences), sequence quality given as a mean and per sequence quality score, per base sequence content, per sequence GC content, per base N content, sequence length distribution, sequence duplication levels, overrepresented sequences, adapter count and a FastQC status check, enabling a fast quality check.

To create the count matrices, a TxDb object was generated using the *makeTxDbFromGFF()* function of the GenomicFeatures (*185*) package version 1.34.8 in R version 3.6 and the GTF file including all annotated transcripts of the GRCm38 mus musculus genome. For the count of reads, a list of exons grouped by genes is required, which was created with the *exonsBy()* function of GenomicFeatures. Finally, the count matrix was generated using the *summarizeOverlaps()* function of the GenomicAlignments (*185*) package version 1.18.1 in R 3.6 with following parameters: paired-end reads, fragments allowed and a not empty intersection mode. Only for zygotes, 2-cell embryos and blastocysts the counts were calculated strand-specific. Per stage, a count matrix including counts for all samples (columns) in all GRCm38 annotated transcripts (rows) was calculated and stored in an RData file for further analysis.

PCA plots were created using batch corrected read counts in order to identify further batch effects and overall group differences between HFD and LFD offspring.

Bioinformatic preprocessing of small RNA-Seq data was performed in collaboration with Marc Horlacher (Institute of computational biology, Helmholtz Zentrum München) using an in-house smRNA-Seq pipeline by Xavier Pastor which is based on the Nextflow smrnaseq

pipeline (*186*). First, quality control of raw reads of all samples was performed via FastQC version 0.11.7, which was followed by adapter trimming via TrimGalore! version 0.4.5. Poly-A tails, which can be present in pri-miRNA were trimmed as well. Reads with a length < 15 after trimming were discarded and post-trimming quality control was performed via FastQC. Next, reference transcripts for different small RNA families (hairpin miRNA, mature miRNA, snRNA, snoRNA, tRNA and piRNA) were obtained from RNAcentral (*187*) and a read alignment was performed via Bowtie version 1.2.2 (*188*) including the instruction to report only the single best alignment and discard all others. Reads are aligned sequentially for each RNA family, e.g. reads are first aligned to hairpin miRNAs and only remaining unmapped reads were then aligned to mature miRNAs in the next step. This is to prevent reads from being discarded due to multiple-alignment, as e.g. hairpin and mature miRNAs can have overlapping sequences. Of note, this approach can potentially introduce biases in terms of alignment order, which were not fully explored here. Resulting alignment BAM files were then sorted and indexed with SAMtools version 1.8 and raw read counts of transcripts were computed via SAMtools idxstats. Transcripts with low read counts were excluded from the analysis as well by removing all transcripts with a count of < 5 in 13 different samples (with 13 being the number of samples in the group with the lowest number of samples).

2.2.4.7   Statistical analysis of sequencing data

Statistical analysis of RNA-Seq data was performed in collaboration with Karolina Worf (long RNA-Seq) and Marc Horlacher (small RNA-Seq) from the Institute of computational biology at the Helmholtz Zentrum München.

Differential expression between HFD and LFD sample groups was obtained using the DESeq2 (*189*) package version 1.24.0 in R version 3.6 while using the count matrix and condition table including all covariates for each stage as input. In case of fetal liver samples of TS20, TS22 and TS23 as well as liver, SAT and WAT samples of 3 weeks old mice, differential expression analysis was performed once for all samples together and once only for male and only for female samples, resulting in three analysis steps per tissue. Of the 142,647 transcripts given in a count matrix, only those with a count threshold of > 20 in ≥ 50% of the samples of a diet were retained. Due to batches in several processing steps, the following covariates were included in the models in addition to the diet: library preparation dates for zygotes and 2-cell embryos, library preparation dates and IVF dates for blastocysts, RNA extraction dates and library amplification dates for all fetal liver stages as well as organ withdrawal dates and RNA integrity number (RIN) for all organs of 3 weeks old mice. In DESeq2, for each transcript a negative binomial generalized linear model (GLM) is fitted to get coefficients for each model variable.

Differential expression analysis of small RNAs of HFD and LFD samples was performed with DESeq2 version 1.24.0 and R version 3.6.1 with raw count matrices obtained from Bowtie alignments as input. To control for potential batch effects, (1) a factor variable of the RNA extraction date and (2) a factor variable of the sequencing batch as covariates were included into the model. Furthermore, in order to identify hidden batches in the count data, which may compromise the analysis svaseq was used (*190*). Two significant hidden batch variables were identified and subsequently included as covariates in the DESeq2 model.

2.2.4.8   Pathway analysis and target prediction

GeneOntology (GO) (*191*) term analysis of significantly (p < 0.01) regulated genes was performed using the GeneRanker tool from the Genomatix software (http://www.genomatix.de/). Biological processes with 10-8,000 total genes per GO term were included in the analysis and manually sorted regarding their biological function.

Target prediction analysis of significantly (p < 0.01) regulated miRNAs was performed using the target search tool of miRDB (http://www.mirdb.org/index.html) (*192*). Only target genes with a prediction score of ≥ 70 were included and compared to selected sets of significantly regulated genes.

3. RESULTS

3.1 Increased susceptibility to metabolic disorders in offspring of HFD-treated parents

Our previous studies on intergenerational epigenetic inheritance of DIO and T2D demonstrated that a challenge with HFD in the parental generation altered epigenomic signatures in the gametes of males and females (*D. Kaspar et al, unpublished*). Coinciding, an increased susceptibility to obesity and glucose intolerance in offspring of HFD-treated parents was observed (*162*). Inheritance via the germline was evident because IVF was used for fertilization and foster mothers were used during gestation and lactation. Therefore, those altered epigenetic signatures could be the cause for the altered metabolic phenotype in HFD offspring. Furthermore, parental HFD treatment resulted in a sex-specific metabolic phenotype in the offspring that was also parent-of-origin specific (*162*). In order to further investigate these findings and the responsible mechanisms, phenotype and transcriptome of the F1 generation was examined.

3.1.1 Phenotype of parental F0 generation

First, new cohorts of C57BL/6NTac mice were purchased at the age of 4-6 weeks. Until the age of 9 weeks, mice were acclimated to the new environment. Starting from the age of 9 weeks, male (mF0) and female (fF0) mice were randomly assigned to either HFD or LFD treatment for 6 weeks. Body weight was monitored throughout the experiment and metabolic health was assessed via ipGTT at the age of 15 weeks (Figure 3.1).
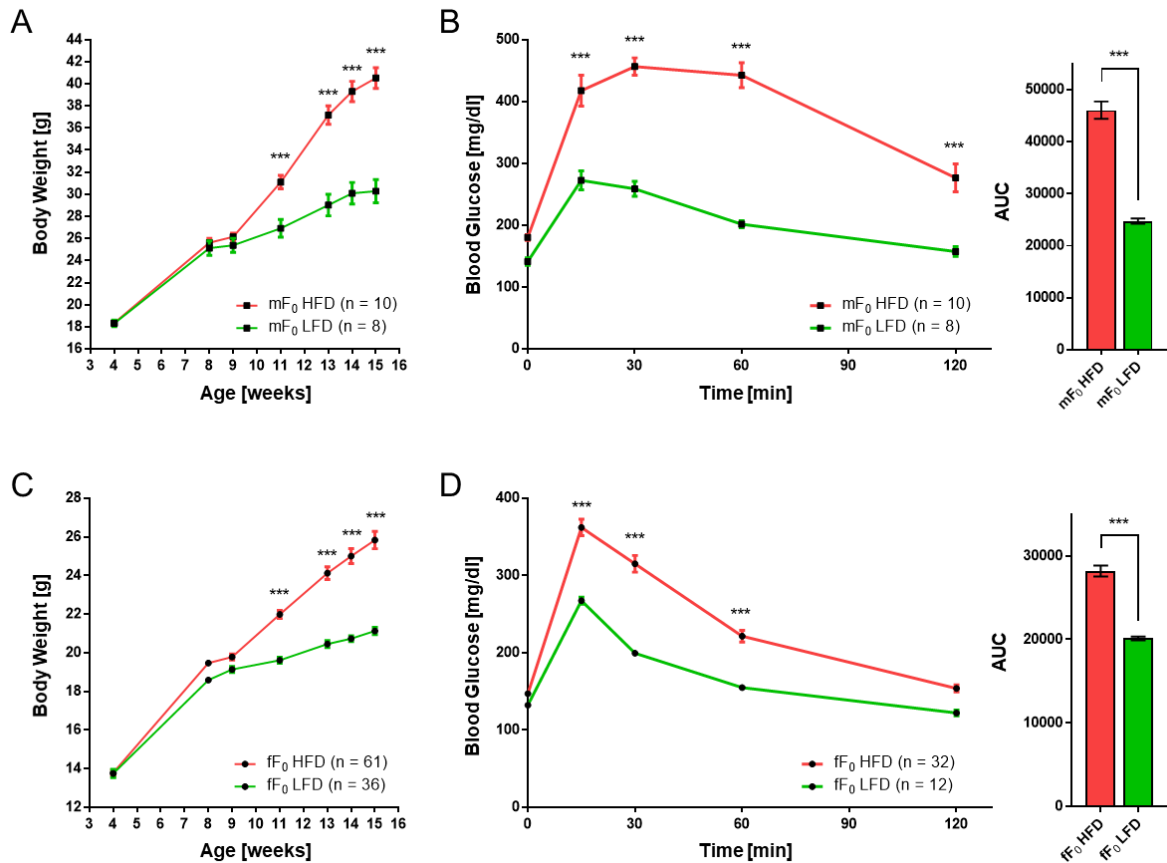
FIGURE 3.1 | BODY WEIGHT AND GLUCOSE TOLERANCE OF F0 GENERATION

Body weight trajectories of (A) male and (C) female parental generation under HFD (red) or LFD (green) treatment from 9-15 weeks of age and assessment of glucose tolerance through ipGTT at the age of 15 weeks of HFD- (red) versus LFD-treated (green) male (B) and female (D) mice. Measurement of blood glucose levels before and two hours after glucose injection (left panels) and corresponding calculated area under the curve (AUC; right panels) are displayed. Error bars display SEM values. Differences were considered statistically significant at $p < 0.05$ using a two-way ANOVA (Sidak's multiple comparison) or two-tailed Student's test (* < 0.05, ** < 0.01, *** < 0.001).

In both, males and females, HFD feeding leads to a highly significant increase in body weight (40.0 g mF0 HFD vs. 30.0 g mF0 LFD; 27.0 g fF0 HFD vs. 21.0 g fF0 LFD). Glucose tolerance is significantly impaired in HFD- compared to LFD-treated male and female mice as demonstrated by significantly higher blood glucose levels after glucose injection and still elevated levels after 2 hours, especially in males. Measurement of the area under the curve (AUC) confirms the significance of the difference (AUC 46,077 in mF0 HFD vs. AUC 24,752 in mF0 LFD; AUC 28,197 in fF0 HFD vs. AUC 20,124 in fF0 LFD).

3.1.2 *In vitro* fertilization in order to obtain the F1 generation

HFD mice showing this metabolic phenotype indicated by obesity and glucose intolerance as well as metabolically healthy LFD mice were sacrificed at the age of 15 weeks to harvest their gametes. Sperm and oocytes were used to conduct IVF and resulting 2-cell embryos were transferred into healthy foster mothers in order to exclude confounding factors during fertilization, gestation and lactation. Numbers of gamete donors, oocyte and 2-cell embryo yield, foster mothers and resulting pups are given in Table 3.1. If possible, resulting litters of the same experimental group were balanced between different foster mothers in order to achieve a litter size of approx. 7-10 pups per foster mother. Therefore, an increased litter size between birth and weaning is apparent.

TABLE 3.1 | IVF AND EMBRYO TRANSFER RESULTS

	group ID	# male donors	# female donors	oocyte yield /donor	# 2-cell embryos	# foster mothers (gestation)	# foster mothers (lactation)	Ø litter size (birth)	Ø litter size (weaning)	# mice
per IVF	**F1 (HxH)**	1	12	25.3	252	7	6	7.1	8.3	50
	F1 (HxH)	1	10	27.6	215	6	4	5.2	7.8	31
	F1 (HxH)	1	5	36.2	139	6	4	5.0	7.5	30
	F1 (HxH)	1	5	29.4	102	3	3	7.3	7.3	31
	F1 (LxL)	1	12	21.5	197	7	5	7.9	10.8	55
	F1 (LxL)	1	10	23.4	177	5	3	5.0	8.3	25
	F1 (LxL)	1	5	19.6	74	4	4	7.8	7.8	22
	F1 (LxL)	1	5	9.0	32	1	1	8.0	8.0	8
	F1 (LxL)	1	11	17.3	154	3	3	11.7	11.7	35
sum	**F1 (HxH)**	4	32	-	708	22	17	24.6	30.9	142
	F1 (LxL)	5	43	-	634	20	16	40.3	46.5	145
average	**F1 (HxH)**	1	8	29.6	177	5.5	4.3	6.2	7.7	35.5
	F1 (LxL)	1	9	18.2	127	4.0	3.2	8.1	9.3	29.0

In total, four independent IVFs were conducted in order to produce the group of HFD offspring and five independent IVFs in the case of LFD offspring. Each individual IVF was conducted with the sperm of one distinct F0 male and the combined oocytes of 5 to 12 F0 females. In sum, 4 male sperm donors plus 32 female oocyte donors were used to produce the HFD offspring (F1 (HxH)) and 5 male sperm donors plus 43 female oocyte donors were used to produce the LFD offspring (F1 (LxL)). Therefore, each individual from the F1 generation

can be allocated to a specific male F0 individual (father) but not to a specific female F0 individual (mother). An average oocyte yield per female donor is ranging from 25.3 to 36.2 in HFD-treated females and from 9.0 to 23.4 in LFD-treated females. Of note, only intact oocytes were counted. Therefore, the total number of 2-cell embryos per IVF ranged between 102 and 252 in F1 (HxH) with 708 in sum and between 32 and 197 in F1 (LxL) with 634 in sum. The majority of the intact 2-cell embryos was transferred into healthy foster mothers. In total, 22 foster mice were used for F1 (HxH) and 20 for F1 (LxL). After birth, small litters derived from the same father were combined if possible in order to achieve comparable litter sizes reducing the number of foster mice during lactation to 17 in the case of F1 (HxH) and 16 in the case of F1 (LxL). Average litter size is therefore increased between birth and weaning from 6.2 to 7.7 for F1 (HxH) and from 8.1 to 9.3 for F1 (LxL). In total, 142 pups originating from HFD-treated parents and 145 pups originating from LFD-treated parents were produced.

3.1.3   Phenotype of F1 generation

Resulting offspring was weaned at the age of 21 days onto normal chow and body weight was measured (Figure 3.2). Here, 7-8 pups per group and sex but from different litters were sacrificed for further experiments.

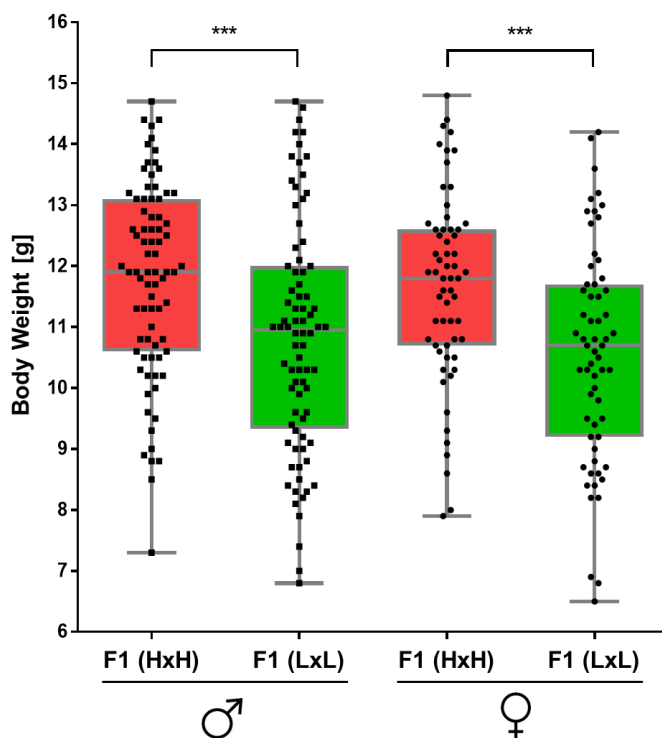**FIGURE 3.2 | BODY WEIGHT OF F1 GENERATION AT 3 WEEKS OF AGE**

Body weight of male (left) and female (right) F1 mice derived from HFD (red) or LFD (green) treated parents at the age of 3 weeks. Data represented as median with 25-75 percentile, Error bars display min-max values. Differences were considered statistically significant at $p < 0.05$ using a two-tailed Student's test (* < 0.05, ** < 0.01, *** < 0.001).

Body weight measurement at 3 weeks of age shows a similar widespread distribution in sons of HFD (7.3 g - 14.7 g) and LFD (6.8 g - 14.7 g) treated parents as well as in daughters of HFD (7.9 g - 14.8 g) and LFD (6.5 g - 14.2 g) treated parents. Nevertheless, in average, HFD offspring is significantly heavier than LFD offspring in males (14.2 g vs. 10.8 g) and in females (11.7 g vs. 10.6 g). Therefore, significant differences in body weight between HFD and LFD offspring are apparent already at the age of 3 weeks.

After weaning, remaining pups were kept on normal chow for 6 weeks followed by a HFD challenge for 6 weeks. Metabolic phenotyping was conducted throughout this time by measuring body weight on a weekly basis from 9 to 15 weeks of age (Figure 3.3) and assessing glucose tolerance via ipGTT at the age of 15 weeks (Figure 3.4).
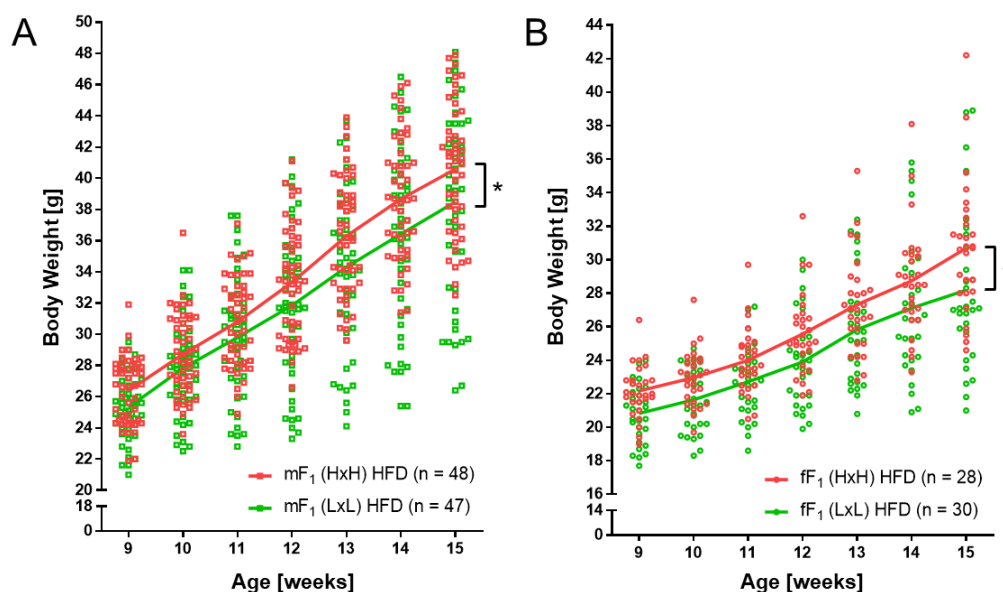
FIGURE 3.3 | BODY WEIGHT OF F1 GENERATION

Body weight trajectories of male (A) and female (B) F1 (HxH) (red) or F1 (LxL) (green) from 9-15 weeks of age. Error bars display SEM values. Differences were considered statistically significant at $p < 0.05$ using a two-way ANOVA (Sidak's multiple comparison) (* < 0.05, ** < 0.01, *** < 0.001).

During HFD challenge, in average all male and female mice increase their body weight although a high variance between the different individuals is apparent. Offspring of both HFD- and LFD-treated parents are able to reach severe overweight, especially individuals that start with higher body weight at the age of 9 weeks (approximately > 27 g in males and > 23 g in females), however this is neither a necessary nor a sufficient cause of developing overweight. Still, more individuals originating from LFD-treated parents increase their body weight only mildly. In average, offspring of HFD-treated parents gain slightly but significantly more weight compared to offspring of LFD-treated parents over the course of 6 weeks. In these cohorts, there was no difference between the sexes regarding the body weight development.

At the age of 15 weeks, male HFD offspring was heavier in average than LFD offspring (40.6 g vs. 38.5 g) and female HFD offspring was heavier in average than LFD offspring (30.7 g vs. 28.2 g).
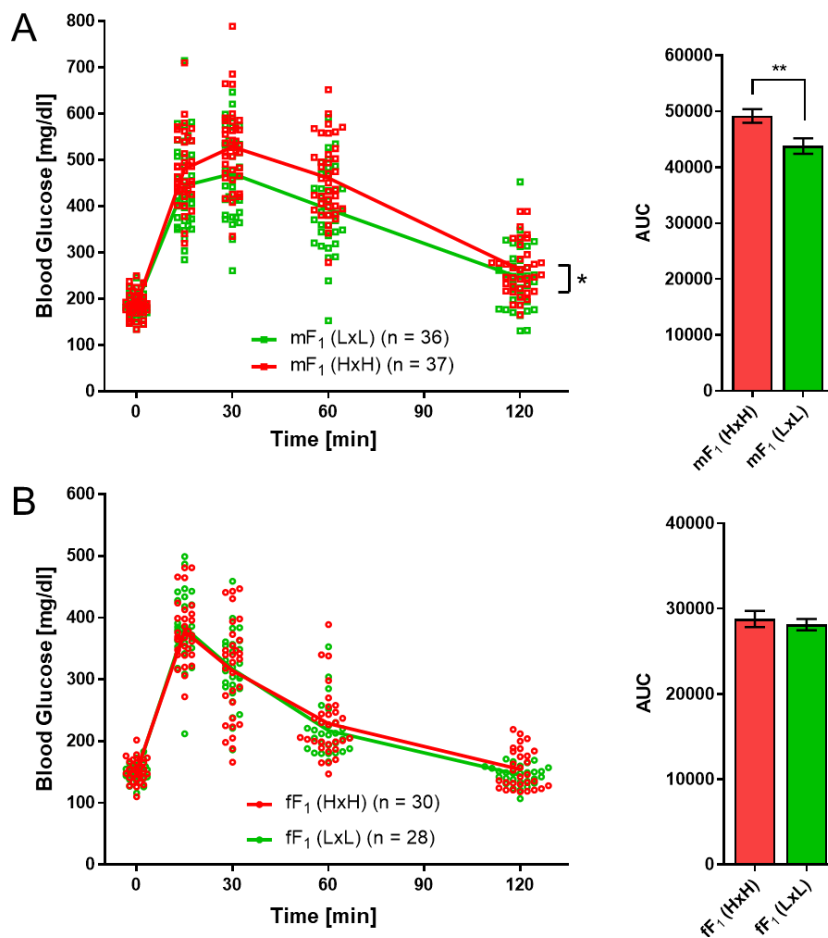
FIGURE 3.4 | GLUCOSE TOLERANCE OF F1 GENERATION

Assessment of glucose tolerance through ipGTT at the age of 15 weeks of F1 (HxH) (red) versus F1 (LxL) (green) male (A) and female (B) mice. Measurement of blood glucose levels before and two hours after glucose injection (left panels) and corresponding calculated area under the curve (AUC; right panels) are displayed. Error bars display SEM values. Differences were considered statistically significant at $p < 0.05$ using a two-way ANOVA (Sidak's multiple comparison) or two-tailed Student's test (* < 0.05, ** < 0.01, *** < 0.001).

Individuals of HFD and LFD offspring overlap regarding their blood glucose levels during ipGTT but in general, male LFD offspring show lower glucose levels. Therefore, ipGTT at the age of 15 weeks revealed a slightly but significantly decreased glucose tolerance in male HFD offspring compared to LFD offspring (AUC 49,173 vs. AUC 43,787). Females on the other hand, show no difference in glucose tolerance between offspring groups with very similar blood glucose levels of the analyzed individuals (AUC 28,791 vs. AUC 28,122). Therefore, the sex-specific metabolic phenotype that was found in previous studies (*162*) could be confirmed in these cohorts.

3.2 Parental HFD-induced transcriptomic alterations in the F1 generation at 3 weeks of age

Metabolic changes were evident in offspring of HFD-treated parents compared to offspring of LFD-treated parents in adulthood as well as at the age of 3 weeks. Based on these changes, transcriptome analysis of relevant organs at the age of 3 weeks should provide insights into potential metabolic mechanisms. In this project, the concept was to first screen several potentially interesting tissues via microarray for basic transcriptional differences between HFD and LFD offspring at the age of 3 weeks. Next, transcriptomic differences and regulatory pathways should be further explored in specific tissues by RNA sequencing.

3.2.1 Screening of relevant organs in 3 weeks old F1 generation

Therefore, at day 21 after birth, eight mice of each group were randomly selected from different litters, sacrificed and organs that are important for metabolic processes were collected for transcriptome analysis. Collected organs included liver, muscle, brown adipose tissue (BAT), visceral white (WAT) and subcutaneous white adipose tissue (SAT) (Figure 3.5).
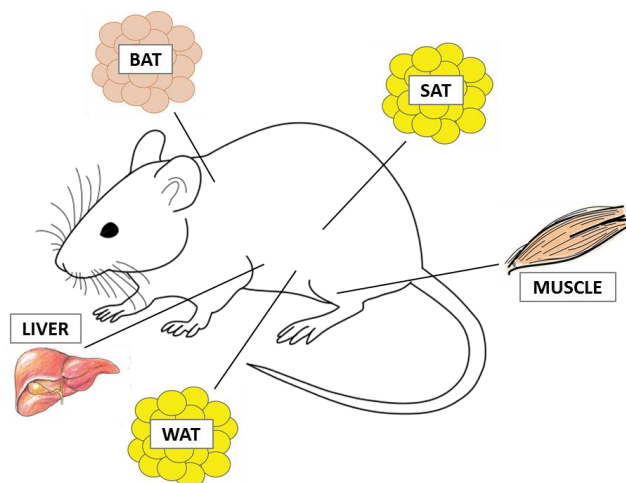
FIGURE 3.5 | SELECTED TISSUES FOR TRANSCRIPTOME SCREENING

Different tissues that play a role in glucose homeostasis were collected at the age of 3 weeks from male and female F1 (HxH) and F1 (LxL) mice. These tissues are liver, muscle, brown adipose tissue (BAT), visceral (WAT) and subcutaneous adipose tissue (SAT).

Total RNA of these tissues was extracted and used for microarrays including a spiked-in polyA control and a negative control. The positive control and quality control of hybridized cDNA fragments (PolyA Control, Log Expression Signal, Relative Log Probe Cell Intensity, Spearman Rank Correlation) confirmed overall good quality of microarray data. Samples that did not pass quality control were considered outliers and removed from the analysis. After

normalization and background correction (average of linear expression values >16 in at least one group), principle component analysis (PCA) of all analyzed probe sets was performed and the first two principle components are plotted for each organ (Figure 3.6). PCA can indicate overall differences between samples and reveal strong batch effects resulting for example from the amplification or hybridization procedure but also from biological differences between different cohorts or organ dissection dates.
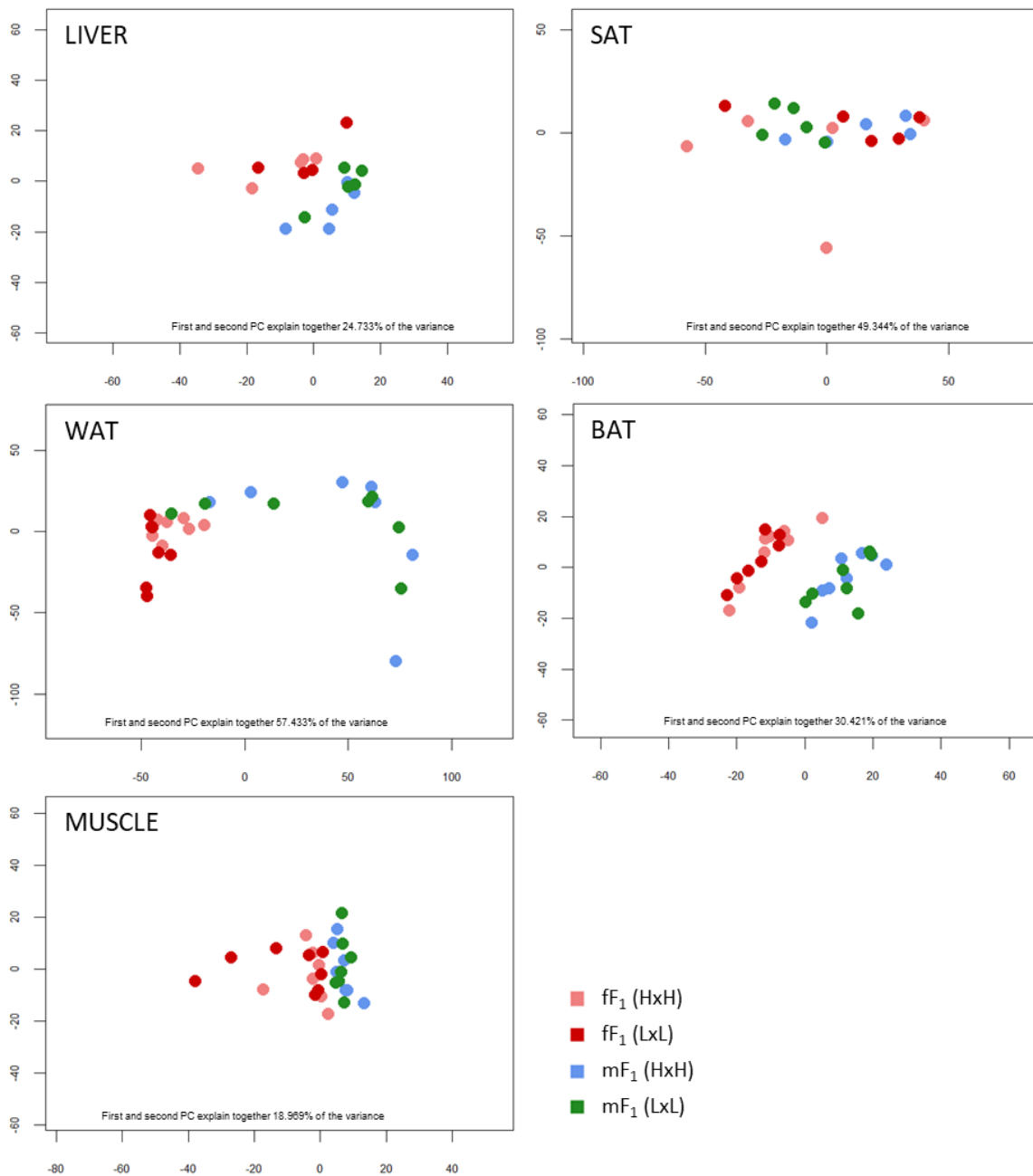
FIGURE 3.6 | PCA OF ORGANS OF 3 WEEKS OLD OFFSPRING IN MICROARRAYS

Principle component analysis of all female (light red) and male (blue) F1 (HxH) as well as female (dark red) and male (green) F1 (LxL) samples considering expression values of all analyzed probe sets.

PCA shows a clustering of the samples according to sex except for SAT, but not according to parental diet. This indicates that rather the sex than the parental diet accounts for the main differences in expression profiles of these samples. Therefore, further analyses were conducted separately for males and females.

Differential expression analysis (DEA) between offspring of HFD- and LFD-treated parents revealed up to a few hundred differentially expressed genes depending on the analyzed organ and the sex, as shown in Figure 3.7.
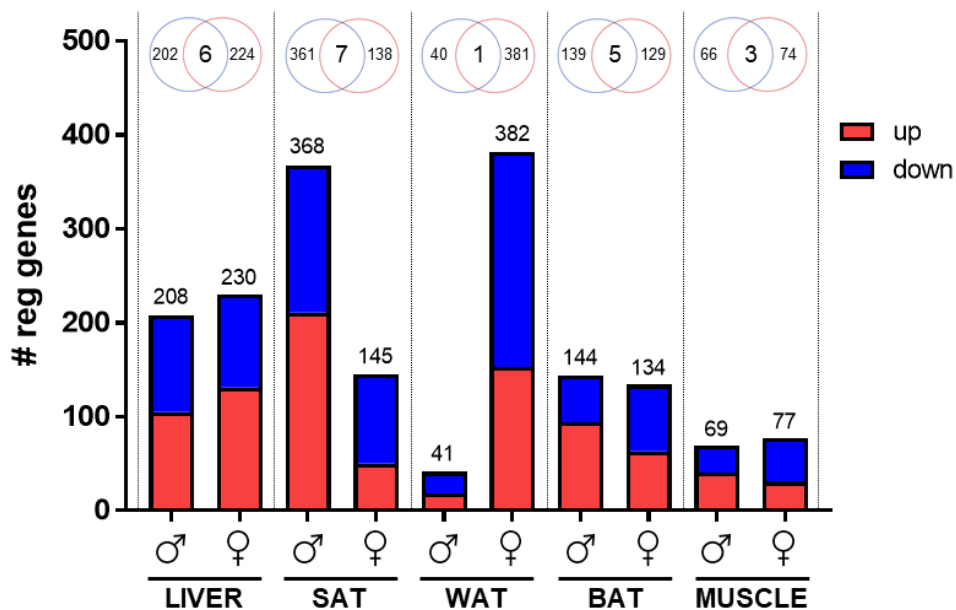
FIGURE 3.7 | NUMBER OF UPREGULATED AND DOWNREGULATED GENES IN ORGANS OF 3 WEEKS OLD OFFSPRING IN MICROARRAYS

Number of significantly ($p < 0.01$) upregulated (red) and downregulated (blue) genes with a linear fold change (FC) > 1.3 between F1 (HxH) and F1 (LxL) male and female organs at 3 weeks of age. Venn diagrams (on top) display the overlap in differentially regulated genes between males and females.

Taking all genes into account that are significantly regulated with $p < 0.01$ and show a linear fold change (FC) > 1.3, liver, SAT and WAT have the highest number of regulated genes (432 in LIVER, 506 in SAT, 422 in WAT) followed by BAT and muscle (273 in BAT, 143 in MUSCLE) with females and males combined. The overlap of regulated genes in males and females, however, is very small with 1-7 genes. Interestingly, the difference in the number of regulated genes between males and females in the white adipose tissues is 2.5 fold higher in males than in females in SAT and 9.3 fold higher in females than in males in WAT.

Overall, differential gene expression analysis reveals significantly regulated genes between F1 (HxH) and F1 (LxL) mice in all organs but varying between different organs and between males and females.

In order to visualize the upregulation and downregulation of these differentially expressed genes within the different groups, they are displayed in heat maps, separately for organs and sexes (Figure 3.8).
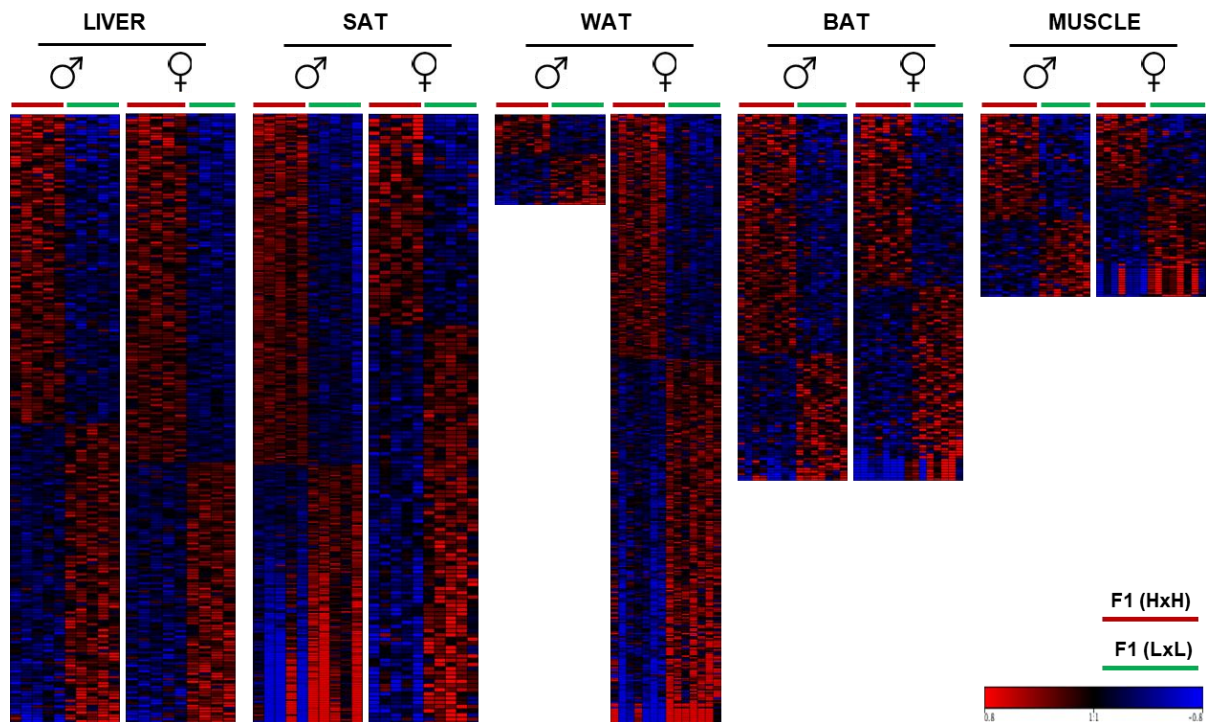
FIGURE 3.8 | HEAT MAPS OF ORGANS OF 3 WEEKS OLD F1 GENERATION IN MICROARRAYS

Heat maps of upregulated (red) and downregulated (blue) genes (p < 0.01; FC > 1.3) between F1 (HxH) and F1 (LxL) male and female organs at 3 weeks of age.

Plotting expression values of all significantly regulated genes for all samples allows a visual comparison between the different groups. Samples were arranged within their respective group without previous clustering. Nevertheless, a distinct color pattern (red vs. blue) is visible showing similar gene expression within each experimental group and gene regulation in the opposite direction between the groups (HFD vs. LFD). This is true for all tissues both in males and females with the exception of a group of strongly downregulated genes in male SAT as well as female WAT, BAT and MUSCLE that are not consistently regulated within the groups. In conclusion, in heat maps displaying expression values of regulated genes with males and females plotted separately, all analyzed tissues can be clustered clearly according to the parental diet.

Next, pathway analysis utilizing GeneOntology (GO) terms was performed with significantly regulated genes (p < 0.05; FC > 1.3), in order to uncover the biological functions and processes these genes are involved in. A selection of interesting and significant terms for each tissue is provided in Figure 3.9.
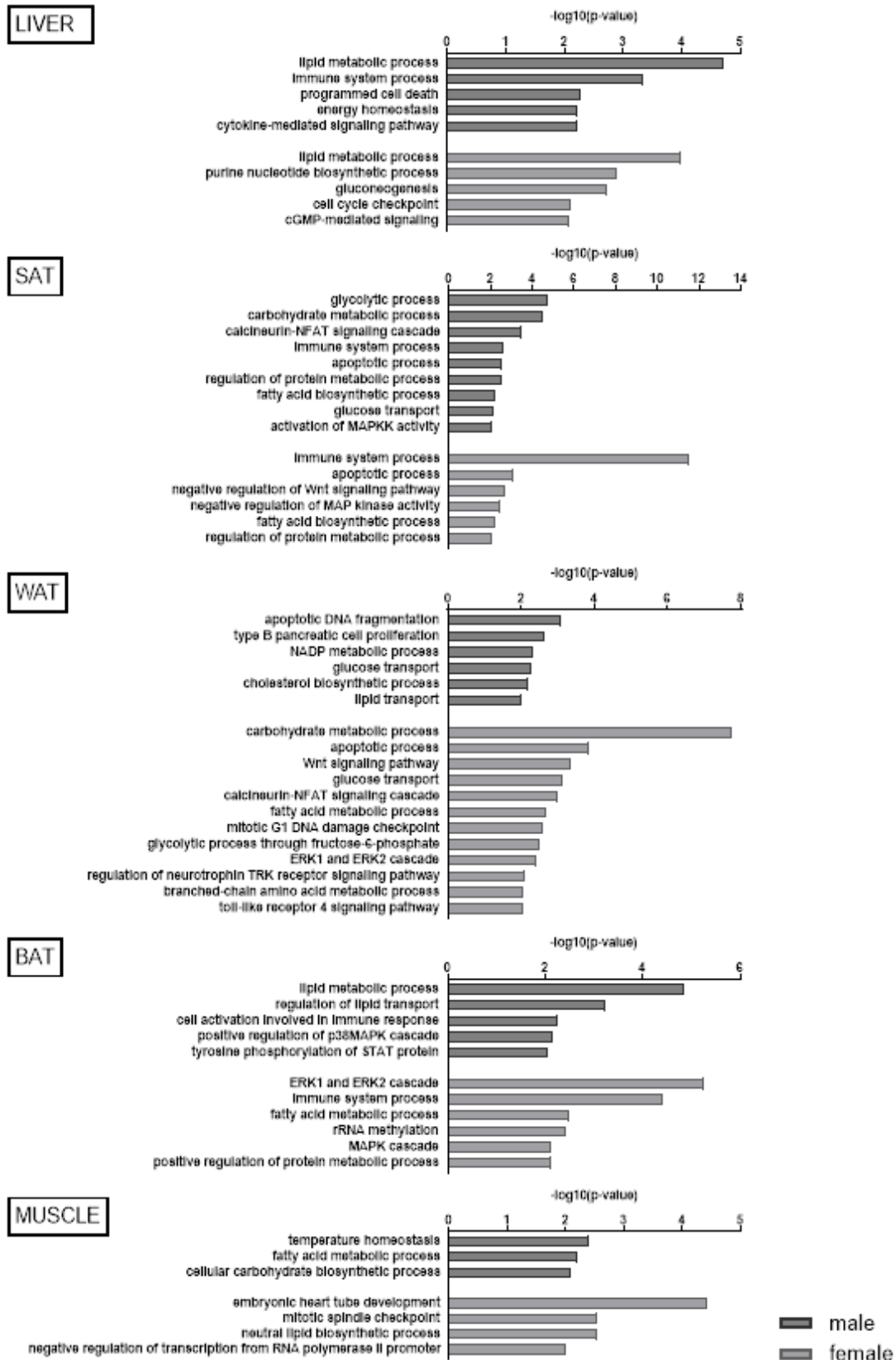
FIGURE 3.9 | AFFECTED GENEONTOLOGY TERMS IN ORGANS OF 3 WEEKS OLD OFFSPRING

Selection of biological processes that are affected by regulated genes (p < 0.05; FC > 1.3). Analysis was performed by using the GeneRanker tool from Genomatix. Displayed are the -log10(p-value) values for each GO term in dark gray for males and light gray for females.

Affected biological processes are especially metabolism related processes such as lipid and fatty acid metabolism, carbohydrate and protein metabolism as well as gluconeogenesis, glycolysis and energy homeostasis. Furthermore, immune response is affected in some tissues, but very significantly in female SAT. Some regulated signaling pathways such as MAPK (ERK) cascade and Wnt signaling in all adipose tissues (WAT, SAT, BAT) might be of interest. Further affected processes are related to the cell cycle and apoptosis.

Indeed, this first screening showed transcriptomic differences between offspring depending on the parental diet in several organs at the age of 3 weeks. Mostly affected are liver, visceral and subcutaneous adipose tissue with strong sex differences especially in the adipose tissues.

3.2.2   RNA Sequencing in affected organs of 3 weeks old offspring

In order to analyze these organ samples from 3 weeks old F1 mice in depth and to also include transcripts that are not pre-bound to the microarray as probe sets, we conducted sequencing of total RNA from the same tissue samples plus from some additional samples in the case of liver and SAT.

Quality of reads after trimming of adapter sequences was adequate and comparable between the different samples. For further analysis, only transcripts with a read count >20 in at least half of the samples in at least one group were incorporated. PCA from all sequencing reads was performed to show overall differences and similarities between the analyzed tissues and within the tissues between offspring of HFD- and LFD-treated parents (Figure 3.10). For Figure 3.10 A, normalized raw counts were used to calculated and plot the PCA, whereas for Figure 3.10 B-D, batch corrected normalized counts were used. The organ withdrawal date and the RIN value were included as covariates in all these PCAs and further differential expression analysis. Additionally, the sex was included as a covariate for the combined analysis of males and females.
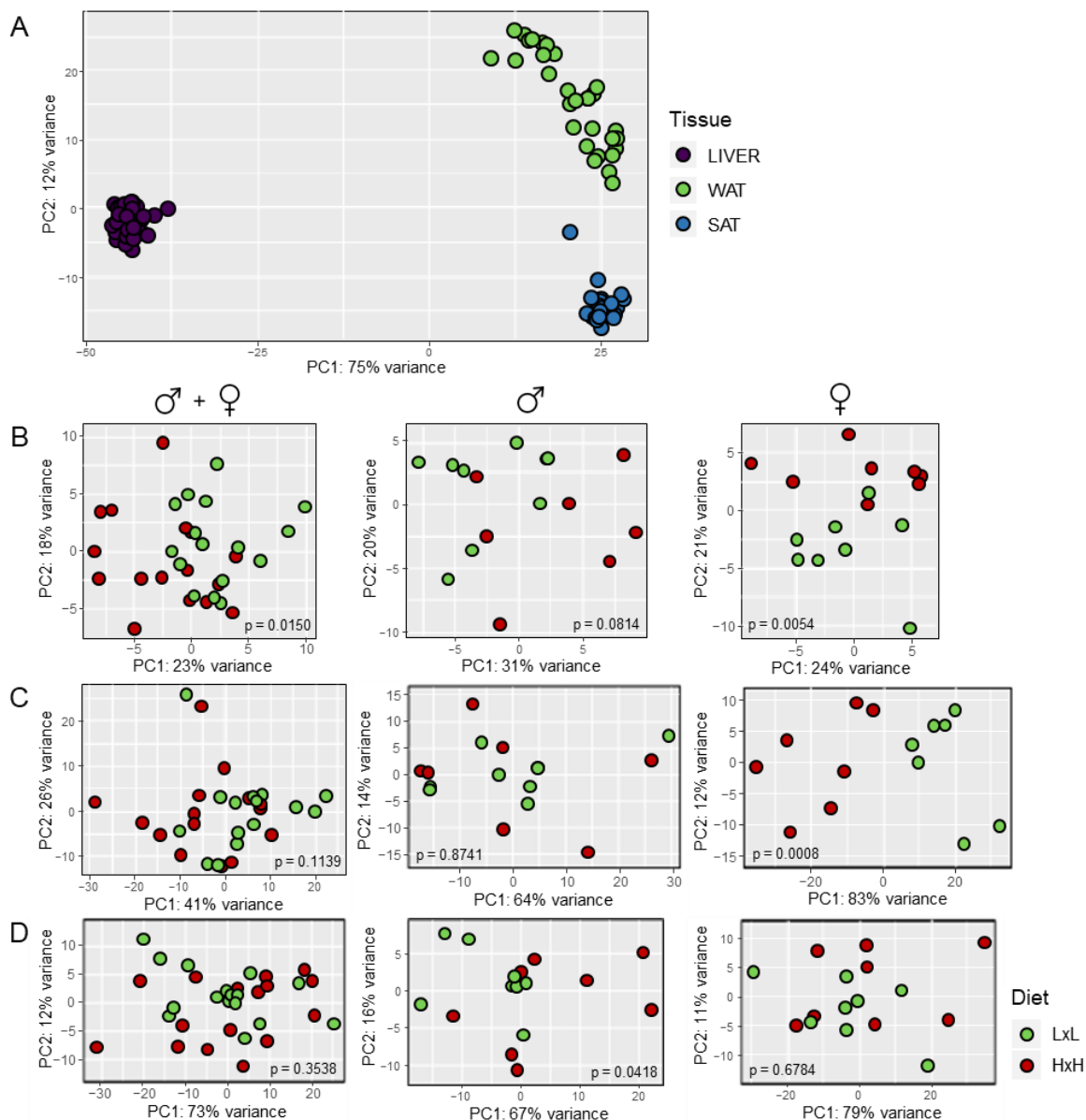
FIGURE 3.10 | PCA PLOTS OF LONG TRANSCRIPTS IN ORGANS OF 3 WEEKS OLD OFFSPRING

PCA of all samples of 3 weeks old F1 mice considering counts of all analyzed sequencing reads. A shows the comparison of liver (purple), WAT (green) and SAT (blue). B, C and D show the PCAs of liver (B), WAT (C) and SAT (D) samples separately for mixed analysis of males and females together (left), analysis of only males (middle) and analysis of only females (right). For B, C, D, the corresponding parental diet (LFD in green vs. HFD in red) is indicated. Plots always display the first principle component (PC) on the x-axis and the second PC on the y-axis. An empirical p-value is calculated and depicted in each PCA plot.

As expected, each of the analyzed tissues cluster together and apart from the other tissues indicating major overall transcriptomic differences between the different tissues. Also, the adipose tissues (WAT and SAT) are more similar regarding their expressed genes compared to liver. By plotting each tissue (liver, WAT and SAT) individually, differences in the

transcriptomes according to the parental diet can be visualized. Additionally, by using a PCA cluster analysis an empirical p-value can be calculated that provides a quantitative measure of the difference between the analyzed groups. In liver (Figure 3.10 B), samples - although overlapping - clearly cluster into two separate groups that are characterized by the parental diet. This is true for the combined analysis of males and females (p = 0.0150) but also for the separate analyses of only males (p = 0.0814) and only females (p = 0.0054). In WAT (Figure 3.10 C), a clear clustering according to the parental diet is displayed in females (p = 0.0008) but not in males (p = 0.8741) or the combined analysis of males and females (p = 0.1139). Also in SAT (Figure 3.10 D), only males (p = 0.0418) cluster according to the parental diet but not females (p = 0.6784) or males and females together (p = 0.3538).

Overall, it is remarkable that by including all sequencing reads at least in some cases such as female WAT the samples cluster according to the parental diet indicating that the parental diet strongly influences the transcriptome in these tissues.

As no other batch effects are observable in these PCA plots, these normalized and batch-corrected sequencing counts were used for differential expression analysis.

3.2.3   Analysis of differentially expressed transcripts in 3 weeks old HFD versus LFD offspring

In order to find the transcripts and genes that are differentially expressed between HFD and LFD offspring, differential expression analysis was performed using DESeq2, which resulted in a number of regulated transcripts for all analyzed tissues. Tissues and sexes were analyzed separately by always comparing offspring of different parental diets (HFD vs. LFD). Number of upregulated and downregulated transcripts with p < 0.01 per organ and sex as well as the number of these transcripts overlapping between sexes and organs are shown in Figure 3.11.
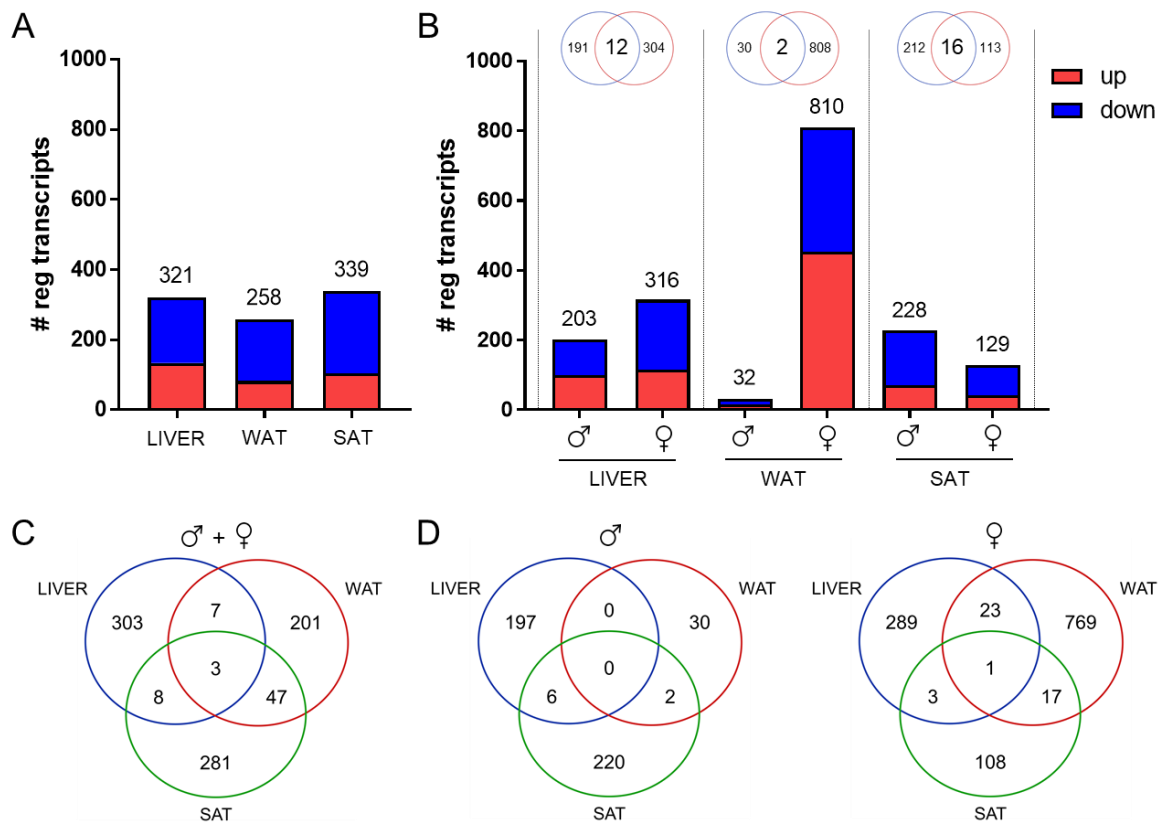
FIGURE 3.11 | NUMBER AND OVERLAP OF REGULATED LONG TRANSCRIPTS IN ORGANS OF 3 WEEKS OLD OFFSPRING

Number of significantly (p < 0.01) upregulated (red) and downregulated (blue) transcripts between F1 (HxH) and F1 (LxL) organs at 3 weeks of age in the mixed analysis (A) and separate analysis for males and females (B) are displayed. In addition, Venn diagrams above the bars in B show overlap of differentially regulated transcripts between males and females. C and D show Venn diagrams displaying significantly regulated transcripts (p < 0.01) between F1 (HxH) and F1 (LxL) overlapping between the tissues in the (C) combined analysis of males and females or the (D) separate analysis of only males (left panel) or only females (right panel). Statistical analysis was performed either of males and females together (A, C), only males or only females (B, D).

Differential gene expression analysis reveals a number of significantly regulated transcripts between F1 (HxH) and F1 (LxL) mice in all organs. Taking all transcripts into account that are significantly regulated with p < 0.01, statistical analysis of males and females together (Figure 3.11 A) by correcting for sex differences yields 321 (liver), 258 (WAT) and 339 (SAT) differentially regulated transcripts. Interestingly, separate statistical analysis for males and females (Figure 3.11 B) shows an enormous sex difference in WAT with 25 times more significantly regulated transcripts in females than in males that is somehow blunted in the combined analysis of males and females. Additionally, the overlap of regulated transcripts between males and females is very low in all three tissues. A detailed overview of regulated

transcripts that overlap between males and females in liver, WAT and SAT is given in Table 3.2.

TABLE 3.2 | OVERLAPPING REGULATED TRANSCRIPTS IN 3 WEEKS OLD MALES AND FEMALES

	Gene symbol	Transcript ID	Males FC	Females FC
LIVER				
	Hsd3b5	ENSMUST00000044094	4.45	2.36
	Dpys	ENSMUST00000150196	1.55	1.43
	C730036E19Rik	ENSMUST00000188305	1.50	1.57
	Acadl	ENSMUST00000027153	-1.16	-1.39
	Uroc1	ENSMUST00000046128	-1.23	-1.57
	Igsf11	ENSMUST00000023478	-1.30	-1.39
	Ddah1	ENSMUST00000029845	-1.35	-1.50
	Ppl	ENSMUST00000035672	-1.42	-1.75
	Pctp	ENSMUST00000020864	-1.45	-1.72
	Sult2a2	ENSMUST00000086148	-1.60	-1.34
	Sult2a6	ENSMUST00000076576	-1.62	-1.68
	Ehhadh	ENSMUST00000023559	-1.66	-1.58
WAT				
	Gas6	ENSMUST00000033828	1.31	1.93
	Olfr542-ps1	ENSMUST00000218525	-2.00	-3.82
SAT				
	Lep	ENSMUST00000069789	1.75	1.41
	Npr3	ENSMUST00000066529	1.66	1.42
	Apmap	ENSMUST00000046399	-1.37	-1.30
	Car5b	ENSMUST00000033739	-1.41	-1.37
	Mup18	ENSMUST00000098040	-1.54	-2.14
	Tst	ENSMUST00000058659	-1.55	-1.51
	Adcyap1r1	ENSMUST00000070756	-1.60	-1.47
	mt-Tp	ENSMUST00000082423	-1.60	-1.49
	Ppfia2	ENSMUST00000217854	-1.64	-1.82
	Gm5182	ENSMUST00000217708	-1.70	-1.52
	Gm28424	ENSMUST00000187393	-1.76	-1.67
	Mup11	ENSMUST00000098046	-1.79	-2.20
	Mup13	ENSMUST00000098042	-1.87	-1.99
	Mup14	ENSMUST00000125461	-1.94	-2.09
	Fasn	ENSMUST00000055655	-2.05	-2.02
	Gm29163	ENSMUST00000188029	-2.16	-2.58

In liver, 12 transcripts of 203 transcripts in males or 316 transcripts in females are overlapping, all of which are regulated in the same direction. In WAT, 2 transcripts of 32 transcripts in males or 810 transcripts in females are overlapping, both of which are regulated in the same direction. In SAT, 16 transcripts of 228 transcripts in males or 129 transcripts in females are overlapping, all of which are regulated in the same direction.

Comparison of transcriptome differences between liver, WAT and SAT in the combined analysis of males and females (Figure 3.11 C) as well as the separate analysis of males and females (Figure 3.11 D) shows only very little overlap.

In the combined analysis of males and females 3 transcripts are regulated in all three tissues. 7 transcripts are regulated in liver and WAT and 8 transcripts in liver and SAT, most of them in the same direction. 47 transcripts are regulated in the same direction in WAT and SAT. However, since transcripts that are significantly regulated in the combined analysis of males and females fail to lead to a clear clustering according to parental diet (see Figure 3.12), they are not listed specifically.

A detailed overview of regulated transcripts that overlap between liver, WAT and SAT (see Figure 3.11 C, D) for males and females separately is given in Table 3.3 and Table 3.4, respectively.

TABLE 3.3 | OVERLAPPING REGULATED TRANSCRIPTS IN MALE LIVER, WAT AND SAT

Gene symbol	Transcript ID	Liver FC	WAT FC	SAT FC
Gm7329	ENSMUST00000185915	-1.73	ns	-1.80
Zbtb16	ENSMUST00000093852	-1.63	ns	-1.54
Tob1	ENSMUST00000041589	-1.30	ns	-1.35
Rora	ENSMUST00000034766	-1.21	ns	-1.35
Snx12	ENSMUST00000120389	-1.19	ns	-1.26
Acsl5	ENSMUST00000043150	-1.26	ns	1.18
Lep	ENSMUST00000069789	ns	2.90	1.75
Npr3	ENSMUST00000066529	ns	2.45	1.66

In males, no transcript is significantly regulated in all three tissues. 5 transcripts are downregulated in liver and SAT encoding 4 protein-coding genes and 1 pseudogene, whereas 1 transcript is downregulated in liver but upregulated in SAT. 2 transcripts encoding protein coding genes *Lep* and *Npr3* are upregulated in the adipose tissues WAT and SAT.

TABLE 3.4 | OVERLAPPING REGULATED TRANSCRIPTS IN FEMALE LIVER, WAT AND SAT

Gene symbol	Transcript ID	Liver FC	WAT FC	SAT FC
mt-Tp	ENSMUST00000082423	-1.63	-2.50	-1.49
Gm47503	ENSMUST00000215636	1.81	2.24	ns
Srsf3	ENSMUST00000233885	1.50	2.04	ns
AU022252	ENSMUST00000141112	-1.29	-1.65	ns
Gm28439	ENSMUST00000187714	-1.46	-2.41	ns
mt-Nd4	ENSMUST00000082414	-1.46	-2.40	ns
mt-Nd5	ENSMUST00000082418	-1.46	-2.50	ns
mt-Nd1	ENSMUST00000082392	-1.50	-2.56	ns
mt-Nd6	ENSMUST00000082419	-1.50	-2.64	ns
mt-Nd2	ENSMUST00000082396	-1.60	-2.94	ns
Lgalsl	ENSMUST00000047028	-1.57	-2.03	ns

Gm13339	ENSMUST00000120651	-1.73	-2.56	ns
Eef1a1	ENSMUST00000042235	-1.24	1.52	ns
Rps3a1	ENSMUST00000029722	-1.21	1.74	ns
Rps6-ps4	ENSMUST00000118499	-1.22	1.73	ns
Rps6	ENSMUST00000102814	-1.26	1.72	ns
Tpt1-ps3	ENSMUST00000121046	-1.28	1.58	ns
Rpl10-ps3	ENSMUST00000076364	-1.36	1.64	ns
Rpl10-ps6	ENSMUST00000121321	-1.39	1.66	ns
Rpl39-ps	ENSMUST00000146505	-1.45	1.80	ns
Akr1c13	ENSMUST00000021634	-1.39	3.07	ns
Mesd	ENSMUST00000094215	-1.39	1.57	ns
Gm3379	ENSMUST00000222259	-1.44	1.64	ns
Gm9843	ENSMUST00000052867	-1.78	2.72	ns
Ppa1	ENSMUST00000020286	-1.33	ns	-1.28
Acadsb	ENSMUST00000015829	-1.52	ns	-1.30
Pkp2	ENSMUST00000039408	-1.30	ns	1.48
Esr1	ENSMUST00000105588	ns	6.34	1.80
Gm42031	ENSMUST00000209823	ns	6.30	1.32
Gm4316	ENSMUST00000212411	ns	2.54	1.17
Chsy1	ENSMUST00000036372	ns	2.16	1.20
Gas6	ENSMUST00000033828	ns	1.93	1.44
Tst	ENSMUST00000058659	ns	-2.49	-1.51
Thrsp	ENSMUST00000043077	ns	-2.76	-1.48
Adcyap1r1	ENSMUST00000070756	ns	-2.77	-1.47
Arl4a	ENSMUST00000136441	ns	-2.77	-1.36
Apmap	ENSMUST00000046399	ns	-2.80	-1.30
Sik2	ENSMUST00000177203	ns	-2.90	-1.40
Chpt1	ENSMUST00000117579	ns	-3.14	-1.51
Cdo1	ENSMUST00000234064	ns	-3.62	-1.49
Slc43a1	ENSMUST00000145004	ns	-3.63	-1.46
Retsat	ENSMUST00000070597	ns	-3.67	-1.45
Gm35665	ENSMUST00000206742	ns	-5.09	-1.70
Cst7	ENSMUST00000089200	ns	-5.77	-1.46

In females, 1 transcript encoding the mitochondrial encoded tRNA proline (*mt-Tp*) is downregulated in all three tissues. 2 transcripts are upregulated and 9 transcripts downregulated in both liver and WAT, whereas 12 transcripts are regulated in different directions. These transcripts include several mitochondrial NADH dehydrogenases and ribosomal proteins. 2 transcripts are downregulated in both liver and SAT, whereas 1 transcript is regulated in different directions. In the adipose tissues WAT and SAT, 5 transcripts are upregulated and 12 transcripts are downregulated in both including *Tst*, *Sik2*, *Cdo1*, and *Retsat*.

In order to visualize the difference between HFD and LFD offspring, these sets of significantly regulated transcripts are displayed in heat maps with hierarchical clustering of the transcripts in rows and the analyzed samples in columns (Figure 3.12).
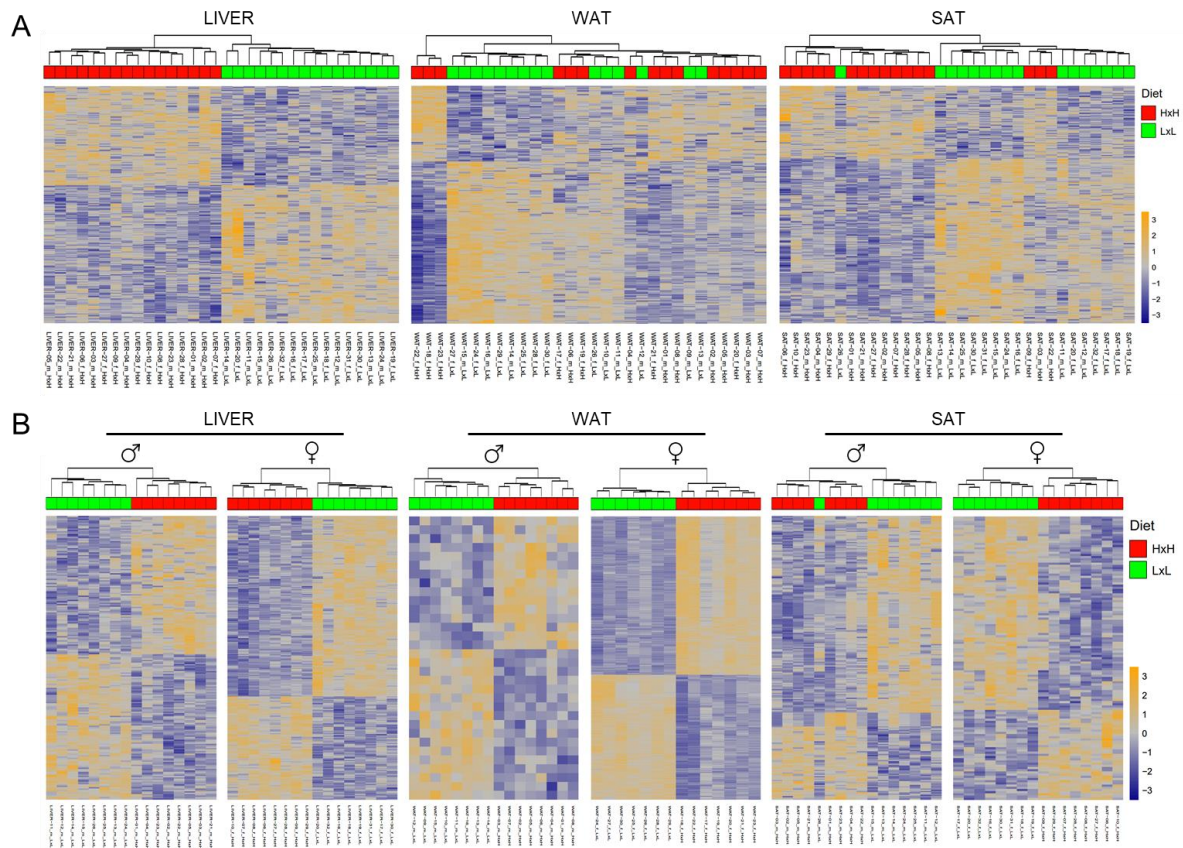
FIGURE 3.12 | HEAT MAPS OF REGULATED LONG TRANSCRIPTS IN ORGANS OF 3 WEEKS OLD OFFSPRING

Heat maps of upregulated (yellow) and downregulated (blue) transcripts (p < 0.01) between F1 (HxH) (red) and F1 (LxL) (green) male and female tissue samples at 3 weeks of age. A displays the differentially expressed set of transcripts in the combined analysis of males and females. B displays differentially expressed sets of transcripts for the separate analysis of males and females.

By hierarchical clustering according to differentially expressed transcripts, only liver samples (males and females together) can be clearly separated in two groups indicating parental HFD and parental LFD treatment. WAT and SAT samples can also be separated in the two groups, but the classification by hierarchical clustering is not completely unambiguous (Figure 3.12 A). In the separate analysis of males and females, samples cluster distinctly according to the parental diet in all analyzed tissues (Figure 3.12 B). Therefore, employing these sets of significantly regulated transcripts enables the distinction between offspring derived from HFD- and offspring of LFD-treated parents indicating specific transcriptomic differences already at the age of 3 weeks.

3.2.4 Analysis of regulated pathways in affected organs

In order to elucidate the pathways and biological processes these regulated transcripts are involved in, their associated genes were analyzed in a gene set enrichment analysis. Therefore, GO term analysis was performed with significantly regulated genes (p < 0.01). A selection of interesting and significantly affected terms in males and females is provided in Figure 3.13 and Figure 3.14, respectively.

FIGURE 3.13 | AFFECTED GENEONTOLOGY TERMS IN ORGANS OF 3 WEEKS OLD F1 MALES

Selection of biological processes that are affected by significantly regulated genes (p < 0.01) in 3 weeks old males. Analysis performed by using the GeneRanker tool from Genomatix. Displayed are the -log10(p-value) values for each GO term.

In 3 weeks old males, genes whose expression is altered by parental HFD are predominantly involved in several metabolic processes and signaling pathways. In liver, many processes involved in the lipid metabolism are over-represented, but also glucose metabolism and ERK1 and ERK2 cascade. In WAT, glucose metabolism and several different signaling pathways are affected by these regulated genes. In SAT, lipid, protein and glucose metabolism but also gene expression and the immune response are affected.
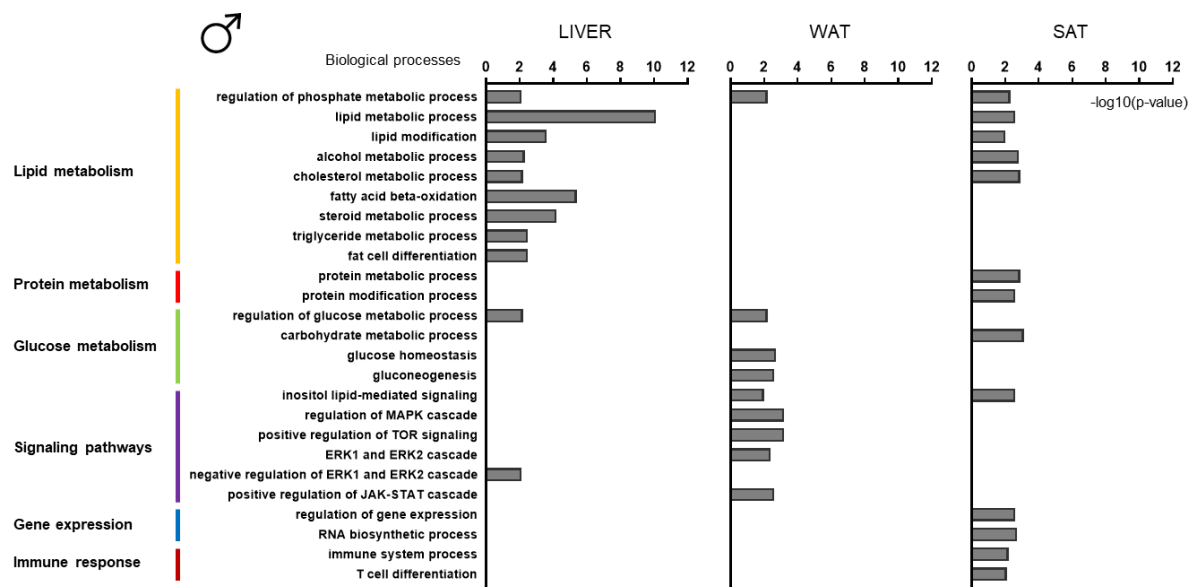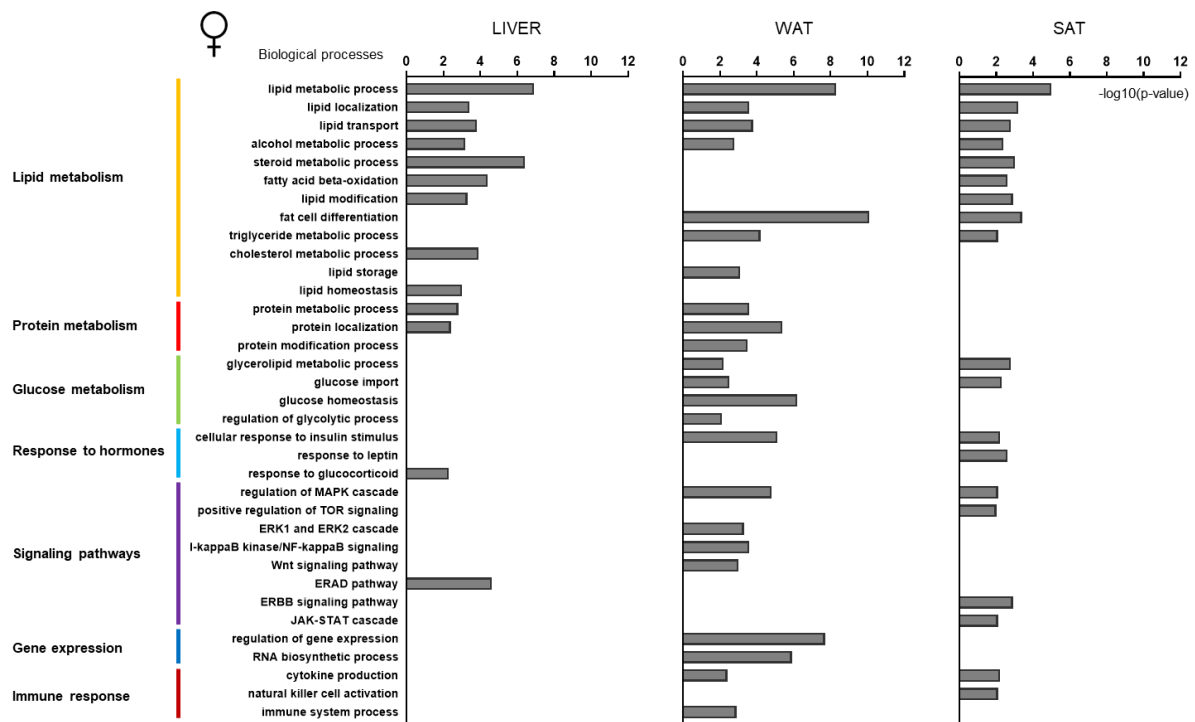
FIGURE 3.14 | AFFECTED GENEONTOLOGY TERMS IN ORGANS OF 3 WEEKS OLD F1 FEMALES

Selection of biological processes that are affected by significantly regulated genes (p < 0.01) in 3 weeks old females. Analysis performed by using the GeneRanker tool from Genomatix. Displayed are the −log10(p-value) values for each GO term.

In 3 weeks old females, genes whose expression is altered by parental HFD are predominantly involved in several metabolic processes, the response to hormones and signaling pathways, similar to males. In liver, many processes involved in the lipid and protein metabolism are affected, but also the response to glucocorticoids and the ERAD pathway. In WAT, lipid, protein and glucose metabolism, but also the response to insulin and several signaling pathways such as ERK1 and ERK2 cascade and Wnt signaling are affected. Additionally, processes involved in gene expression and the immune response are over-represented. In SAT, many processes of the lipid and glucose metabolism are affected but also the response to insulin and leptin. Additionally, the signaling pathways MAPK cascade, TOR signaling and JAK-STAT cascade as well as the immune response are affected.

Although only very few specific transcripts and genes are regulated in both male and female tissues at this age, many similar biological processes are affected by these different regulated genes in both males and females. Especially the lipid metabolism but also glucose metabolism is strongly affected by a parental HFD in the offspring's tissues.

Overall, transcriptome analysis of specific organs could substantiate differences between offspring of HFD- and LFD-treated parents already at the age of 3 weeks in addition to the phenotypic difference in weaning body weight (Figure 3.2).

3.3 Transcriptomic alterations in liver tissue of HFD offspring during organogenesis

Transcriptome analysis of 3 weeks old mice revealed differences depending on the parental diet in line with phenotypic differences at this age and in adulthood. In order to investigate if these transcriptomic differences can be detected even earlier, liver tissue was harvested and analyzed at several stages during organogenesis. These stages include Theiler stages (TS) TS20 (E12), TS22 (E14) and TS23 (E15). The sex of each individual fetus was determined by PCR screening for the *Sry* gene that is only present at the Y chromosome in males. Final RNA-Seq analysis was subsequently conducted with 8-10 samples per parental diet, fetal stage and sex, except for female offspring of LFD-treated parents at TS20. In this group, only 4 samples were available.

Quality of reads after trimming of adapter sequences was adequate and comparable between the different samples. For further analysis, only transcripts with a read count >20 in at least half of the samples in at least one group were incorporated.

PCA from all sequencing reads was performed to show overall differences and similarities between the analyzed fetal stages and within the stages between offspring of HFD- and LFD-treated parents (Figure 3.15). The dates of RNA extraction and cDNA amplification were included as covariates in these PCAs and further differential expression analysis. Additionally, the sex was included as a covariate for the combined analysis of males and females.
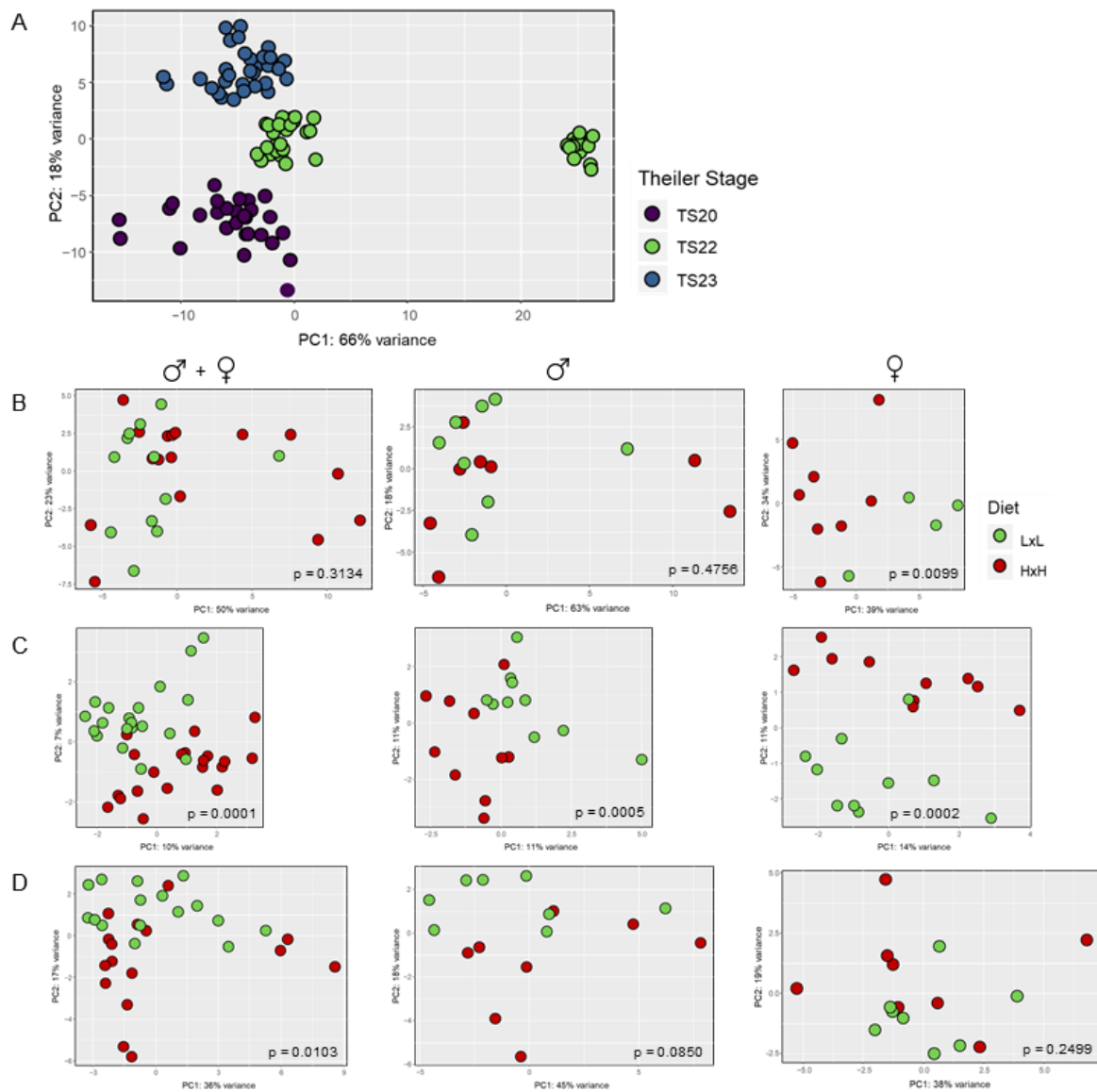
FIGURE 3.15 | PCA PLOTS OF FETAL LIVER

PCA of all liver samples of fetal F1 mice considering normalized raw counts (A) and batch corrected normalized counts (B-D) of all analyzed sequencing reads. A shows the comparison of TS20 (purple), TS22 (green) and TS23 (blue). B, C and D show the PCAs of TS20 (B), TS22 (C) and TS23 (D) samples separately for mixed analysis of males and females together (left), analysis of only males (middle) and analysis of only females (right). For B, C, D, the corresponding parental diet (LFD in green vs. HFD in red) is indicated. Plots always display the first principle component (PC) on the x-axis and the second PC on the y-axis. An empirical p-value is calculated and depicted within each PCA plot.

In the comparison of samples of all developmental stages PC1 separates the samples of TS22 in two clusters that can be explained by a batch effect during cDNA amplification. By considering only PC2 the different developmental stages clearly cluster in the three different groups (TS20, TS22 and TS23) with the strongest differences between TS20 and TS23. Separate analysis of the developmental stages can visualize transcriptome differences

according to the parental diet. In TS20 (Figure 3.15 B), only females cluster clearly in two separate groups (p = 0.0099) whereas males (p = 0.4756) and males and females together (p = 0.3134) do not. In TS22 (Figure 3.15 C), males and females together (p = 0.0001), males (p = 0.0005) and females (p = 0.0002) clearly form separate clusters according to the parental diet. In TS23 (Figure 3.15 D), males and females together (p = 0.0103) although still overlapping and males (p = 0.0850) clearly cluster according to the parental diet whereas females (p = 0.2499) do not.

Overall, transcriptome of liver tissue differs significantly between the three developmental stages. However, a clear distinction between liver tissue of the different parental diets is not always possible but the groups show a tendency of clustering together. Therefore, at these stages of development, a distinct and separate analysis of males and females is reasonable.

As no other batch effects are observable in these PCA plots, these normalized and batch corrected sequencing counts were used for differential expression analysis.

3.3.1 Analysis of differentially expressed transcripts in developing liver tissue

In order to examine the transcripts accountable for the differences between liver tissue of HFD and LFD offspring, differential expression analysis was performed using DESeq2 resulting in a few hundred regulated transcripts for all Theiler stages. Stages and sexes were analyzed separately by always comparing offspring of different parental diets (HFD vs. LFD). Number of upregulated and downregulated transcripts with p < 0.01 per Theiler stage and sex as well as the number of these transcripts overlapping between sexes and stages are shown in Figure 3.16.
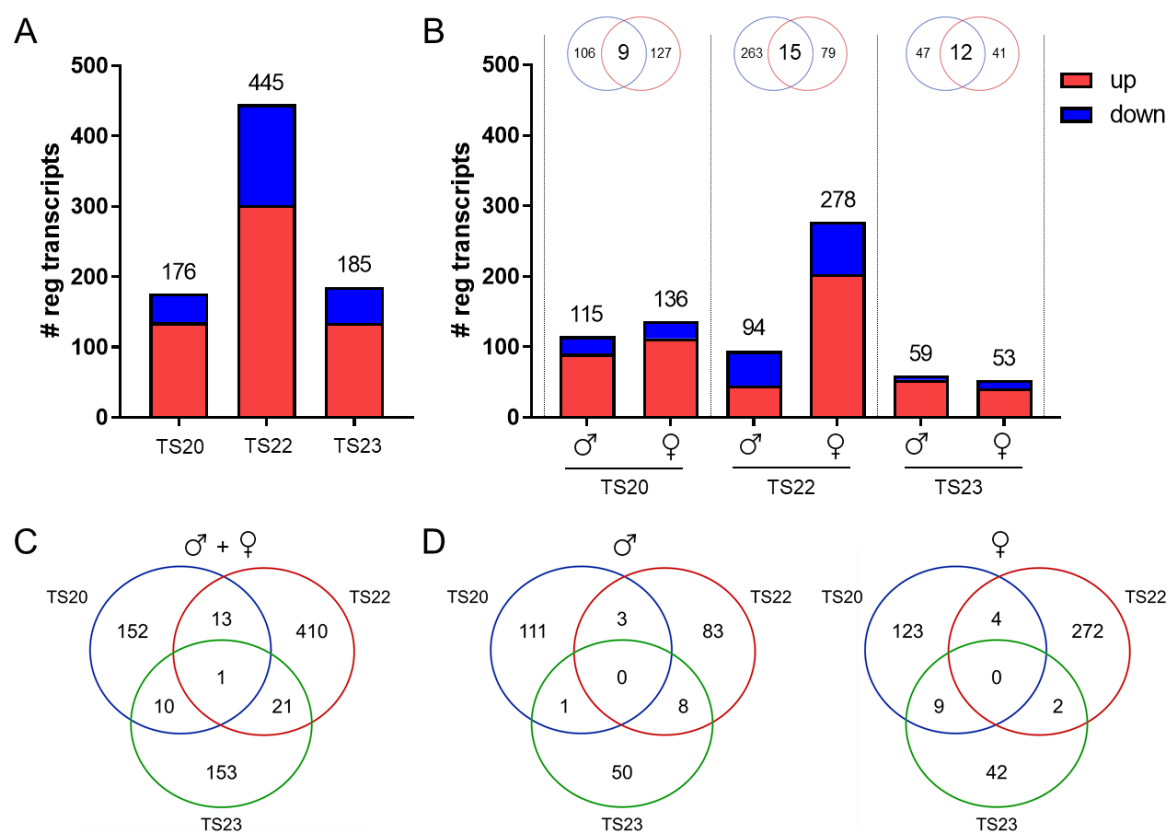
FIGURE 3.16 | NUMBER AND OVERLAP OF REGULATED LONG TRANSCRIPTS IN FETAL LIVER

Number of significantly (p < 0.01) upregulated (red) and downregulated (blue) transcripts between F1 (HxH) and F1 (LxL) fetal liver tissues in the mixed analysis (A) and separate analysis for males and females (B). Venn diagrams display overlap in differentially regulated transcripts between males and females. C and D show Venn diagrams displaying significantly regulated transcripts (p < 0.01) between F1 (HxH) and F1 (LxL) overlapping between the different fetal stages. Statistical analysis was performed either of males and females together (A, C), only males or only females (B, D).

Differential gene expression analysis reveals a number of significantly regulated transcripts between F1 (HxH) and F1 (LxL) mice at all developmental stages. Taking all transcripts into account that are significantly regulated with p < 0.01, statistical analysis of males and females together (Figure 3.16 A) by correcting for sex differences yields 176 (TS20), 445 (TS22) and 185 (TS23) differentially regulated transcripts. Separate statistical analysis for males and females (Figure 3.16 B) shows 115 and 136 (TS20), 94 and 278 (TS22), 59 and 53 (TS23) regulated transcripts for males and females, respectively. So, only for TS22 a difference between the sexes is apparent. The overlap of regulated transcripts between males and females is very low at all three developmental stages as shown by the Venn diagrams in Figure 3.16 B. A detailed overview of regulated transcripts that overlap between males and females in TS20, TS22 and TS23 is given in Table 3.5.

TABLE 3.5 | OVERLAPPING REGULATED LONG TRANSCRIPTS IN MALE AND FEMALE FETAL LIVER

Gene symbol	Transcript ID	Males FC	Females FC
TS20			
Gm24245	ENSMUST00000157318	2.44	2.06
Chd9	ENSMUST00000209474	1.64	2.57
Gm13340	ENSMUST00000117219	1.61	1.47
Gm42031	ENSMUST00000209823	1.59	2.01
Gm42429	ENSMUST00000198579	1.53	2.49
Gm46620	ENSMUST00000236930	1.52	2.07
Gm43305	ENSMUST00000199958	1.51	1.78
Gm13341	ENSMUST00000120780	1.44	1.41
Gm42427	ENSMUST00000200473	1.42	1.81
TS22			
Hba-x	ENSMUST00000020531	1.77	1.81
Hbb-y	ENSMUST00000033229	1.73	2.07
Emd	ENSMUST00000088313	1.45	1.47
Calm2	ENSMUST00000040440	1.34	1.29
Mthfd2	ENSMUST00000005810	1.26	1.39
Asb4	ENSMUST00000043294	1.25	1.39
Hspe1	ENSMUST00000075242	1.25	1.43
Pgam1	ENSMUST00000011896	1.23	1.35
Pdia6	ENSMUST00000057288	1.21	1.28
Gm6210	ENSMUST00000204734	1.20	1.27
Gm3362	ENSMUST00000148102	1.18	1.27
Prelid3b	ENSMUST00000016401	1.18	1.20
Rps16-ps2	ENSMUST00000140155	1.17	1.24
Hmgn1	ENSMUST00000050884	1.15	1.22
Tomm20	ENSMUST00000179857	1.15	1.15
TS23			
Hamp	ENSMUST00000062620	1.61	2.24
Trf	ENSMUST00000035158	1.50	1.33
Elane	ENSMUST00000046091	1.47	1.29
Gm10524	ENSMUST00000181931	1.44	1.21
Pcbd1	ENSMUST00000020298	1.41	1.34
Fgb	ENSMUST00000048246	1.35	1.18
Serpina1c	ENSMUST00000074051	1.34	1.18
Pla1a	ENSMUST00000002926	1.34	1.27
Serpina1d	ENSMUST00000078869	1.32	1.19
Gc	ENSMUST00000049209	1.30	1.20
Ttr	ENSMUST00000075312	1.28	1.17
Alb	ENSMUST00000031314	1.24	1.17

At TS20, 9 transcripts of 115 transcripts in males or 136 transcripts in females are overlapping, all of which are upregulated. Most of them are predicted genes with unknown function. At TS22, 15 transcripts of 94 transcripts in males or 278 transcripts in females are overlapping, all of which are upregulated and most of them protein-coding genes. At TS23, 12 transcripts of 59 transcripts in males or 53 transcripts in females are overlapping, all of which are upregulated and most of them protein-coding genes.

Comparison of transcriptome differences between TS20, TS22 and TS23 in the combined analysis of males and females (Figure 3.16 C) as well as the separate analysis of males and females (Figure 3.16 D) shows only very little overlap.

In the mixed analysis of males and females, 1 transcript *Gm42429* is upregulated in all three developmental stages. 13 transcripts are regulated in TS20 and TS22, 11 of which are upregulated. 10 transcripts are regulated in TS20 and TS23, 8 of which are upregulated and 1 is downregulated in both stages. 21 transcripts are regulated in TS22 and TS23, only 1 of which is upregulated in both stages whereas 20 transcripts are regulated in different directions. However, since transcripts that are significantly regulated in the combined analysis of males and females fail to lead to a clear clustering according to parental diet (see Figure 3.17), they are not listed here.

A detailed overview of regulated transcripts that overlap between the different Theiler stages for males and females separately is given in Table 3.6 and Table 3.7, respectively.

TABLE 3.6 | OVERLAPPING REGULATED TRANSCRIPTS IN MALE FETAL LIVER

Gene symbol	Transcript ID	TS20 FC	TS22 FC	TS23 FC
Gm42429	ENSMUST00000198579	1.53	1.48	ns
Emd	ENSMUST00000088313	1.51	1.45	ns
Gm14681	ENSMUST00000118047	1.54	-1.27	ns
Chd9	ENSMUST00000209474	1.64	ns	2.00
Camp	ENSMUST00000112022	ns	1.78	1.73
Afp	ENSMUST00000042755	ns	-1.07	1.18
Alb	ENSMUST00000031314	ns	-1.11	1.24
C3	ENSMUST00000024988	ns	-1.13	1.32
Serpina1d	ENSMUST00000078869	ns	-1.15	1.32
Serpina1c	ENSMUST00000074051	ns	-1.19	1.34
Gc	ENSMUST00000049209	ns	-1.26	1.30
Proz	ENSMUST00000033822	ns	-1.45	1.36

In the analysis of only males, no transcript is found to be regulated in all three developmental stages. 3 transcripts are regulated in TS20 and TS22, 2 of which are upregulated. 1 transcript is upregulated in both stages TS20 and TS23. 8 transcripts are regulated in TS22 and TS23, only 1 of which is upregulated in both stages whereas 7 transcripts are regulated in different directions.

TABLE 3.7 | OVERLAPPING REGULATED TRANSCRIPTS IN FEMALE FETAL LIVER

Gene symbol	Transcript ID	TS20 FC	TS22 FC	TS23 FC
Hbb-bs	ENSMUST00000023934	1.70	1.28	ns
Rhd	ENSMUST00000030627	1.42	1.17	ns
Asb4	ENSMUST00000043294	-1.45	1.39	ns
Fbn2	ENSMUST00000025497	-1.58	1.24	ns
Stfa3	ENSMUST00000068182	2.66	ns	1.43
Gm42429	ENSMUST00000198579	2.49	ns	1.41
H2ac11	ENSMUST00000091741	1.91	ns	1.21
Gc	ENSMUST00000049209	1.74	ns	1.20
Gm10524	ENSMUST00000181931	1.60	ns	1.21
H2bc4	ENSMUST00000018246	1.59	ns	1.21
Alb	ENSMUST00000031314	1.42	ns	1.17
Serpina1c	ENSMUST00000074051	1.37	ns	1.18
Lyz2	ENSMUST00000092163	1.37	ns	1.24
Klf3	ENSMUST00000196764	ns	-1.21	-1.28
Hif3a	ENSMUST00000108492	ns	-1.14	1.18

In the analysis of only females, no transcript is found to be regulated in all three developmental stages. 4 transcripts are regulated in TS20 and TS22, 2 of which are upregulated. 9 transcripts are upregulated in both stages TS20 and TS23. 2 transcripts are regulated in TS22 and TS23, only 1 of which is downregulated in both stages.

In order to visualize the difference between HFD and LFD fetal liver, these sets of significantly regulated transcripts are displayed in heat maps with hierarchical clustering of the transcripts in rows and the analyzed samples in columns (Figure 3.17).
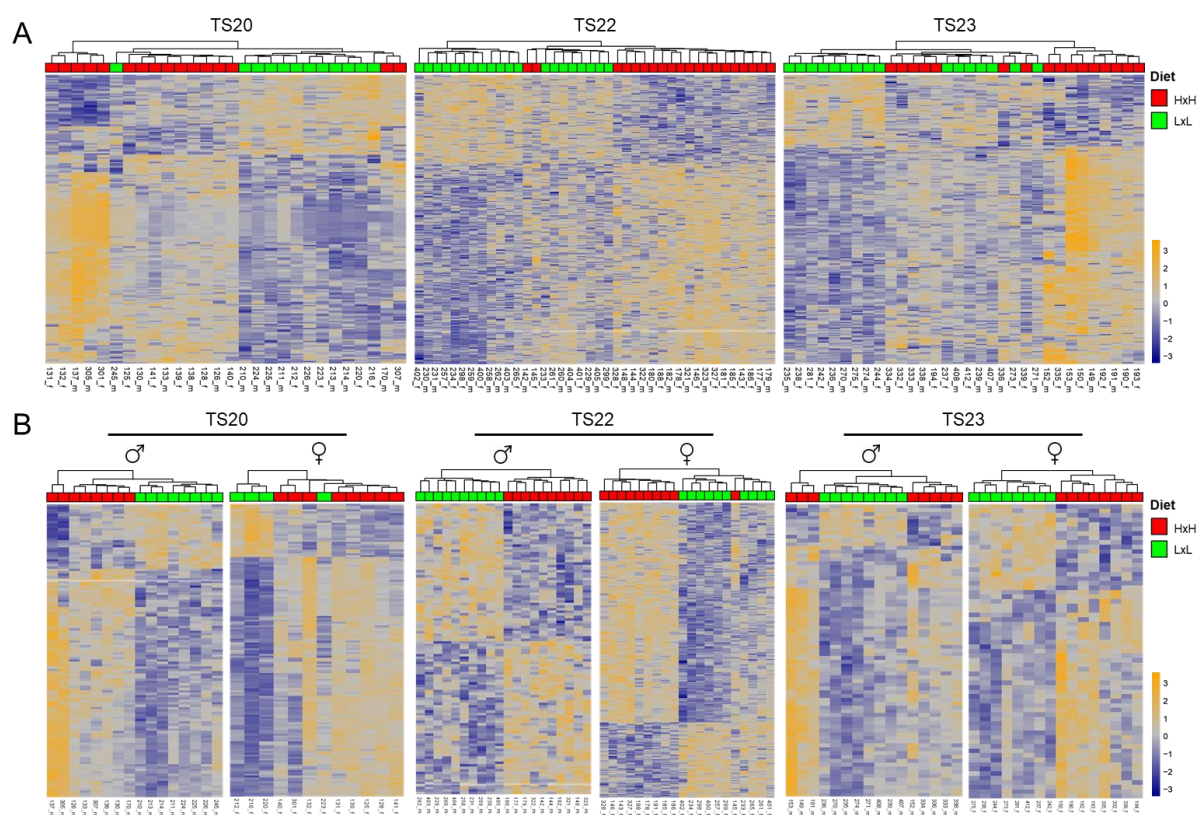
FIGURE 3.17 | HEAT MAPS OF REGULATED LONG TRANSCRIPTS IN FETAL LIVER

Heat maps of upregulated (yellow) and downregulated (blue) transcripts (p < 0.01) between F1 (HxH) (red) and F1 (LxL) (green) male and female fetal liver samples. A displays the differentially expressed set of transcripts in the combined analysis of males and females. B displays differentially expressed sets of transcripts for the separate analysis of males and females.

By hierarchical clustering according to differentially expressed transcripts, only samples of TS22 (males and females together) can be clearly separated in two groups indicating parental HFD and parental LFD treatment. Samples of TS20 and TS23 can also be separated in the two groups, but a distinct classification by hierarchical clustering is not possible (Figure 3.17 A). In the separate analysis of males and females, samples cluster according to the parental diet in nearly all analyzed stages except for females in TS20 and TS23 (Figure 3.17 B).

Therefore, employing these sets of significantly regulated transcripts enables the distinction between offspring derived from HFD- and LFD-treated parents already at this early stage of development.

3.3.2   Analysis of regulated pathways in affected liver tissue during organogenesis

Pathway (GO term) analysis was performed with associated genes of these significantly regulated transcripts (p < 0.01) to uncover the biological functions and processes they are affecting. A selection of interesting and significantly affected terms in males and females is provided in Figure 3.18 and Figure 3.19, respectively.
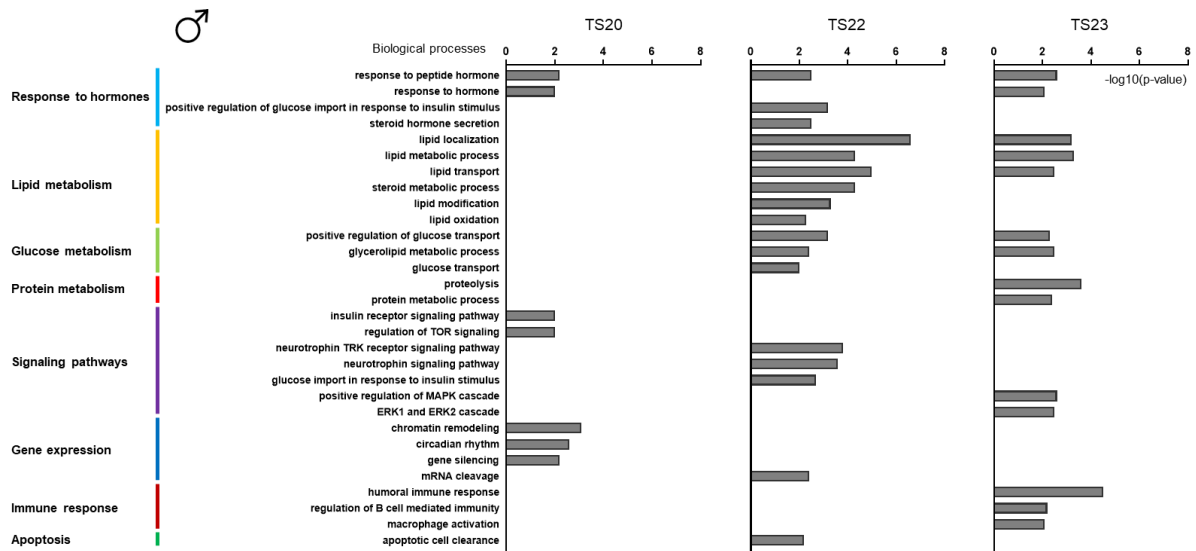
FIGURE 3.18 | AFFECTED GENEONTOLOGY TERMS IN MALE FETAL LIVER

Selection of biological processes that are affected by significantly regulated genes (p < 0.01) in male fetal liver of TS20, TS22 and TS23. Analysis performed by using the GeneRanker tool from Genomatix. Displayed are the -log10(p-value) values for each GO term.

In male fetal liver, genes whose expression is affected by parental HFD are predominantly involved in several metabolic processes, signaling pathways and the response to hormones in all analyzed Theiler stages. At TS20, response to hormones and insulin signaling are affected but also gene silencing and circadian rhythm. At Ts22, various processes of lipid and glucose metabolism are affected as well as the response to hormones, several signaling pathways, mRNA cleavage and apoptotic processes. At TS23, response to hormones as well as lipid, glucose and protein metabolism are affected processes but also immune response and signaling pathways such as MAPK cascade and ERK1 and ERK2 cascade.
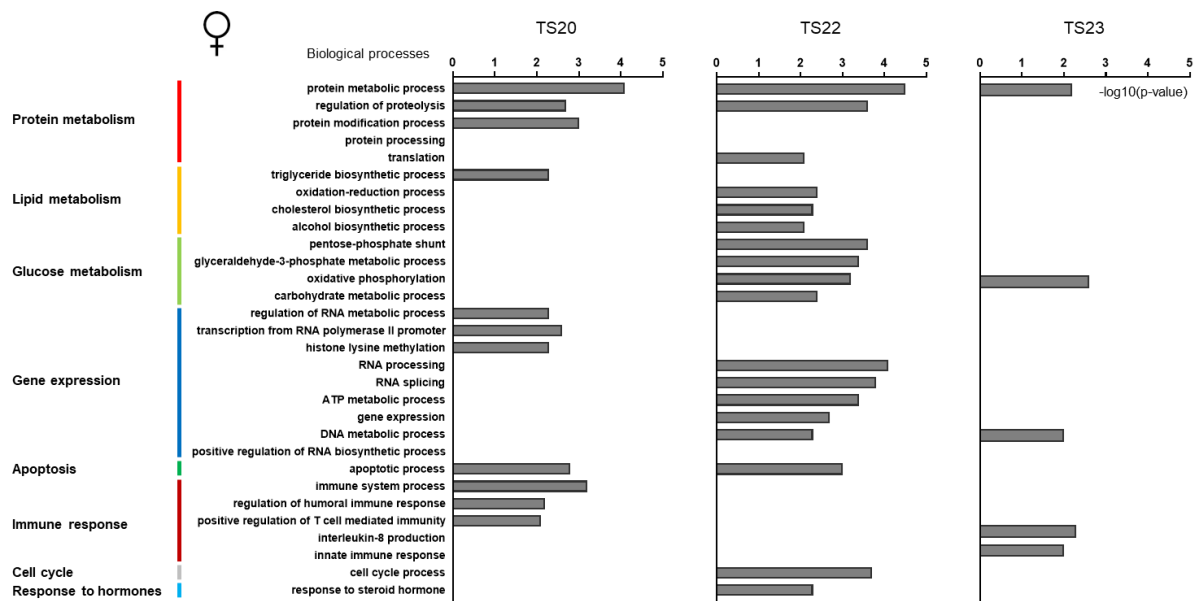
FIGURE 3.19 | AFFECTED GENEONTOLOGY TERMS IN FEMALE FETAL LIVER

Selection of biological processes that are affected by significantly regulated genes (p < 0.01) in female fetal liver of TS20, TS22 and TS23. Analysis performed by using the GeneRanker tool from Genomatix. Displayed are the -log10(p-value) values for each GO term.

In female fetal liver, genes whose expression is affected by parental HFD are predominantly involved in several metabolic processes and regulation of gene expression throughout the analyzed Theiler stages. At TS20, protein and lipid metabolism as well as transcription and histone methylation are affected but also immune response and apoptosis. At Ts22, various processes of protein, lipid and glucose metabolism are affected as well as gene expression, apoptosis, cell cycle processes and response to hormones. At TS23, only a few processes involved in protein and glucose metabolism are affected as well as gene expression and immune response.

3.4 Parental HFD-induced alterations in the expression of long and small RNAs in preimplantation embryos

Parental HFD induced an increased susceptibility to develop a metabolic phenotype in adulthood and increased body weight already at the age of 3 weeks in the offspring. Additionally, changes in the transcriptome of developing liver tissue as well as liver, WAT and SAT at the age of 3 weeks were detected. Based on the fact that IVF was used to procreate the offspring, these molecular and metabolic alterations must have been transmitted through the gametes and the early embryonic stages. In order to find epigenetic signatures that could potentially be causal for the transmission, differential expression of small and long RNAs in preimplantation embryos was analyzed next. Three stages during preimplantation phase were selected for analysis: The zygotic stage, a few hours after fertilization; the 2-cell stage, after the first cell division with the beginning of transcription; the blastocyst stage, before hatching from the zona pellucida starts.

3.4.1 Preimplantation development is not altered by parental HFD

Preimplantation embryos for analysis were produced via IVF with oocytes and sperm from parental F0 mice that had been treated with either HFD or LFD for 6 weeks. Harvested cumulus-oocyte complexes from several females were co-incubated with capacitated sperm cells and after fertilization cultured until the blastocyst stage. At three stages during early embryonic development, samples were taken and snap-frozen in liquid nitrogen. These samples consist of a number of pooled single embryos that met pre-defined quality standards such as no contamination with sperm cells and cumulus cells, intact and round zona pellucida as well as intact embryonic cells (Figure 3.20).

Pictures of examples for preimplantation embryos meeting the quality criteria are shown in Figure 3.20 A-C. A shows an intact zygote with two pronuclei and two polar bodies indicating successful fertilization. B shows an intact 2-cell embryo with two similar cells after the first mitotic cell division. C shows an intact blastocyst with a clear inner structure. It consists of the outer layer (trophoblast) surrounding the inner cell mass (ICM) and the blastocoel. Figure 3.20 D-F, on the other hand, provides examples of preimplantation embryos not meeting the quality criteria. D shows an oocyte that has not been fertilized and many sperm cells attached to it. E shows an intact 2-cell embryo, however, many sperm cells are attached to it potentially enabling contamination. F shows a blastocyst that is already in the hatching process. Obviously, only embryos of good quality were collected and further used for transcriptome analysis.
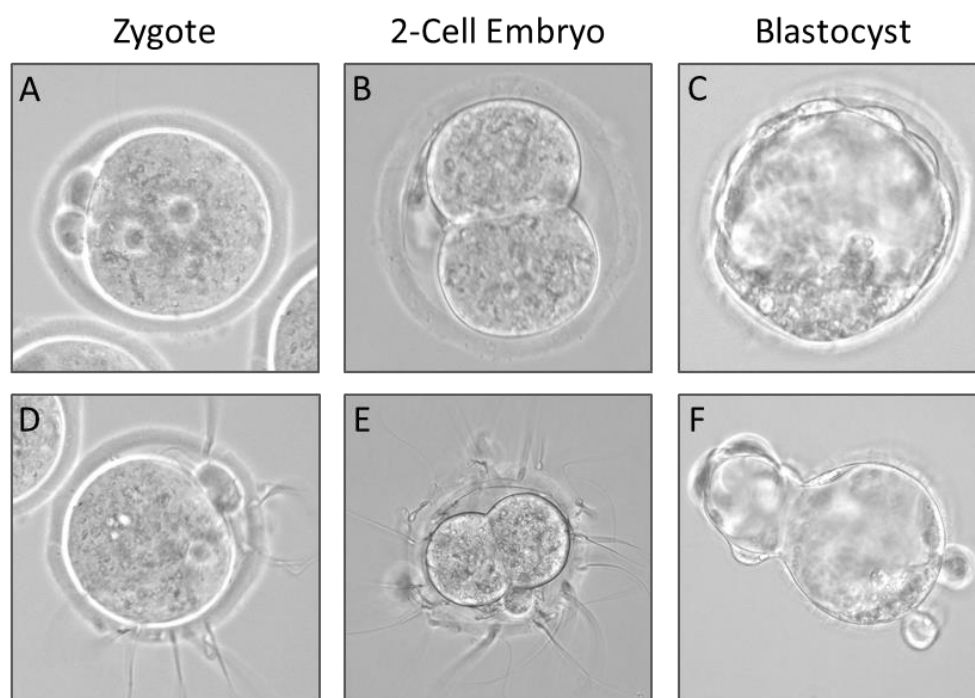
FIGURE 3.20 | MICROSCOPIC IMAGES OF PREIMPLANTATION EMBRYOS

Microscopic images of preimplantation embryos indicate quality standards for further use in analysis. A-C show embryos at three different developmental stages of good quality with an intact zona pellucida and no contamination with spermatozoa or somatic cells, whereas D-F show embryos of poor quality.

For zygotes, in average 42.9 embryos were pooled (20-85), for 2-cell embryos, in average 30.5 embryos were pooled (10-45) and for blastocysts, in average 11.3 embryos were pooled (3-21). In Table 3.8, number of independent IVFs, number of sperm and oocyte donors as well as total number of used embryos and embryos per sample are shown for each developmental stage and each parental diet group.

TABLE 3.8 | IVF RESULTS

	Group ID	# IVFs	# sperm donors	# oocyte donors	# embryos	# embryos/ sample
Zygote	*F1 (HxH)*	14	14	111	577	41
	F1 (LxL)	16	16	144	711	44
2-Cell Embryo	*F1 (HxH)*	19	19	132	585	31
	F1 (LxL)	14	14	111	423	30
Blastocyst	*F1 (HxH)*	13	13	67	147	11
	F1 (LxL)	17	17	94	192	11

3.4.2   Sequencing of long RNAs in preimplantation embryos

Total RNA was isolated from these pools of preimplantation embryos and used for strand-specific library preparation. Paired-end sequencing was performed producing 2x125 bp reads with in average 56.6 million reads per sample (52.0 million for zygotes, 52.1 million for 2-cell embryos, 65.7 million for blastocysts). After adapter and quality trimming, in average 55.9 million reads were counted per sample (51.3 million for zygotes, 51.3 million for 2-cell embryos, 65.0 million for blastocysts). Read counts were normalized for further analyses and in addition, it was corrected for the batch effect of the library preparation date. All normalized reads were included for the PCA in order to detect further batches and overall differences between the samples (Figure 3.21).
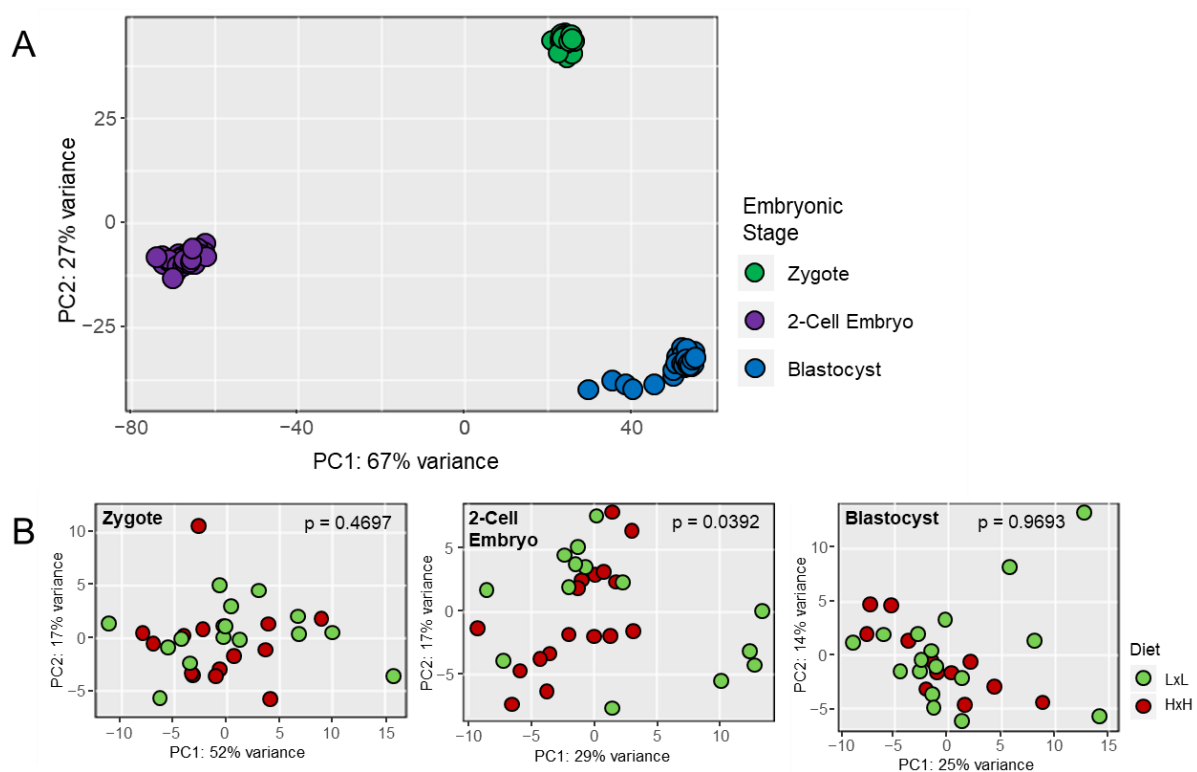
FIGURE 3.21 | PCA PLOTS OF LONG TRANSCRIPTS OF PREIMPLANTATION EMBRYOS

Principle component analysis of preimplantation embryos including all sequencing reads. A shows transcriptomic differences between the different stages. B shows the distribution of the samples for every embryonic stage individually with the parental diet indicated in green (LFD) and red (HFD). An empirical p-value is calculated and depicted in each PCA plot.

PCA of all stages of preimplantation embryos shows a clear separation of zygotes, 2-cell embryos and blastocysts and a clustering within these sample groups (Figure 3.21 A). PCA of each sample group individually shows an equal distribution of the samples throughout the plotted area indicating a successful correction for batch effects and no clustering according to the parental diet (Figure 3.21 B).

3.4.3 Analysis of differentially expressed long transcripts in preimplantation embryos

Differential expression analysis was performed using DESeq2 and resulted in a number of regulated transcripts for all analyzed embryonic stages. Zygotes, 2-cell embryos and blastocysts were analyzed separately by always comparing offspring of HFD-treated parents with offspring of LFD-treated parents.

Number of upregulated and downregulated transcripts with p < 0.01 and the number of these transcripts overlapping between the different stages are shown in Figure 3.22.
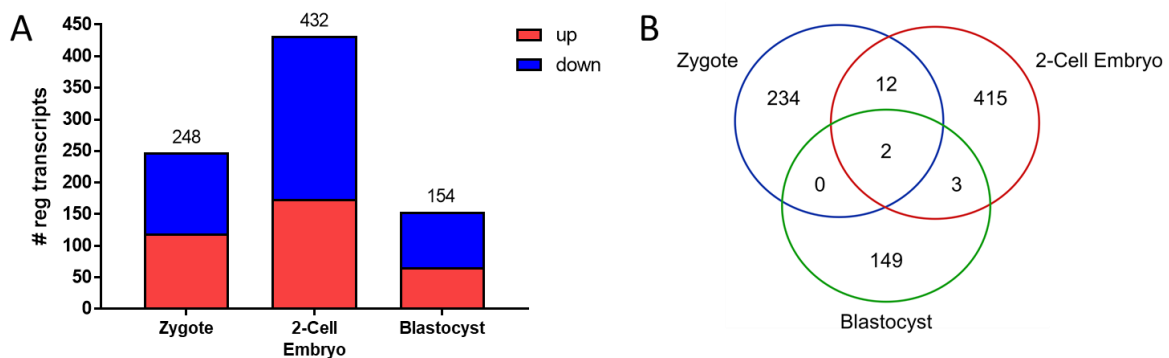
FIGURE 3.22 | NUMBER OF REGULATED LONG TRANSCRIPTS AND OVERLAP IN PREIMPLANTATION EMBRYOS

Number of significantly upregulated (red) and downregulated (blue) transcripts (A) without a certain fold change (p < 0.01) between F1 (HxH) and F1 (LxL) embryonic stages (zygote, 2-cell embryo, blastocyst). Venn diagram (B) displays overlap in differentially regulated transcripts between zygotes, 2-cell embryos and blastocysts.

Differential gene expression analysis reveals a number of significantly regulated transcripts between F1 (HxH) and F1 (LxL) preimplantation embryos. Taking all transcripts into account that are significantly regulated with p < 0.01, the number of regulated transcripts is higher in 2-cell embryos (432 transcripts encoding 419 unique genes) than in zygotes (248 transcripts encoding 246 unique genes) and blastocysts (154 transcripts encoding 153 unique genes). However, if FDR < 0.1 is used to identify significantly regulated transcripts, these numbers are drastically reduced to 36 transcripts in zygotes, 5 transcripts in 2-cell embryos and 1 transcript in blastocysts. 2 transcripts are regulated in all three stages, 12 transcripts are regulated in zygotes and 2-cell embryos and 3 transcripts are regulated in 2-cell embryos and blastocysts (Figure 3.22).

Overlapping regulated transcripts are listed in Table 3.9 including the linear FC with which they are regulated.

TABLE 3.9 | OVERLAPPING REGULATED TRANSCRIPTS IN ZYGOTE, 2-CELL EMBRYO AND BLASTOCYST

Gene symbol	Transcript ID	Zygote FC	2-Cell Embryo FC	Blastocyst FC
Gm7762	ENSMUST00000220595	1.13	1.45	1.31
Myom2	ENSMUST00000033842	1.13	1.15	-1.81
Gm32846	ENSMUST00000205665	1.41	1.70	ns
Odf2l	ENSMUST00000199435	1.25	1.46	ns
Gm47136	ENSMUST00000215837	1.24	1.40	ns
Krt71	ENSMUST00000023710	1.26	1.31	ns
Cldn8	ENSMUST00000049697	1.09	1.47	ns
Dnah12	ENSMUST00000022433	1.13	1.20	ns
Catsper2	ENSMUST00000038073	-1.31	-1.54	ns
Abi3bp	ENSMUST00000231781	-1.38	-1.35	ns
Syde1	ENSMUST00000040580	-1.34	-1.32	ns
Gli3	ENSMUST00000110510	-1.29	-1.29	ns
Amer1	ENSMUST00000084535	-1.14	-1.27	ns
Zscan4-ps3	ENSMUST00000210559	1.15	-1.40	ns
Rbm8a	ENSMUST00000048915	ns	-1.64	-1.60
1700028K03Rik	ENSMUST00000162591	ns	1.50	-1.56
Ranbp17	ENSMUST00000102815	ns	-1.29	1.29

Gm7762 is a protein-coding gene that is significantly ($p < 0.01$) upregulated in all three analyzed embryonic stages. Similarly, the protein-coding gene *Myom2* is significantly upregulated in zygotes and 2-cell embryos but downregulated in blastocysts. 12 transcripts are significantly regulated in both zygotes and 2-cell embryos, 6 of them upregulated (*Gm32846, Odf2l, Gm47136, Krt71, Cldn8, Dnah12*), 5 downregulated (*Catsper2, Abi3bp, Syde1, Gli3, Amer1*) and 1 upregulated in zygotes but downregulated in 2-cell embryos (*Zscan4-ps3*). Downregulated in both 2-cell embryos and blastocysts is *Rbm8a*, whereas *1700028K03Rik* is upregulated in 2-cell embryos and downregulated in blastocysts and *Ranbp17* is downregulated in 2-cell embryos but upregulated in blastocysts.

In order to visualize the difference between HFD and LFD offspring, all samples from zygotes, 2-cell embryos and blastocysts were clustered according to the similarity of their significantly (p < 0.01) regulated transcripts and displayed in heat maps (Figure 3.23).
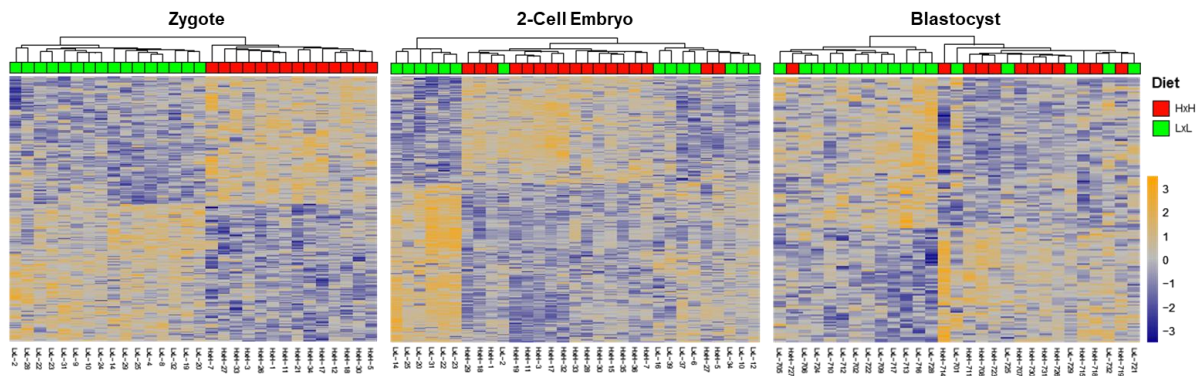
FIGURE 3.23 | HEAT MAPS OF LONG TRANSCRIPTS OF PREIMPLANTATION EMBRYOS

Heat maps of upregulated (yellow) and downregulated (blue) transcripts (p < 0.01) between F1 (HxH) (red) and F1 (LxL) (green) during three embryonic stages (zygote, 2-cell embryo, blastocyst). Samples (columns) and transcripts (rows) are arranged according to their hierarchical clustering.

Hierarchical clustering of samples in heat maps clearly shows a clustering according to the parental diet in zygotes but less clearly in 2-cell embryos and blastocysts. This means that based on the expression levels of these regulated transcripts, zygote samples can be distinguished according to the parental diet. 2-cell embryos and blastocysts cannot be clearly distinguished, nevertheless, samples partially show a clustering according to the parental diet.

In order to examine the significantly regulated transcripts in more detail, a classification according to the Ensembl biotypes was performed and is depicted in Figure 3.24.
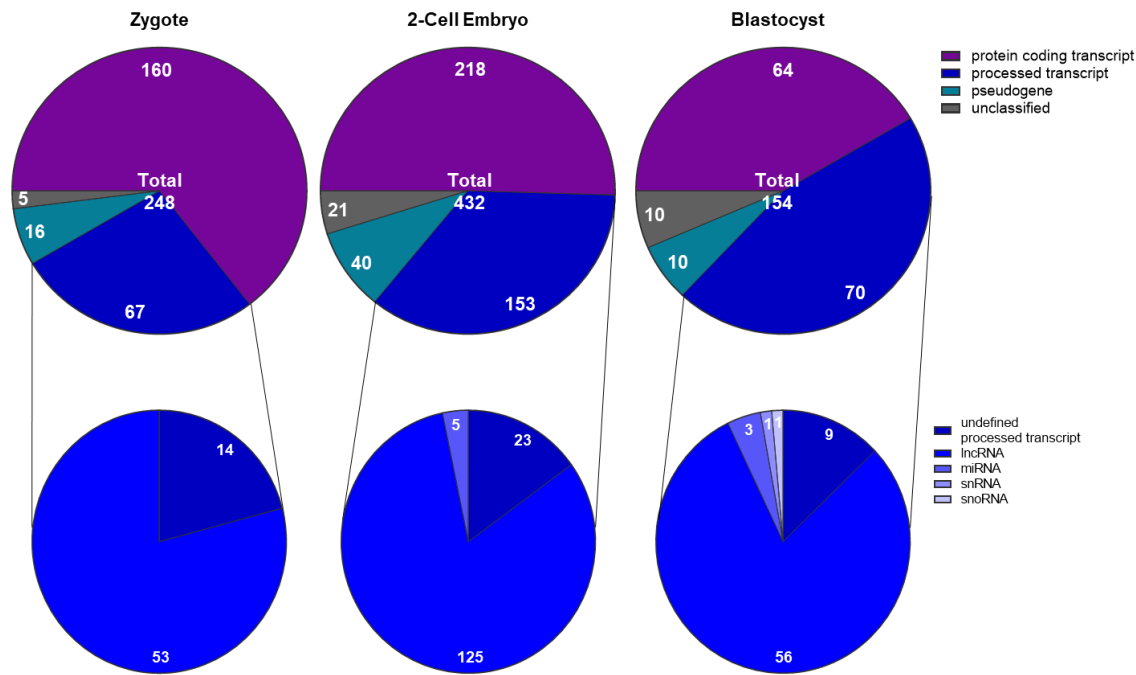
FIGURE 3.24 | BIOTYPES OF REGULATED TRANSCRIPTS IN PREIMPLANTATION EMBRYOS

Classification of significantly regulated transcripts (p < 0.01) in preimplantation embryos. Distinguished classes are protein coding transcripts (purple; "gene/transcript that contains an open reading frame (ORF)"), processed transcripts (dark blue; "gene/transcript that does not contain an ORF"), pseudogenes (cyan; "a gene/transcript that has homology to known protein-coding genes but contains a frameshift and/or stop codon(s) which disrupts the ORF"), and unclassified transcripts (gray). Processed transcripts are further subdivided in unclassified processed transcripts, lncRNAs ("a non-coding gene/transcript >200 bp in length"), miRNAs ("a small RNA (~22bp) that silences the expression of target mRNA"), snRNA ("small RNA molecules that are found in the cell nucleus and are involved in the processing of pre messenger RNAs"), and snoRNA ("small RNA molecules that are found in the cell nucleolus and are involved in the post-transcriptional modification of other RNAs"). Classification of transcripts is based on the Ensembl biotypes (http://www.ensembl.org/info/genome/genebuild/biotypes.html).

Analysis of the regulated transcripts in more detail revealed 64.5% (160) protein coding transcripts, 27.0% (67) processed transcripts, 6.5% (16) transcripts for pseudogenes and 2.0% (5) unclassified transcripts for zygotes. In 2-cell embryos, 50.5% (218) are protein coding transcripts, 35.4% (153) processed transcripts, 9.3% (40) transcripts for pseudogenes and 4.9% (21) unclassified transcripts. Blastocysts contain 41.6% (64) protein coding transcripts, 45.5% (70) processed transcripts, 6.5% (10) transcripts for pseudogenes and 6.5% (10) unclassified transcripts. Subdivision of the class "processed transcripts" shows 20.9% (14) undefined processed transcripts and 79.1% (53) lncRNAs for zygotes, 15.0% (23) undefined processed transcripts, 81.7% (125) lncRNAs and 3.3% (5) miRNAs for 2-cell embryos and 12.9% (9) undefined processed transcripts, 80.0% (56) lncRNAs, 4.3% (3) miRNAs, 1.4% (1) snRNAs and 1.4% (1) snoRNAs for blastocysts.

Interestingly, in each preimplantation stage, at least one third of the regulated transcripts is not protein-coding and, therefore, might have no known biological function assigned.

3.4.4   Regulated pathways of long RNAs in preimplantation embryos

Gene set enrichment analysis was performed for the sets of differentially expressed genes (p < 0.01) from all three preimplantation stages. A selection of interesting and significantly affected terms in zygotes, 2-cell embryos and blastocysts is provided in Figure 3.25.
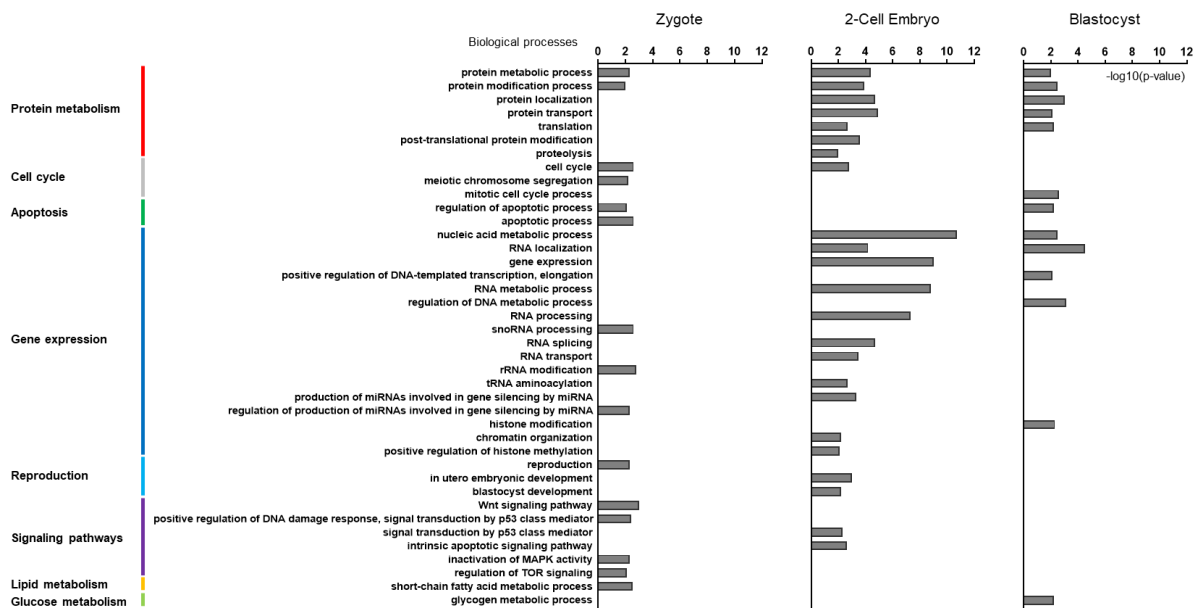
FIGURE 3.25 | AFFECTED PATHWAYS OF REGULATED TRANSCRIPTS IN PREIMPLANTATION EMBRYOS

Selection of biological processes that are affected by significantly regulated genes (p < 0.01) in zygotes, 2-cell embryos and blastocysts. Analysis was performed by using the GeneRanker tool from Genomatix. Displayed are the −log10(p-value) values for each GO term.

In preimplantation embryos, genes whose expression is altered by parental HFD are predominantly involved in metabolic processes, regulation of gene expression and signaling pathways. In zygotes, protein and lipid metabolism, cell cycle and apoptotic processes are affected by parental HFD treatment. Also, different RNA modification processes and gene silencing as well as signaling pathways such as Wnt signaling, MAPK cascade and TOR signaling are affected. In 2-cell embryos, many processes involved in protein metabolism and RNA metabolism including gene expression, gene silencing, RNA processing, and histone modification are affected but also embryonic development and the intrinsic apoptotic signaling pathway. In blastocysts, several protein metabolic and modification processes and glucose metabolism are affected. In addition, cell cycle and apoptotic processes as well as gene expression and histone modification are affected.

3.4.5   Analysis of differentially expressed small RNAs in preimplantation embryos

Total RNA from pools of preimplantation embryos was used for small RNA library preparation. Single-read sequencing was performed producing 1x50 bp reads. After adapter and quality trimming, read counts were normalized for further analyses. However, exclusion of transcripts with low read counts reduced the number of transcripts significantly from initially 85,388 to 7,475. In addition, it was corrected for the batch effects of RNA extraction date and sequencing date as well as the first two hidden batches that were found via surrogate variable analysis (SVA). All normalized reads were included for the PCA in order to detect further batches and overall differences between the samples (Figure 3.26).
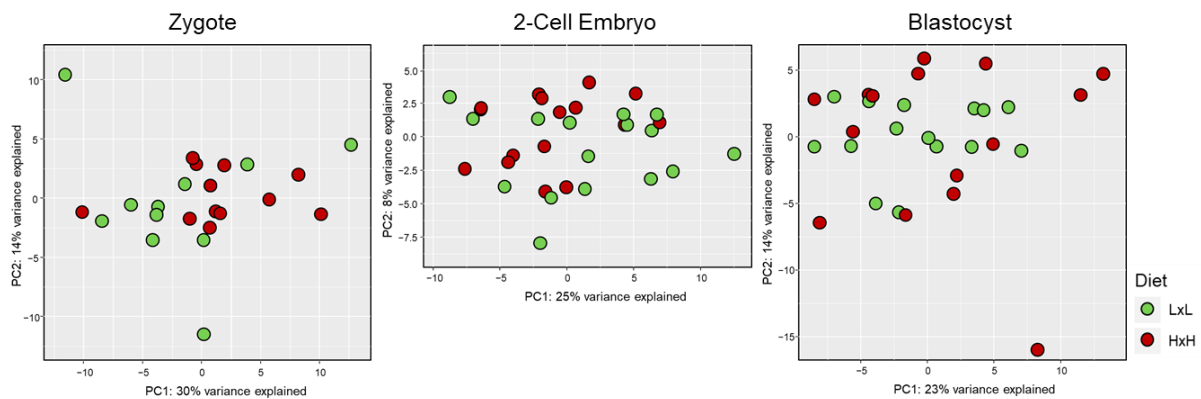
FIGURE 3.26 | PCA PLOTS OF SMALL RNAS OF PREIMPLANTATION EMBRYOS

Principle component analysis of preimplantation embryos including all small RNA sequencing reads shows the distribution of the samples for every embryonic stage individually with the parental diet indicated in green (LFD) and red (HFD).

PCA of each preimplantation stage separately shows an equal distribution of HFD and LFD offspring throughout the plotted area indicating no clustering according to the parental diet. Moreover, correction for batch effects was apparently successful.

Differential expression analysis was performed using DESeq2 and resulted in a number of differentially regulated small RNAs for all analyzed embryonic stages. Zygotes, 2-cell embryos and blastocysts were analyzed separately by always comparing offspring of HFD-treated parents with offspring of LFD-treated parents (HFD vs. LFD).

Number of upregulated and downregulated small RNAs with p < 0.01 and the number of these transcripts overlapping between the different stages are shown in Figure 3.27.
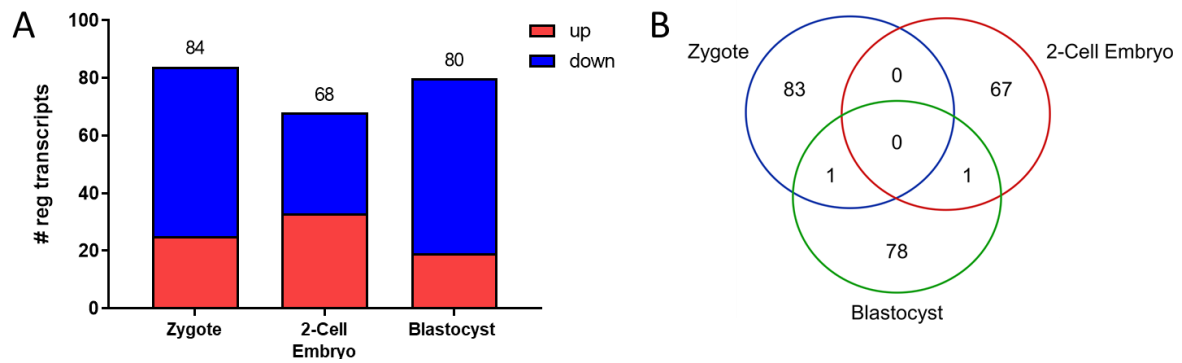
FIGURE 3.27 | NUMBER OF REGULATED SMALL RNAS AND OVERLAP IN PREIMPLANTATION EMBRYOS

Number of significantly upregulated (red) and downregulated (blue) small RNAs (A) without a certain fold change (p < 0.01) between F1 (HxH) and F1 (LxL) embryonic stages (zygote, 2-cell embryo, blastocyst). Venn diagram (B) displays overlap in differentially regulated small RNAs between zygotes, 2-cell embryos and blastocysts.

Differential gene expression analysis reveals a number of significantly regulated small RNAs between F1 (HxH) and F1 (LxL) preimplantation embryos. Taking all small RNAs into account that are significantly regulated with p < 0.01, the number of regulated small RNAs is higher in zygotes (123 small RNAs) than in 2-cell embryos (68 small RNAs) and blastocysts (80 small RNAs). However, if FDR < 0.1 is used to identify significantly regulated transcripts, these numbers are drastically reduced to 11 small RNAs in zygotes and no small RNAs in 2-cell embryos and blastocysts. 2 small RNAs (miRNA 6237 and tRNA fragment 925B) are regulated in both zygotes and 2-cell embryos and 1 small RNA (miRNA 7055-5p) is regulated in 2-cell embryos and blastocysts.

Significantly regulated small RNAs were sorted in different classes according to their length and function (Figure 3.28).
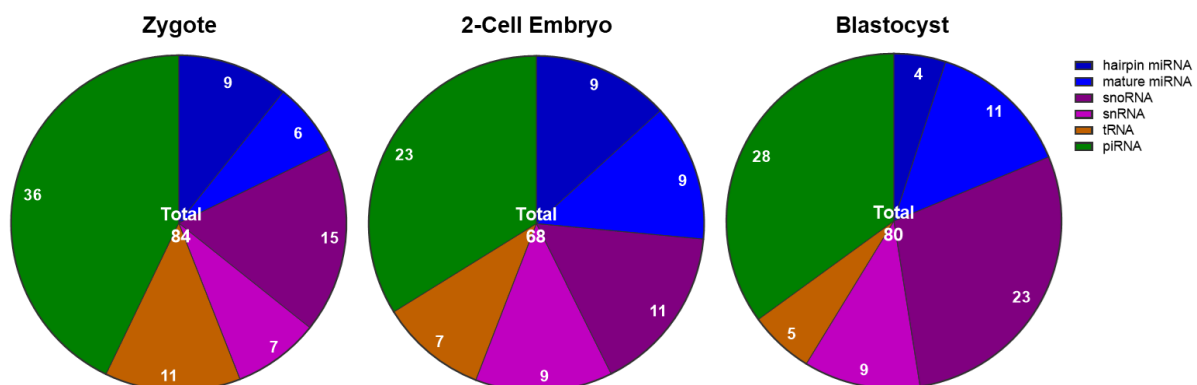
FIGURE 3.28 | CLASSES OF REGULATED SMALL RNAS

Classification of significantly regulated small RNAs (p < 0.01) in preimplantation embryos. Distinguished classes are hairpin miRNAs, mature miRNAs, snoRNAs, snRNAs, tRNAs and piRNAs.

Classification of regulated small RNAs shows a similar distribution in the three embryonic stages with piRNAs representing the largest class of at least one third of all regulated small RNAs. The class of miRNAs is divided in precursor hairpin miRNA and mature miRNA. In zygotes, regulated small RNAs can be distinguished in 10.7% (9) hairpin miRNAs, 7.1% (6) mature miRNAs, 17.9% (15) snoRNAs, 8.3% (7) snRNAs, 13.1% (11) fragmented tRNAs and 42.9% (36) piRNAs. In 2-cell embryos, regulated small RNAs can be distinguished in 13.2% (9) hairpin miRNAs, 13.2% (9) mature miRNAs, 16.2% (11) snoRNAs, 13.2% (9) snRNAs, 10.3% (7) fragmented tRNAs and 33.8% (23) piRNAs. In blastocysts, regulated small RNAs can be distinguished in 5.0% (4) hairpin miRNAs, 13.8% (11) mature miRNAs, 28.8% (23) snoRNAs, 11.3% (9) snRNAs, 6.3% (5) fragmented tRNAs and 35.0% (28) piRNAs.

All samples from zygotes, 2-cell embryos and blastocysts were clustered hierarchically according to their significantly (p < 0.01) regulated small RNAs and displayed in heat maps (Figure 3.29). Here, the different small RNA classes are shown together.
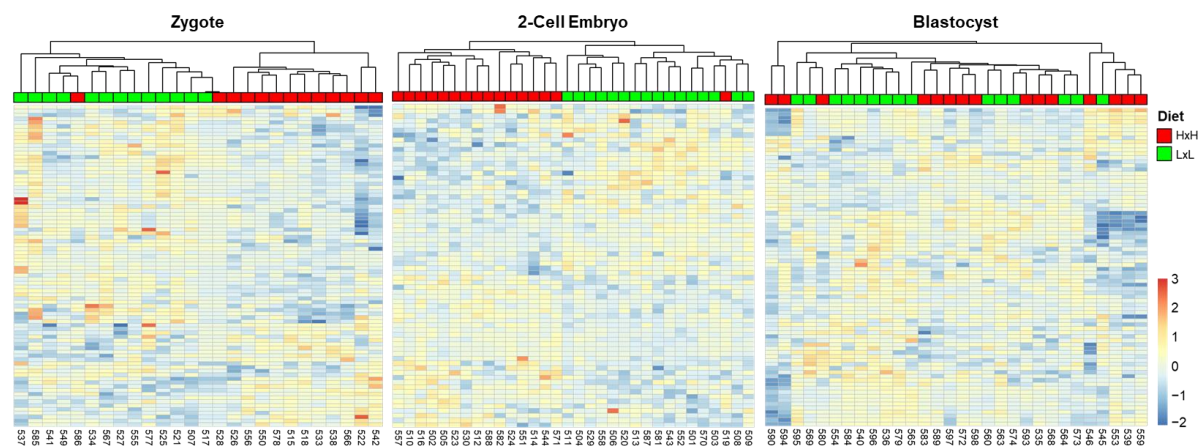
FIGURE 3.29 | HEAT MAPS OF REGULATED SMALL RNAS OF PREIMPLANTATION EMBRYOS

Heat maps of upregulated (red) and downregulated (blue) small RNAs (p < 0.01) between F1 (HxH) (red) and F1 (LxL) (green) preimplantation embryos.

Upregulation or downregulation of specific transcripts is rarely consistent between all samples of one dietary group. Additionally, most significantly regulated transcripts only show small expression differences, indicated by a very faint coloring in the heat map. Nevertheless, hierarchical clustering of samples in heat maps shows a clear clustering according to the parental diet in zygotes and 2-cell embryos but less clearly in blastocysts.

3.4.6 Targets of significantly regulated miRNAs

Especially the class of mature miRNAs is interesting, because miRNAs are known to be involved in gene silencing but also in gene activation. Therefore, an HFD-induced increase in specific miRNAs could provoke a decrease in expression of certain target genes (gene silencing) or an increase in target gene expression (gene activation). Potential target genes of regulated miRNAs are displayed in Table 3.10, Table 3.11 and Table 3.12.

TABLE 3.10 | POTENTIAL TARGET GENES OF REGULATED MIRNAS IN ZYGOTES

		Potential targets					
		Zygote		2-Cell Embryo		Blastocyst	
miRNA (Zygote)	FC	Gene Symbol	FC	Gene Symbol	FC	Gene Symbol	FC
miR-28a-3p	2.62	-		-		-	
miR-7040-5p	2.01	-		-		-	
miR-7669-3p	1.76	Ift52	1.07	Cyp2c67	-1.49	Pla2g4b	1.87
		Igf2bp3	-1.10	Rbm8a	-1.64	Rbm8a	-1.60
				Cdk5r1	-1.36		
				Kcns1	1.84		
miR-184-5p	-2.84	Ect2	-1.32	Rnf20	-1.58	-	
		Wls	-1.31	Prrc2c	-1.49		
miR-1188-3p	-1.99	-		Leng8	-1.57	Fgf4	1.58
				Uspl1	-1.32		
				Brix1	1.23		
miR-1902	-1.89	-		Sap130	-1.45	Acad11	-2.12
				Bach2	1.21	Esyt2	-2.41

Table 3.10 shows the regulated mature miRNAs that are significantly regulated in zygotes and their potential target genes among the significantly regulated genes in zygotes, 2-cell embryos and blastocysts. Two upregulated miRNAs (miR-28a-3p and miR-7040-5p) do not share any potential target genes with the regulated genes in preimplantation embryos. Upregulated miR-7669-3p correlates with slightly upregulated *Ift52* and downregulated *Igf2bp3* in zygotes, downregulated *Cyp2c67*, *Rbm8a*, *Cdk5r1* and upregulated *Kcns1* in 2-cell embryos as well as upregulated *Pla2g4b* and downregulated *Rbm8a* in blastocysts. Downregulated miR-184-5p correlates with downregulated *Ect2* and *Wls* in zygotes as well as downregulated *Rnf20* and *Prrc2c* in 2-cell embryos. Downregulated miR-1188-3p has no potential target genes in the regulated genes in zygotes, but correlates with downregulated *Leng8* and *Uspl1* and upregulated *Brix1* in 2-cell embryos and upregulated *Fgf4* in blastocysts. Downregulated miR-1902 has no potential target genes in the regulated genes in zygotes, but correlates with downregulated *Sap130* and upregulated *Bach2* in 2-cell embryos and downregulated *Acad11 and Esyt2* in blastocysts.

TABLE 3.11 | POTENTIAL TARGET GENES OF REGULATED MIRNAS IN 2-CELL EMBRYOS

		Potential targets			
		2-Cell Embryo		Blastocyst	
miRNA (2-Cell Embryo)	*FC*	*Gene Symbol*	*FC*	*Gene Symbol*	*FC*
miR-7055-5p	**2.54**	*Cdc14b*	**-1.47**	*Pogz*	**-1.50**
		Senp2	**-1.37**		
miR-6237	**2.40**	*Lrif1*	**1.90**	*Cdc73*	**-1.95**
		Zfp735	**1.30**	*Dpysl2*	**-1.45**
		Lcp2	**1.41**		
		Raph1	**-1.16**		
		Kpna1	**-1.87**		
miR-7042-5p	**2.38**	*Jam2*	**1.19**	*Sema5a*	**-1.73**
		Cdk5r1	**-1.36**	*Usp15*	**-1.64**
		Sgk3	**1.52**		
		Sf3b2	**-1.49**		
miR-7044-3p	**2.25**	-		-	
miR-2861	**1.47**	*Jam2*	**1.19**	*Rrbp1*	**1.71**
				Trip12	**-1.36**
miR-6368	**1.42**	*Ywhaq*	**1.68**	*Ablim1*	**-2.13**
		Kif5b	**-1.83**	*Kif5b*	**-1.68**
		Cd247	**1.66**	*Sema5a*	**-1.73**
		Sgk3	**1.52**		
miR-1894-3p	**1.26**	*Kif5b*	**-1.83**	*Kif5b*	**-1.68**
		Stk38l	**-1.29**		
miR-20a-5p	**-2.50**	*Sertad2*	**-1.49**	*Rb1cc1*	**-1.50**
		Atad2	**-1.53**	*Ccng2*	**-2.13**
		Pbx3	**-1.60**	*Pkd2*	**-2.14**
		Ankrd17	**-1.40**	*Dennd5b*	**-1.45**
		Tet1	**-1.55**	*Dpysl2*	**-1.45**
		Gad2	**1.55**	*Vldlr*	**-1.69**
		Tle4	**-1.73**	*Ccnd1*	**2.13**
		Slc25a36	**-1.84**		
		Rock2	**-1.24**		
		D030056L22Rik	**-1.45**		
miR-743a-3p	**-1.93**	*Cetn3*	**1.53**	*Akap11*	**-2.37**
		Rraga	**1.34**	*Sf1*	**-1.39**
		Sertad2	**-1.49**	*Kif5b*	**-1.68**
		Rwdd2b	**1.20**	*Pogz*	**-1.50**
		Sod2	**-1.42**	*Rbm25*	**-1.65**
		Hipk1	**-1.82**	*Ccng2*	**-2.13**
		Kif5b	**-1.83**		
		Atad2	**-1.53**		
		Ctsa	**-1.55**		
		Zfp182	**1.40**		
		Ubn2	**-1.81**		
		Pikfyve	**-1.64**		
		Dag1	**-1.28**		

Table 3.11 shows the regulated mature miRNAs that are significantly regulated in 2-cell embryos and their potential target genes among the significantly regulated genes in 2-cell embryos and blastocysts. The upregulated miRNAs miR-7755-5p, miR-6237, miR-7042-5p,

miR-7044-3p, miR-2861, miR-6368 and miR-1894-3p correlate with downregulated genes *Cdc14b, Senp2, Raph1, Kpna1, Cdk5r1, Sf3b2, Kif5b* and *Stk38l* in 2-cell embryos and *Pogz, Cdc73, Dpysl2, Sema5a, Usp15, Trip12, Ablim1* and *Kif5b* in blastocysts potentially indicating a transcriptional inhibition. Downregulated miRNAs miR-20a-5p and miR-743a-3p correlate with upregulated genes *Gad2, Cetn3, Rraga, Rwdd2b* and *Zfp182* in 2-cell embryos and *Ccnd1* in blastocysts potentially indicating a decreased transcriptional inhibition.

TABLE 3.12 | POTENTIAL TARGET GENES OF REGULATED MIRNAS IN BLASTOCYSTS

| | | Potential targets | |
| | | Blastocyst | |
miRNA (Blastocyst)	FC	Gene Symbol	FC
miR-98-3p	2.57	4932438A13Rik	-2.07
		Dcaf1	-1.36
		Camk2d	-1.41
		Eps15l1	-1.49
		Rb1cc1	-1.50
		Rnf115	-1.96
miR-3112-5p	-3.93	Abca3	-1.37
		Nepro	-1.41
		Vldlr	-1.69
miR-32-5p	-3.00	4932438A13Rik	-2.07
		Golga4	-1.34
		Fnbp4	-1.63
		Glyr1	-1.23
		D1Ertd622e	-2.34
		Rrbp1	1.71
miR-465a-5p	-2.78	Cfap20	-1.89
		Stag2	-1.73
		Ppig	2.17
		Usp15	-1.64
miR-7055-5p	-2.59	Pogz	-1.50
miR-466f-3p	-2.32	Cdc73	-1.95
		Timm10	1.28
		Ube4a	2.12
		Trip12	-1.36
		Gm8300	-1.97
		Camk2d	-1.41
		Clip1	-2.11
miR-6988-5p	-2.22	Gm8300	-1.97
miR-463-5p	-2.14	Ppig	2.17
miR-871-3p	-2.01	Akap11	-2.37
		Tmem44	1.94
		Asb1	1.44
miR-465b-5p	-2.00	Cfap20	-1.89
		Stag2	-1.73
		Ppig	2.17
		Usp15	-1.64
miR-465d-3p	-1.63	Rbm25	-1.65
		Efcab11	-1.75

Table 3.12 shows the regulated mature miRNAs that are significantly regulated in blastocysts and their potential target genes among the significantly regulated genes in blastocysts. The upregulated miR-98-3p correlates with downregulated genes *4932438A13Rik*, *Dcaf1*, *Camk2d*, *Eps15l1*, *Rb1cc1* and *Rnf115* in blastocysts potentially indicating an increased transcriptional inhibition. The downregulated miRNAs miR-3112-5p, miR-32-5p, miR-465a-5p, miR-7055-5p, miR-466f-3p, miR-6988-5p, miR-463-5p, miR-871-3p, miR-465b-5p and miR-465d-3p correlate with upregulated genes *Rrbp1*, *Ppig*, *Timm10*, *Ube4a*, *Tmem44* and *Asb1* in blastocysts potentially indicating a decreased transcriptional inhibition.

3.5 Parental HFD-induced alterations of the transcriptome are not consistent during the course of development

3.5.1 Differentially expressed transcripts between liver tissue during development

Differential expression analysis revealed transcriptomic differences between HFD and LFD offspring already at the age of 3 weeks. Especially in liver these differences were found independent of a sex-specific or combined analysis. Moreover, transcriptomic differences were also present in the developing liver tissue during organogenesis. In order to find genes potentially involved in the transmission of metabolic changes induced by parental HFD, regulated transcripts in liver were compared between the different developmental stages (Figure 3.30).
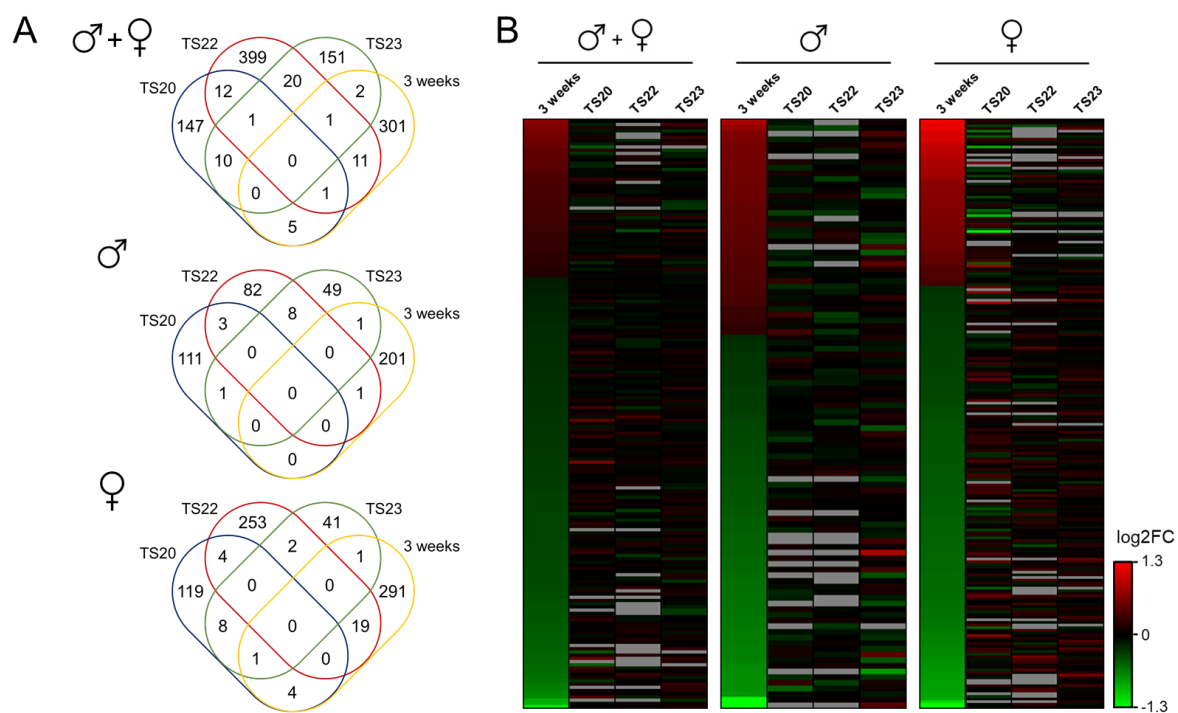
FIGURE 3.30 | COMPARISON OF REGULATED LONG TRANSCRIPTS BETWEEN LIVER TISSUES

Comparison of regulated transcripts in liver tissue throughout the different developmental stages. A shows the significantly regulated transcripts (p < 0.01) overlapping between TS20, TS22, TS23 and 3 weeks of age in males and females (upper panel), males (middle panel) and females (lower panel) in Venn diagrams. B displays the log2 fold changes (log2FC) of significantly regulated transcripts (p < 0.01) at 3 weeks of age compared to their log2FC during organogenesis as heat maps. Red indicates upregulation and green downregulation whereas gray indicates a missing value due to filtering prior to statistical analysis.

Only very few significantly regulated transcripts in liver tissue overlap during organogenesis and the age of 3 weeks independent of analyzing the sexes together or separately (Figure 3.30 A). These overlapping transcripts are listed in Table 3.13. In most cases, transcripts that are significantly regulated at the age of 3 weeks do not show a similar upregulation or downregulation during organogenesis (Figure 3.30 B) and as shown in Figure 3.30 A, the majority of these transcripts are not significantly regulated.

TABLE 3.13 | OVERLAPPING REGULATED TRANSCRIPTS IN LIVER BETWEEN 3 WEEKS OF AGE AND ORGANOGENESIS

	Gene symbol	Transcript ID	3 weeks FC	TS20 FC	TS22 FC	TS23 FC
Males + Females						
	Pkp2	ENSMUST00000039408	-1.20	1.26	-1.16	ns
	F11	ENSMUST00000034064	1.23	ns	-1.31	1.28
	Usp36	ENSMUST00000151433	-1.42	-1.36	ns	ns
	Cpox	ENSMUST00000060077	-1.28	1.20	ns	ns
	Gm13340	ENSMUST00000117219	-1.23	1.52	ns	ns
	Gm13339	ENSMUST00000120651	-1.44	1.40	ns	ns
	Gm13341	ENSMUST00000120780	-1.21	1.40	ns	ns
	Pxmp4	ENSMUST00000000896	-1.27	ns	-1.15	ns
	Cers6	ENSMUST00000028426	-1.31	ns	-1.10	ns
	Josd1	ENSMUST00000023061	-1.17	ns	-1.09	ns
	mt-Cytb	ENSMUST00000082421	-1.17	ns	-1.11	ns
	Snx12	ENSMUST00000120389	-1.17	ns	-1.12	ns
	Ddi2	ENSMUST00000102484	-1.17	ns	-1.08	ns
	Gm8355	ENSMUST00000177767	-1.21	ns	1.17	ns
	Tubb2a	ENSMUST00000056427	-1.44	ns	1.17	ns
	Scd2	ENSMUST00000026221	-1.28	ns	1.12	ns
	Cyb5b	ENSMUST00000034400	-1.21	ns	1.25	ns
	Gpam	ENSMUST00000235957	-1.32	ns	1.09	ns
	Gm7694	ENSMUST00000179801	1.59	ns	ns	1.27
	Pctp	ENSMUST00000020864	-1.55	ns	ns	1.21
Males						
	Snx12	ENSMUST00000120389	-1.19	ns	-1.17	ns
	Ifi211	ENSMUST00000009340	-1.43	ns	ns	1.84
Females						
	Alb	ENSMUST00000031314	-1.19	1.42	ns	1.17
	Gm47503	ENSMUST00000215636	1.81	1.47	ns	ns
	9530086O07Rik	ENSMUST00000203503	1.53	-2.26	ns	ns
	Gm13341	ENSMUST00000120780	-1.21	1.41	ns	ns
	Gm13340	ENSMUST00000117219	-1.23	1.47	ns	ns
	mt-Cytb	ENSMUST00000082421	-1.36	ns	-1.16	ns
	Ncapg2	ENSMUST00000222761	1.64	ns	-1.14	ns
	Ncapg2	ENSMUST00000084828	1.59	ns	-1.12	ns
	Rpl39-ps	ENSMUST00000146505	-1.45	ns	1.24	ns
	Rpl23a-ps3	ENSMUST00000104925	-1.37	ns	1.23	ns

Rpl19-ps11	ENSMUST00000122422	-1.46	ns	1.28	ns
Usp39	ENSMUST00000070345	-1.70	ns	1.32	ns
Mesd	ENSMUST00000094215	-1.39	ns	1.18	ns
Prelid3b	ENSMUST00000016401	-1.30	ns	1.20	ns
Ubqln4	ENSMUST00000008748	-1.40	ns	1.24	ns
Rps6	ENSMUST00000102814	-1.26	ns	1.33	ns
Rps3a1	ENSMUST00000029722	-1.21	ns	1.15	ns
Cct6a	ENSMUST00000201414	-1.25	ns	1.14	ns
Sdhd	ENSMUST00000000175	-1.24	ns	1.15	ns
Gm6210	ENSMUST00000204734	-1.56	ns	1.27	ns
Gm26384	ENSMUST00000102183	-1.64	ns	1.45	ns
Gm11808	ENSMUST00000089430	-1.49	ns	1.23	ns
Gm8355	ENSMUST00000177767	-1.21	ns	1.22	ns
Gm9843	ENSMUST00000052867	-1.78	ns	1.30	ns
Gm10222	ENSMUST00000088336	-1.59	ns	ns	1.30

In the combined analysis of males and females, 2 genes were regulated in liver tissue at 3 weeks of age and two stages of organogenesis. *Pkp2* is downregulated at the age of 3 weeks and at TS22 but upregulated at Ts20, whereas coagulation factor XI (*F11*) is upregulated at the age of 3 weeks and at TS23 but downregulated at Ts22. 5 transcripts are regulated at 3 weeks of age and at TS20 but only *Usp36* is downregulated at both stages. 11 transcripts are regulated at the age of 3 weeks and at TS22 but only 6 of those (*Pxmp4*, *Cers6*, *Josd1*, *mt-Cytb*, *Snx12*, *Ddi2*) are downregulated at both stages. 2 transcripts are regulated at the age of 3 weeks and at TS23 but only *Gm7694* is upregulated at both stages.

In the analysis of male liver tissues, *Snx12* is downregulated at 3 weeks of age and at TS22 and one transcript is regulated at 3 weeks of age and at TS23 but in different directions.

In the analysis of female liver tissues, *Alb1* is downregulated at 3 weeks of age but upregulated at TS20 and TS23. 4 transcripts are regulated at 3 weeks of age and at TS20 but only *Gm47503* is upregulated at both stages. 19 transcripts are regulated at 3 weeks of age and at TS22 but only *mt-Cytb* is downregulated at both stages. 1 transcript is regulated at 3 weeks of age and at TS23 but not in the same direction.

Therefore, comparison of the significantly ($p < 0.01$) regulated transcripts between liver tissue at 3 weeks of age and liver tissue during different stages of organogenesis yields no transcript that is consistently regulated in offspring liver due to parental HFD treatment.

3.5.2 Regulated pathways in liver tissues during the course of development

Although no transcripts are significantly regulated consistently in liver tissue of all developmental stages in HFD compared to LFD offspring, different transcripts can still be involved in similar biological processes. Therefore, affected GO terms by significantly regulated genes of the different developmental stages were compared and are shown in Table 3.14.

TABLE 3.14 | COMPARISON OF AFFECTED BIOLOGICAL PROCESSES IN LIVER

Biological processes	Males				Females			
	3 weeks	TS20	TS22	TS23	3 weeks	TS20	TS22	TS23
Lipid metabolism	+	-	+	+	+	+	+	-
Glucose metabolism	+	-	+	+	-	-	+	+
Protein metabolism	-	-	-	+	+	+	+	+
Gene expression (DNA/RNA metabolism)	-	+	+	-	-	+	+	+
Signaling pathways	+	+	+	+	+	-	-	-
Response to hormones	-	+	+	+	+	-	+	-
Immune response	-	-	-	+	-	+	-	+
Apoptosis	-	-	+	-	-	+	+	-

Metabolic processes such as lipid, glucose and protein metabolism were found to be affected in liver tissue at the age of 3 weeks, however, differences exist between males and females. Similarly, most of these metabolic processes were also affected during organogenesis in male and female liver tissue. Especially many GO terms involved in the lipid metabolism were affected in liver tissue of HFD offspring. The group of nucleic acid metabolism including regulation of gene expression and splicing is not significantly affected at the age of 3 weeks but is affected during organogenesis in males and females. The group "signaling pathways" includes a broad range of various pathways such as insulin signaling, TRK receptor signaling, MAPK cascade, JAK-STAT cascade, TOR signaling and Wnt signaling. Some of these are affected in male liver tissue at the age of 3 weeks and also during organogenesis and females at the age of 3 weeks. The response to different hormones such as an insulin stimulus, leptin or glucocorticoids is summarized as "response to hormones". This group is mainly affected in

male liver during organogenesis and female liver at 3 weeks of age and TS22. The groups "immune response" and "apoptosis" are not affected in liver tissue at 3 weeks of age but at a few stages during organogenesis in males and females.

3.5.3 Alterations in the transcriptome from early embryo to juvenile mouse

HFD-induced changes in gene expression in the preimplantation embryo that are still altered during organogenesis and in metabolically active tissues in the juvenile mouse could hint to their involvement in the epigenetic transmission of this metabolic phenotype. In order to investigate this possibility and find potential candidate genes, expression of significantly (FDR < 0.1) regulated transcripts during the preimplantation stages was compared to their expression in liver tissue during organogenesis and different tissues at the age of 3 weeks. Therefore, log2FC values for the same gene between HFD and LFD offspring over all the analyzed developmental stages and tissues were plotted in a heat map (Figure 3.31).
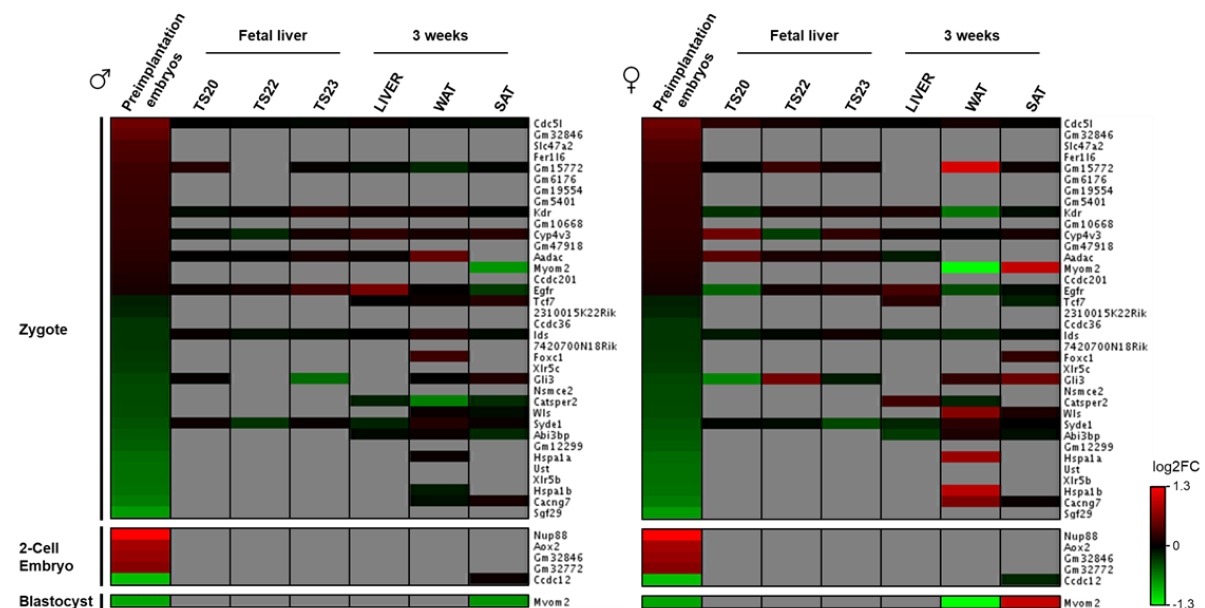
FIGURE 3.31 | COMPARISON OF REGULATED TRANSCRIPTS THROUGHOUT DEVELOPMENT

Comparison of regulated transcripts in preimplantation embryos throughout the different analyzed developmental stages and tissues in males (left) and females (right). Displayed are the log2FC of significantly regulated transcripts (FDR < 0.1) in preimplantation embryos compared to their log2FC (not significant) during organogenesis and at 3 weeks of age as heat maps. Red indicates upregulation and green downregulation whereas gray indicates a missing value due to filtering prior to statistical analysis.

Various genes that are significantly regulated (FDR < 0.1) in zygotes (36), 2-cell embryos (5) and blastocysts (1) are not or lowly expressed in the analyzed tissues during organogenesis and

at 3 weeks of age and therefore have no log2FC value assigned (indicated by gray area). In both males and females, some genes are consistently expressed throughout the developmental stages such as *Cdc5l*, *Kdr*, *Cyp4v3*, *Egfr*, *Ids*, and *Syde1* and some genes are expressed in most of the analyzed stages such as *Gm15772*, *Aadac*, *Gli3*, and *Abi3bp*. However, most of these genes do not show a relevant upregulation or downregulation. Interestingly, *Gli3* is significantly downregulated at the zygotic stage and also in the male fetal liver at TS23 as well as in females at TS20 but upregulated in female fetal liver at TS22. *Tcf7, Catsper2* and *Abi3bp* which are significantly but mildly downregulated in zygotes are not expressed in the fetal liver tissue but are expressed in tissues at 3 weeks of age in a sex-specific manner. Furthermore, other genes that are significantly regulated in zygotes are only expressed in both or either of the adipose tissues at 3 weeks of age and often in a sex-specific manner such as *Myom2*, *Foxc1*, *Wls*, *Hspa1a*, *Hspa1b*, and *Cacng7*. Interestingly, *Myom2* which is mildly upregulated in zygotes and downregulated in blastocysts, is downregulated in male SAT at 3 weeks of age whereas in females it is downregulated in WAT and upregulated in SAT at 3 weeks of age.

In this comparison of significantly regulated transcripts at early embryonic stages with their expression during later development yields no transcripts that are consistently regulated throughout development due to parental HFD treatment.

4. Discussion

With this comprehensive transcriptome analysis covering important developmental stages of the F1 generation we aim to find commonly regulated transcripts or regulatory elements that could hint to a mechanism and/or involved epigenetic regulators for the intergenerational epigenetic inheritance of DIO and T2D.

In a great number of rodent studies, the consequences of different dietary regimes such as LPD and HFD on the offspring's metabolic phenotype have been tested (reviewed in (*2*)). It has been shown that nutrition in the parental generation can have profound effects on the progeny by intergenerational and transgenerational epigenetic inheritance. Previous work in our lab could show intergenerational inheritance of HFD-induced obesity and glucose intolerance exclusively through the gametes. Sex-specific and parent-of-origin specific metabolic differences were found in adult offspring undergoing HFD challenge (*162*). Therefore, the aim of this work was to elucidate the mechanistic link between parental dietary treatment and offspring's metabolic phenotype by analyzing transcriptome differences throughout development.

4.1 Transcriptome in tissues of young HFD offspring and during organogenesis

The F0 generation that derived from wildtype and unchallenged ancestors was treated with either HFD or LFD from the age of 9 to 15 weeks. HFD-treated males and females thereby significantly increased their body weight and glucose intolerance (Figure 3.1) similar to what was shown in our previous study (*162*) and numerous other studies (*193-196*). Production of the F1 generation via IVF and embryo transfer into healthy foster mothers excluded confounding factors and therefore, real intergenerational epigenetic inheritance could be achieved with transmission of parental information exclusively via the gametes. In the F1 generation, HFD offspring showed slightly but significantly increased body weight in both males and females compared to LFD offspring already at the age of 3 weeks (Figure 3.2) as well as in adulthood after undergoing an HFD challenge (Figure 3.4). This finding is in contrast to previous results (*162*) in which increased obesity was only observed in females. However, impaired glucose tolerance was found only in male F1 (HxH), consistent with previous results (*162*). These results prove once more the intergenerational epigenetic inheritance of an HFD-induced metabolic phenotype via the gametes.

4.1.1   3 weeks old F1 generation

At the age of 3 weeks, the transcriptome of several organs was screened using microarrays revealing sex-specific differences between HFD and LFD offspring (Figure 3.7). The set of significantly regulated genes allows a clustering according to the parental diet (Figure 3.8) and shows that biological processes affected by these genes are often metabolism-related but also involved in immune response, apoptosis and different signaling pathways such as MAPK cascade and Wnt signaling (Figure 3.9). Nevertheless, they are also sex-specific in part. These major sex differences in the transcriptome and the affected processes might explain the sex-specificity in the metabolic phenotype in adult mice.

Similar to this first transcriptomic screening, RNA sequencing was performed on liver, WAT and SAT showing distinct clustering with more similarities between the adipose tissues. Separately plotted, liver samples cluster according to parental diet in males and females, WAT samples only cluster in females and SAT samples cluster only weakly in males (Figure 3.10). Significantly regulated transcripts were found in all three tissues with very little overlap between males and females in each tissue (Figure 3.11 A, B). Corresponding heat maps show clustering according to the parental diet especially when males and females were analyzed separately (Figure 3.12). These findings are similar to the results of the microarray analysis and also here, a drastic difference between males and females was observed in WAT. Due to these differences and the sex-specific metabolic phenotype in adulthood, transcriptomes of males and females were analyzed separately. Moreover, overlap of significantly regulated transcripts between the tissues is also relatively low (Figure 3.11 C, D). Interesting regulated genes in liver, WAT and SAT are highlighted below.

Liver:

- In males and females, dimethylarginine dimethylaminohydrolase 1 (*Ddah1*) is significantly regulated and was reported to be protective against HFD-induced hepatic steatosis and insulin resistance (*197*). Therefore, downregulation of this gene in males (-1.35) and females (-1.50) could be contributing to the metabolic phenotype in adulthood. Enoyl Coenzyme A hydratase domain containing 2 (*Echdc2*), enoyl-Coenzyme A, hydratase (*Ehhadh*) and insulin induced gene 2 (*Insig2*) are involved in lipid metabolism and regulated in male (*Echdc2* +1.68; *Ehhadh* -1.66; *Insig2* -2.22) and female (*Echdc2* -1.71; *Ehhadh* -1.58; *Insig2* -1.77) liver. Moreover, in *ob/ob* mice, additional deletion of phosphatidylcholine transfer protein (*Pctp*) led to improved glucose tolerance (*198*) and in wildtype mice, *Pctp* deficiency caused an increase in hepatic insulin sensitivity as well as altered glucose metabolism and body fat composition (*199*) indicating a pathogenic role in the formation of diabetes. In line

with these metabolic alterations, downregulation of *Pctp* in males (-1.45) and females (-1.72) could play a role in altering the metabolic phenotype in HFD offspring.

- In males, upregulated genes ATPase, Cu++ transporting, beta polypeptide (*Atp7b*) (+1.42) and catechol-O-methyltransferase (*Comt*) (+1.38) were shown to increase metabolic dysfunction in mice (*200, 201*), whereas mice with whole-body deletion of downregulated perilipin 2 (*Plin2*) (-1.37) develop obesity (*202*). Deletion of downregulated Kruppel-like factor 11 (*Klf11*) (-1.37) induces MODY VII and neonatal diabetes in humans but increased insulin sensitivity in mice (*203, 204*). Therefore, these genes are potentially involved in parental HFD-induced metabolic disorders.

- In females, Rho-associated coiled-coil containing protein kinase 2 (*Rock2*), which contributes to glucose intolerance and insulin resistance is upregulated (+1.42) (*205*). Downregulated NADH:ubiquinone oxidoreductase subunit AB1 (*Ndufab1*) (-1.40) is reported to be protective against obesity and insulin resistance (*206*). Moreover, dysfunction of downregulated genes Trk-fused gene (*Tfg*) (-1.41) and glutathione S-transferase (*Gstp*) (-1.42) leads to increased glucose intolerance (*207, 208*), which is in line with the observed metabolic phenotype in adulthood.

WAT:

- In males, gene expression of the adipocytokine leptin (*Lep*) is significantly increased (+2.90) in offspring of HFD-treated parents, which is in line with the enhanced body weight compared to LFD offspring these mice exhibit and with increased leptin levels in adiposity (*209*). The natriuretic peptide receptor 3 (*Npr3*), which is significantly upregulated (+2.45) is a promising candidate gene for obesity (*210*) and its deletion was shown to be protective against DIO (*211*). Knockout of kinesin family member 5B (*Kif5b*) in adipose tissue was shown to increase obesity and insulin resistance in DIO mice (*212*) corresponding to its downregulation (-1.64) in male offspring of HFD-treated parents.

- In females, Kruppel-like factor 9 (*Klf9*) is downregulated (-1.87) in HFD offspring while loss of *Klf9* function predisposes mice to obesity (*213*). Deficiency of thiosulfate sulfurtransferase (*Tst*) was reported to lead to exacerbated obesity and diabetes in mice (*214*). Therefore, downregulation of *Tst* (-2.49) is in line with the increased body weight at the age of 3 weeks. Salt inducible kinase 2 (*Sik2*) increases glucose uptake in adipocytes (*215*) and deletion of retinol saturase (*Retsat*) was shown to increase adiposity and alter hepatic lipid composition by indirectly influencing PPARG activity (*216, 217*). Both of these genes are downregulated (*Sik2* -2.90; *Retsat* -3.67) in HFD offspring indicating a role in the metabolic differences between HFD and LFD offspring. Uncoupling protein 3 (*Ucp3*) is involved in lipid homeostasis and strongly

downregulated (-6.03) in HFD offspring indicating a role in the formation of the observed metabolic phenotype (*218*). Furthermore, the family members of peroxisome proliferator-activated receptors (Ppar) function as master regulators of various cellular processes such as adipogenesis, lipid metabolism and glucose homeostasis. Two of the three subtypes, Ppar gamma (*Pparg*) (-4.97) and Ppar alpha (*Ppara*) (-5.77) are downregulated in female WAT. Although *Pparg* increases insulin sensitivity and is required for differentiation of adipose tissue, its inhibition was also shown to ameliorate DIO and T2D (*219, 220*). Furthermore, lipin 1 (*Lpin1*) plays an important role in lipid metabolism as catalyzing enzyme in triglyceride synthesis and is markedly downregulated in females (-3.49). However, *Lpin1* deletion leads to lipodystrophy while promotion of obesity was rather achieved by *Lpin1* overexpression (*221*). HFD feeding also increased *Lpin1* expression in rats (*222*).

SAT:

- Similar to male WAT, adipocytokine-encoding *Lep* (*209*) and candidate obesity gene *Npr3* (*210*) are significantly increased in male (*Lep* +1.75; *Npr3* +1.66) and female (*Lep* +1.41; *Npr3* +1.42) HFD offspring. Similar to female WAT, downregulation of *Tst* in males (-1.55) and females (-1.51) corresponds to the increased body weight of HFD offspring (*214*).

- In males, upregulation of aryl-hydrocarbon receptor (*Ahr*) (+1.58) could lead to increased body weight in HFD offspring since whole-body deletion of *Ahr* protects mice from DIO (*223*). Downregulation of peroxiredoxin 4 (*Prdx4*) (-1.50), which confers protection against T2D (*224*), and cadherin 13 (*Cdh13*) (-1.62), which is reduced in obese mouse models (*225*) are in line with the observed metabolic phenotype in HFD offspring.

- In females, promotion of adipogenesis by cysteine dioxygenase 1 (*Cdo1*) might be reduced by *Cdo1* downregulation (-1.49) in HFD offspring (*226*). *Retsat* (-1.45) as well as *Sik2* (-1.40) - similar to female WAT - are downregulated in females indicating a role in the metabolic differences between HFD and LFD offspring. Moreover, family with sequence similarity 13, member A (*Fam13a*) is notably downregulated in female offspring of HFD-treated parents (-1.67) corresponding to the observed exacerbated metabolic phenotype in *Fam13a*-deficient mice (*227*).

This analysis clearly shows transcriptomic alterations in metabolically active tissues between 3 weeks old offspring of HFD- and LFD-treated parents. Some significantly regulated candidate genes such as *Ddah1*, *Plin2*, *Rock2*, *Lep*, *Npr3*, *Tst*, *Retsat* and *Lpin1* that could be causative for the metabolic differences in these mice were identified. Similar to the sex-specific

metabolic phenotype described in (*162*) these transcriptomic differences are sex-specific. Only a few regulated genes including *Lep*, *Npr3*, *Retsat*, *Sik2* and *Tst*, overlap between the different tissues at the age of 3 weeks.

Similarly, according to GO term analyses of all significantly regulated genes, metabolism-related processes are strongly affected in 3 weeks old HFD-derived offspring. In males, lipid metabolism is clearly affected in liver, whereas in WAT, glucose metabolism and different signaling pathways are over-represented. In SAT, lipid, glucose and protein metabolism as well as gene expression and hormone response are influenced by regulated genes (Figure 3.13). In females, lipid metabolism is mainly affected in all three tissues, whereas in WAT, also glucose and protein metabolism as well as different signaling pathways and immune response are over-represented (Figure 3.14).

4.1.2   Organogenesis of liver tissue

In order to trace the transcriptomic differences that were found in tissues of 3 weeks old offspring back to developing tissue during organogenesis, liver tissue transcriptome of F1 (HxH) and F1 (LxL) fetuses was analyzed at TS20, TS22 and TS23. During these Theiler stages, liver tissue is developing rapidly and phenotypic classification of fetuses is relatively simple. Overall, the different Theiler stages could be distinguished based on their transcriptomic pattern. Separation of the samples based on the parental diet is only possible in TS20 females, at TS22 and slightly in TS23 males (Figure 3.15). Significantly regulated transcripts were found in all Theiler stages in a sex-specific manner and with very few transcripts overlapping between the different Theiler stages. Hierarchical clustering in heat maps according to the parental diet was shown more clearly when males and females were plotted separately. Importantly, this analysis indicates that parental HFD causes different transcriptomic changes in the developing offspring depending on the sex (Figure 3.17). Interestingly, none or very few transcripts are regulated in all three or two of the analyzed Theiler stages, respectively. This suggests that the HFD-induced transcriptomic alterations in the developing liver are highly dynamic. Another explanation would be that the HFD-induced transcriptomic differences are negligible compared to the transcriptomic changes ongoing due to fetal development. Interesting genes that are differentially regulated during organogenesis are highlighted below.

TS20:

- In males and females, differentially expressed transcripts at this stage are mostly predicted genes with unknown function. Interestingly, chromodomain helicase DNA

binding protein 9 (*Chd9*) is upregulated in both males (+1.64) and females (+2.57), hinting at altered chromatin structure during liver formation in HFD offspring (*228*).

- In males, *Sik2* is downregulated (-1.75) while Sik2-deficiency in mice is associated with impaired glucose and insulin tolerance (*229*). Interestingly, *Sik2* is downregulated in female WAT and SAT at the age of 3 weeks as well.

- In females, ankyrin repeat and SOCS box-containing 4 (*Asb4*), which was reported to be involved in the control of feeding behavior and metabolic rate (*230*) is significantly downregulated (-1.45). Likewise, overexpression of *Asb1* (+1.48) has no apparent deleterious effects according to a study (*231*). Loss of ubiquitin-conjugating enzyme E2L 6 (*Ube2l6*), which is upregulated (+1.73) in females was associated with resistance to obesity (*232*). Conspicuously, many histone variants are upregulated in females suggesting an altered chromatin structure at TS20 due to parental HFD treatment.

TS22:

- In males, insulin-like growth factor binding protein 1 (*Igfbp1*) is significantly downregulated (-1.42), while deletion of *Igfbp1* in a mutant mouse model resulted in increased body weight and fat mass (*233*).

- In females, caseinolytic mitochondrial matrix peptidase proteolytic subunit (*Clpp*) is significantly upregulated (+1.52). As loss of *Clpp* was shown to be protective against DIO and insulin resistance (*234, 235*) this upregulation during organogenesis could lead to the observed metabolic phenotype after birth. Furthermore, *Asb4* is upregulated (+1.39) in females at TS22, in contrast to its downregulation at TS20 (*230*) suggesting stage-specific alterations in gene expression due to parental HFD.

TS23:

- In males and females, hepcidin antimicrobial peptide (*Hamp*) is strongly upregulated (males +1.61; females +2.24), which fits well with the finding that hepatocytes of *Hamp*-deficient mice exhibit greater insulin sensitivity than those of wildtype mice (*236*). This upregulation of *Hamp* could be a first indication of reduced insulin sensitivity in adulthood. On the other hand, upregulation of pterin 4 alpha carbinolamine dehydratase/dimerization cofactor of hepatocyte nuclear factor 1 alpha (TCF1) 1 (*Pcbd1*) in males (+1.41) and females (+1.34) is in contrast to impaired glucose tolerance observed in *Pcbd1*-deficient mice (*237, 238*).

- In males, neutrophil expressed elastase (*Elane*), which was shown to be elevated in HFD-fed mice and to increase the immune response (*239*) is upregulated (+1.47). Similar to males and females at TS20, the chromatin modifier *Chd9* is upregulated (+2.00) in males at TS23 (*228*). In addition, betaine-homocysteine methyltransferase

(*Bhmt*) is involved in the regulation of hepatic gluconeogenesis and its deficiency reduces body fat content in mice (*240, 241*). Therefore, upregulation of *Bhmt* (+1.42) in males during liver formation insinuates metabolic dysfunction in adulthood.

- In females, phosphoglucomutase 2 (*Pgm2*), which is involved in glucose metabolism is downregulated (-1.55) suggesting metabolic differences during liver formation.

Accordingly, GO terms that are affected by differentially expressed genes in males are regulation of gene expression and hormone response at TS20 and mostly metabolic processes at TS22 and TS23 (Figure 3.13). In females, different metabolic processes in all Theiler stages as well as gene expression regulation especially at TS22 and immune response mainly at TS20 and TS23 are over-represented (Figure 3.19).

4.1.3 Comparison of liver tissue during organogenesis and at the age of 3 weeks

Comparison of liver tissues throughout the different developmental stages revealed no transcripts that are significantly altered at all stages. However, comparing expression ratios of genes that are (not necessarily significantly) regulated between the different stages highlights some interesting genes.

- Phosphatidylcholine transfer protein (*Pctp*) is involved in lipid metabolism (*242*). Although its whole-body deficiency caused an increase in hepatic insulin sensitivity in mice, reduction in hepatic glucose production, gluconeogenesis, and glycogenolysis together with low gene expression in liver per se and alterations in body fat composition were observed as well (*199*). Consistently, *Pctp* is significantly downregulated in male (-1.45) and female (-1.72) liver at the age of 3 weeks in HFD offspring, whereas it is mostly higher expressed in HFD male (TS20 +1.04; TS22 +1.08; TS23 +1.25) and female (TS20 +1.20; TS22 -1.02; TS23 +1.17) offspring during liver formation although not significantly. Here, downregulation of *Pctp* in liver seems to impact lipid and glucose metabolism at the age of 3 weeks but not during organogenesis.

- Several members of the Kruppel-like factor (Klf) family are involved in the regulation of glucose homeostasis (*243*). Knock-out of *Klf3* led to leaner mice that are protected against DIO and glucose intolerance (*244, 245*). In developing liver of HFD offspring, *Klf3* was significantly downregulated in females at TS22 (-1.21) and TS23 (-1.28), whereas at the age of 3 weeks, downregulation in males (-1.23) and upregulation in females (+1.13) was apparent but not significant. Interestingly, *Klf11*, which is involved in lipid metabolism while KLF11 deficiency leads to increased insulin sensitivity and

resistance to DIO (*204*) was significantly downregulated in male liver (-1.37) at the age of 3 weeks. Moreover, *Klf9* is downregulated in female WAT (-1.87) corresponding to the observation that deletion of *Klf9* predisposes mice to obesity (*213*).

Overall, analysis of tissues during organogenesis and in juvenile mice substantiates transcriptomic differences between offspring of HFD-treated parents and offspring of LFD-treated parents already in these early stages of development. Although comparison of liver transcriptome analyses could not reveal particular genes that are responsible for the formation of the epigenetically transmitted metabolic phenotype, candidate genes that might be involved in the process were identified. However, the rapidly changing transcriptome during organ formation, which is suggested by clustering in the PCA might have blunted the small differences due to the parental diet and renders the comparison to other developmental stages complicated. Nevertheless, *Pctp* and certain members of the *Klf* family might be interesting candidate genes.

Additionally, comparison of the GO terms affected by the regulated genes of each stage shows high similarities, especially within the same tissues and within the same sex. Overall, mostly affected by parental HFD are metabolic processes such as lipid, glucose and protein metabolism. Interestingly, the same metabolic processes are affected by different genes in each tissue showing that although parental HFD influences gene expression differently in males and females as well as at different developmental stages, the impact on cellular processes might be the same. These sex-specific metabolic changes on the molecular level are in line with the sex-specific metabolic changes in HFD-derived F1 mice at the age of 3 weeks and in adulthood.

4.2 Transcriptome in preimplantation embryos

4.2.1 Long RNA transcripts

Sequencing of long RNAs in preimplantation embryos yielded 248 significantly regulated (p < 0.01) transcripts in zygotes, 432 in 2-cell embryos and 154 in blastocysts. On the basis of these transcripts, a clear distinction between HFD and LFD offspring through hierarchical clustering was only possible in zygotes. Taking only genes into account that were regulated with FC > 1.3, 40 genes were found in zygotes, 242 in 2-cell embryos and 99 in blastocysts. A high proportion of these regulated genes are required during oogenesis or spermatogenesis or in embryonic development. Some genes are involved in metabolic processes for instance in insulin action such as three genes of the heat shock protein family that are all downregulated in zygotes. Furthermore, many genes are involved in DNA/RNA metabolism for example as transcriptional regulators (several zinc finger proteins (*Zfp*), *Rbm8a*) (*246*), in splicing (*Cdc5l*, *Srsf6*, *Rbm25*) or miRNA processing (*Drosha*) (*247*). Additionally, genes that act as epigenetic regulators by DNA/tRNA (de-)methylation (*Pgk2*, *Lcmt2*, *Tet1*, *Nsun2*) (*248-250*) and histone modification (*Ctbp2*, *Esco2*, *Kansl3*, *Usp16*, *Setd3*, *Rnf20*, *Usp22*, *Cdc73*) (*251*) are differentially regulated. Potential candidate genes and their functions are described in more detail in chapter 4.2.3.

GO terms that are mostly affected by differentially regulated genes in preimplantation embryos are related to protein metabolism as well as DNA/RNA metabolism (Figure 3.25). The term protein metabolism includes formation and degradation of proteins as well as their modification. In order to start development in the early embryo, transcription starts in the ZGA and produces amongst others many genes involved in translation and protein modification. Parental HFD seems to alter the expression of some of these genes, which in turn could lead to altered proteins or protein content in the early embryo or later on. DNA/RNA metabolism includes terms for example related to gene expression, RNA processing, gene silencing via miRNAs or histone modification. Expression of many genes involved in these metabolic processes are altered in HFD-derived early embryos. This way, the expression of numerous other genes can be affected and altered already in the preimplantation embryo or later in development. Especially the epigenetic changes via miRNAs and on histones could have long-lasting effects on transcription of other genes. In zygotes, signaling pathways such as canonical Wnt signaling pathway (regulated genes: *Arntl*, *Wls*, *Gli3*, *Bcl9*, *Tcf7*, *Amer1* and *Fzd7*) and MAPK cascade (regulated genes: *Spred1* and *Spred2*) are also affected hinting at an influence on basic molecular pathways of parental HFD. On the one hand, the canonical Wnt signaling pathway mediates regulation of gene transcription via

accumulation of the transcriptional co-activator β-catenin and on the other hand, it is involved in embryonic development for example by controlling body axis patterning and cell fate determination. Despite the crucial role of Wnt genes and the Wnt signaling pathway, no negative impact on embryonic development was observed in this mouse model of parental HFD indicating no or only a mild effect on this signaling pathway. The MAPK cascade is a signal transduction pathway that modulates transcription and is involved in many other biological processes. In this model of parental HFD, *Spred1* and *Spred2* that act as inhibitors of the MAPK signaling pathway (*252*) are only slightly downregulated in zygotes suggesting minimal impact on the function of the MAPK signaling pathway.

4.2.2   Small RNA transcripts and miRNA target genes

Sequencing of small RNAs in preimplantation embryos yielded a small number of significantly regulated small RNAs (Figure 3.27). In the literature, miRNAs, piRNAs and tsRNAs are the small RNA classes most commonly associated with epigenetic inheritance of metabolic disorders (*63, 158, 171, 173, 253, 254*). Whereas the mechanisms of miRNA- and piRNA-mediated gene regulation and their roles in epigenetic inheritance are well established, the mechanisms behind tsRNA-mediated epigenetic inheritance are largely unknown.

6 mature miRNAs were found affected by parental HFD in zygotes, 9 in 2-cell embryos and 11 in blastocysts. miR-let-7c, miR-293-5p and miR-880-3p, which were significantly regulated in sperm of HFD-fed F0 and F1 males (*253*) as well as miR-19b, which was shown to induce obesity in mice when injected into naïve zygotes (*173*) were not among the significantly regulated miRNAs in our study. Another study found 11 upregulated and 2 downregulated miRNAs in HFD compared to control diet sperm (*254*), one of which miR-184 is also downregulated in HFD-derived zygotes. However, in HFD sperm the guide strand miR-184-3p was found downregulated whereas in zygotes the almost complementary passenger strand miR-184-5p is downregulated. A recent study investigating the transcriptome of blastocysts derived from obese fathers or mothers identified 11 miRNAs that were regulated in sperm of obese males and their target genes regulated in blastocysts (*255*). However, none of these miRNAs was significantly regulated in preimplantation embryos within our study. In the last years, many miRNAs were associated with metabolic diseases (reviewed in (*256*)) and just very recently, miR-128-1 was linked to obesity in humans and identified as a metabolic regulator in mice (*257*). However, an association to metabolic disorders could not be found for most of the significantly regulated miRNAs in our data. miR-2861, which is upregulated in 2-cell embryos (+1.47), might be an epigenetic regulator by targeting histone deacetylase 5 (*Hdac5*) (*258*). miR-20a-5p, which is downregulated in 2-cell embryos (-2.50) was shown to be downregulated in women with gestational diabetes mellitus (*259*). miR-466f-3p, which is

downregulated in blastocysts (-2.32) might be involved in the insulin signaling pathway (*260*). However, the association studies mentioned above usually investigate miRNAs in metabolically active tissues of adult mice, whereas in this case, miRNA changes were examined in preimplantation embryos.

36 piRNAs were found differentially regulated in zygotes, 23 in 2-cell embryos and 28 in blastocysts of HFD-treated parents, however, piRNA-025883, piRNA-015935 and piRNA-036085, which were found regulated in sperm of HFD-fed F0 and F1 males (*253*) were not among them. 11 tRNAs were found differentially regulated in zygotes, 7 in 2-cell embryos and 5 in blastocysts of HFD- treated parents. Coinciding, tRNA-glycine-GCC fragments (*63*) and fractions of tsRNAs (*171*) were altered in sperm of LPD- or HFD-challenged males, respectively. However, tsRNA content of resulting embryos was not examined in these studies complicating the comparison of results.

Target prediction analysis yielded a list of target genes for each regulated miRNA with some of these genes being also regulated in preimplantation embryos (Table 3.10, Table 3.11, Table 3.12). Target gene expression might be directly inhibited via RNA interference (RNAi) or enhanced via RNA-based gene activation (RNAa) (*62*). Potential candidate genes that are targets of regulated miRNAs and their functions are described in more detail in chapter 4.2.3.

4.2.3   Candidate genes of epigenetic inheritance

Differential gene expression analysis of long and small RNAs in preimplantation embryos identified candidate genes that are potentially involved in the intergenerational epigenetic transmission of the metabolic syndrome. Those genes are described below.

- Although the family of ubiquitin specific peptidases (*Usp*) functions in many different cellular processes (*261, 262*), they are able to act as epigenetic modifiers of the chromatin structure by deubiquitinating histones. *Usp16* (-1.51) and *Usp22* (-1.77) in 2-cell embryos as well as *Usp15* (-1.64) in blastocysts are significantly downregulated indicating a potential role in the epigenetic transmission of a metabolic phenotype to the offspring.
- Leucine carboxyl methyltransferase 2 (*Lcmt2*) and NOL1/NOP2/Sun domain family member 2 (*Nsun2*) are both differentially regulated in 2-cell embryos (*Lcmt2* +1.43; *Nsun2* -1.88) and act as tRNA methyltransferases (*248, 263*). Therefore, they might be involved in altering epigenetic signatures dependent on the parental diet during intergenerational inheritance.
- The large family of zinc finger proteins is involved in a variety of cellular functions but many of these proteins function in the DNA/RNA metabolism for example as

transcriptional regulators (*264*). Several genes encoding zinc finger proteins were found differentially regulated between HFD and LFD-derived preimplantation embryos. *Zfp712* (+2.07), *Zfp953* (+1.86), *Zfp715* (+1.67), *Zfp873* (+1.56), *Zfp442* (+1.44), *Zfp182* (+1.40), *Zfp955a* (+1.33), *Zfp955b* (+1.32), *Zfp735* (+1.30), and *Zfp97* (+1.30) are upregulated while *Zfp36l2* (-1.32) and *Zfp972* (-1.71) are downregulated.

- The E3 ubiquitin ligase *Rnf20* is involved in various processes such as regulation of hepatic lipid metabolism (*265*) and adipocyte differentiation (*266*) as well as regulation of β-cell gene expression and insulin secretion (*267*). It functions as an epigenetic regulator by ubiquitinating histones and is significantly downregulated in 2-cell embryos (-1.58) indicating a potential role in the transmission of transcriptional effects.

- The gene *Drosha* is strongly downregulated in 2-cell embryos (-2.08) of HFD-treated parents. Since the corresponding Drosha protein is required for miRNA processing (*247*), the downregulation could lead to alterations in the availability of necessary miRNAs as well as alterations in the composition of miRNA content in 2-cell embryos and maybe even in later stages.

- The Tet1 protein is essential for the DNA demethylation process (*249, 250*) and especially vital for genome-wide erasure of DNA methylation in the paternal genome after fertilization (*268*). Therefore, downregulation of *Tet1* in 2-cell embryos (-1.55) hints to incomplete erasure of DNA methylation and thus inheritance of specific epigenetic signatures to the offspring. Moreover, *Tet1* is a target of miR-20a-5p (-2.50), which is downregulated in 2-cell embryos.

- Serum/glucocorticoid regulated kinase 3 (*Sgk3*) seems to play a role in glucose homeostasis (*269*) among many other functions. It was found to be upregulated in 2-cell embryos (+1.52) and a target of miR-7042-5p (+2.38) and miR-6368 (+1.42) that are upregulated in 2-cell embryos as well. Furthermore, *Sgk3* is downregulated in female liver at TS22 (-1.27) and could be a candidate gene for HFD-induced intergenerational epigenetic inheritance.

- Rho-associated coiled-coil containing protein kinase 2 (*Rock2*) is downregulated in 2-cell embryos (-1.24) and a target of miR-20a-5p that is also downregulated in 2-cell embryos (-2.50). Additionally, *Rock2* is downregulated in female WAT (-1.66) and upregulated in female liver (+1.42) at the age of 3 weeks. Although an attenuation of HFD-induced glucose intolerance and insulin resistance was only shown in male mice with heterozygous *Rock2* deletion (*205*), it might still be an interesting candidate gene for the epigenetic inheritance of HFD-induced metabolic changes.

- Cyclin G2 (*Ccng2*) was shown to suppress Wnt signaling (*270*) and is downregulated in blastocysts (-2.13). Moreover, it is a target gene of miR-20a-5p (-2.50) and miR-743a-3p (-1.93), which are both downregulated in blastocysts.

- Nucleolus and neural progenitor protein (*Nepro*) is significantly downregulated in blastocysts (-1.41) and a target of downregulated miR-3112-5p (-3.93). It is essential for blastocyst formation and therefore vital in preimplantation development (*271*).

- Very low density lipoprotein receptor (*Vldlr*) is a negative regulator of Wnt signaling (*272*) and therefore important in embryonic development. Its downregulation in blastocysts (-1.69) as well as the downregulation of miR-20a-5p (-2.50) in 2-cell embryos and miR-3112-5p (-3.93) in blastocysts, which are both potential regulators of *Vldlr*, makes it an interesting candidate gene for the epigenetic transmission of this metabolic phenotype. However, whereas *Vldlr* deficiency was shown to be protective against HFD-induced obesity and to improve insulin resistance in mice (*273, 274*), overweight 3 weeks old F1 (HxH) females show a strong downregulation of *Vldlr* in liver (-2.66) and no significant regulation in adipose tissues.

- RNA binding motif protein 8a (*Rbm8a*) is downregulated in 2-cell embryos (-1.64) and blastocysts (-1.60) and a target of miR-7669-3p that is upregulated in zygotes (+1.76). Although it has been shown only in neurodevelopment and associated disorders so far (*246*), its crucial role in the degradation of erroneous and dispensable transcripts suggests a regulatory function on the transcript level during early development.

- Similar to its downregulation in male WAT (-1.64), *Kif5b*, which plays a role in obesity and insulin resistance (*212*) is significantly downregulated in 2-cell embryos (-1.83) and blastocysts (-1.68). Additionally, it is a target gene of several miRNAs that are significantly regulated in 2-cell embryos, namely miR-6368 (+1.42), miR-1894-3p (+1.26) and miR-743a-3p (-1.93).

Overall, several candidate genes were identified throughout development that are involved in epigenetic regulation and metabolic processes and could therefore be mediators of intergenerational epigenetic inheritance of metabolic disorders.

More importantly, our comprehensive study demonstrates that the whole process of intergenerational and transgenerational epigenetic inheritance is much more dynamic and versatile than suggested by earlier studies. Their claims that specific miRNAs (*173, 253-255, 257*), piRNAs (*253*) or fragmented tRNAs (*63, 171*) are sufficient and/or causative for epigenetic inheritance of metabolic disorders might be correct but are probably not showing the complete picture.

4.3 Genes and processes altered by parental HFD

Sequencing of long RNA transcripts and differential expression analysis between HFD and LFD offspring could identify specific genes that are altered by parental HFD during development and might therefore play a role in the intergenerational inheritance of a metabolic phenotype. Many genes were found significantly regulated that have a function in gametogenesis and embryogenesis, in epigenetic regulation during fertilization and early development, and in the regulation of metabolic processes such as lipid metabolism and glucose homeostasis. A selection of these genes is depicted in Figure 4.1 and was in part already described in previous chapters.
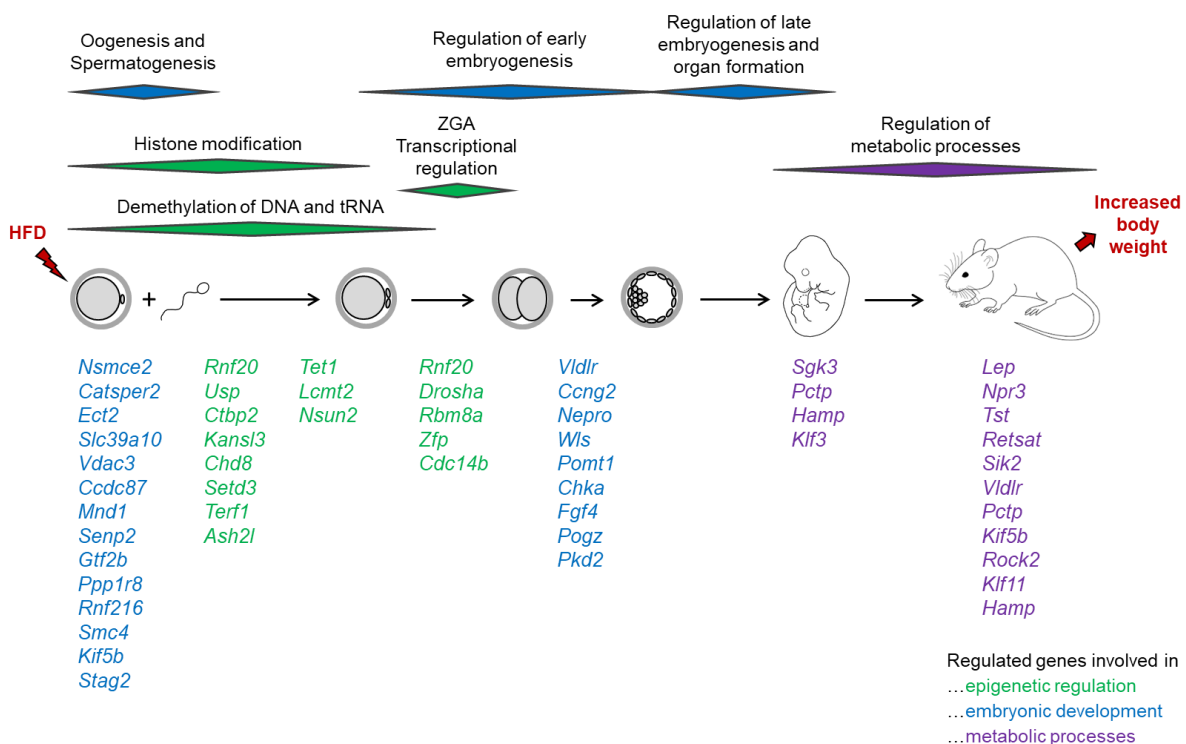
FIGURE 4.1 | GENES AFFECTED BY PARENTAL HFD THROUGHOUT DEVELOPMENT

Overview of important processes that might be altered by parental HFD and their corresponding differentially expressed genes. Depicted are processes and regulated genes throughout development that are involved in epigenetic regulation (green), in embryonic development (blue) and metabolic processes (purple).

Interestingly, many genes that are involved in developmental processes such as during gametogenesis and embryonic development are differentially expressed in preimplantation embryos derived from HFD parents. Moreover, several genes that act as epigenetic regulators through alteration of histone modifications, DNA and tRNA methylation, and gene expression are differentially expressed in HFD-derived preimplantation embryos. On the contrary, genes involved in the regulation of metabolic processes are mainly differentially expressed in

metabolically active tissues of HFD-derived offspring. Some of these regulated genes are also targets of differentially expressed miRNAs in preimplantation embryos. Due to the application of IVF in the production of the analyzed preimplantation embryos and tissues, the molecular information about the parental HFD treatment must have been transmitted via the gametes. Accordingly, every alteration in the epigenetic signatures during fertilization and early embryonic development might play a role in the intergenerational inheritance. *Tet1* is a highly interesting candidate gene as the Tet proteins are crucial for active demethylation of DNA after fertilization (*268*). Although, *Tet3* is reported to be mainly responsible for DNA demethylation in the paternal pronucleus, *Tet1* regulates the DNA methylation status and has a role in the cell specification in blastocysts (*249*). Parental HFD-mediated downregulation of *Tet1* in 2-cell embryos could therefore lead to notably altered methylation statuses of certain genes and affect overall embryonic development. The tRNA methyltransferase *Nsun2* contributes to tRNA stability (*248*) and might increase the abundance of (certain) tRNA fragments through its downregulation in 2-cell embryos. These fragments of tRNA could facilitate intergenerational epigenetic inheritance, which has been demonstrated already in other studies (*63, 173*) even though the mechanisms behind remain to be uncovered. Another promising candidate gene is *Drosha*. Its pivotal function in the processing of miRNA could be compromised by the 2-fold downregulation in HFD-derived 2-cell embryos. Thereby, alterations in the availability of vital miRNAs and/or alterations in the composition of miRNA content might be the consequence, which could ultimately lead to an altered metabolic phenotype. This altered metabolic phenotype is already present at the age of 3 weeks with increased body weight and even detectable in the transcriptome of liver and adipose tissues. Most interestingly, "obesity genes" *Lep* and *Npr3* are considerably upregulated in adipose tissues whereas genes *Tst* and *Retsat* that are protective against diabetes and obesity are significantly downregulated. The protective effect against HFD-induced hepatic steatosis and insulin resistance of *Ddah1* is diminished by its downregulation in liver. Moreover, several of the genes whose hepatic expression was found altered after HFD treatment in a genome-wide sequencing study (*275*) are also differentially regulated in liver of 3 weeks old HFD offspring, namely *Nat8f1*, *Adh4*, *Cyp2c55*, *Cyp4a10*, and *Cyp4a14* in males and *Aldh1b1* and *Gstt3* in females, although only males were examined in the above-mentioned study.

Various potential candidate genes were identified in the comprehensive analysis of significantly regulated genes over the course of development that could be causal for the epigenetic transmission of DIO and T2D. However, validation of these genes and a mechanistic proof is still pending.

Furthermore, over-represented biological processes were investigated and an overview of the affected processes at each developmental stage is presented in Figure 4.2.
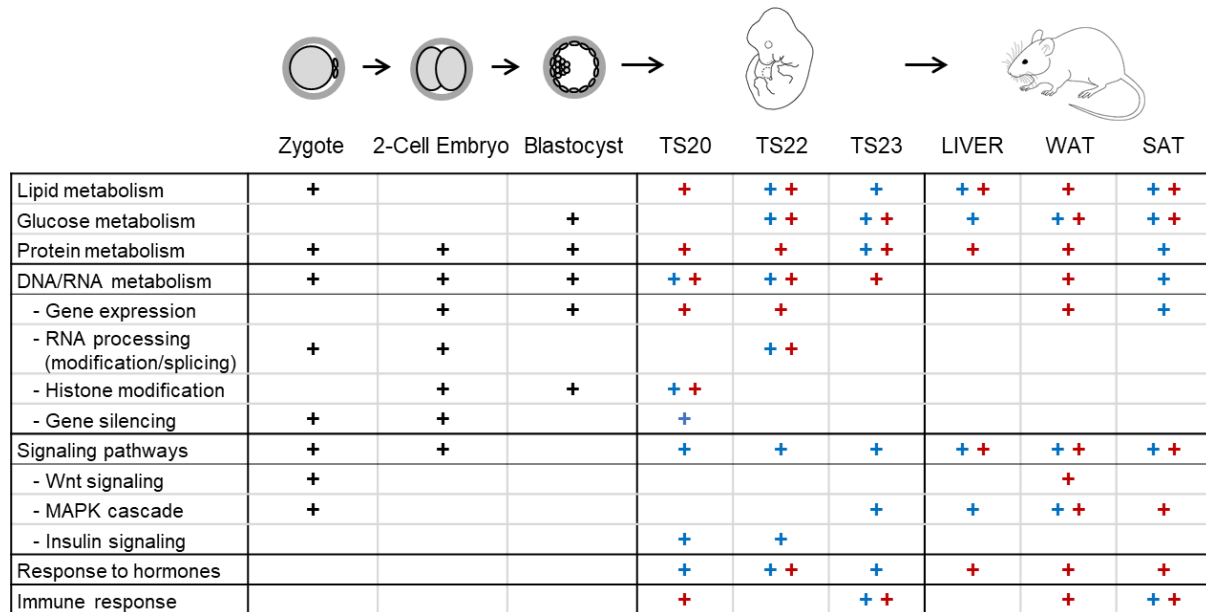

	Zygote	2-Cell Embryo	Blastocyst	TS20	TS22	TS23	LIVER	WAT	SAT
Lipid metabolism	+			+	+ +	+	+ +	+	+ +
Glucose metabolism			+		+ +	+ +	+	+ +	+ +
Protein metabolism	+	+	+	+	+	+ +	+	+	+
DNA/RNA metabolism	+	+	+	+ +	+ +	+		+	+
- Gene expression		+	+	+	+			+	+
- RNA processing (modification/splicing)	+	+			+ +				
- Histone modification		+	+	+ +					
- Gene silencing	+	+		+					
Signaling pathways	+	+		+	+	+	+ +	+ +	+ +
- Wnt signaling	+							+	
- MAPK cascade	+					+	+	+ +	+
- Insulin signaling				+	+				
Response to hormones				+	+ +	+	+	+	+
Immune response				+		+ +		+	+ +

FIGURE 4.2 | GO TERMS AFFECTED BY PARENTAL HFD THROUGHOUT DEVELOPMENT

Overview of important biological processes (GO terms) that are affected by differentially expressed genes in HFD offspring. The character "+" indicates the over-representation of the process stated on the left in the developmental stage or tissue stated above. If applicable, the sex of the analyzed tissues is indicated by blue (male) or red (female) color of the "+".

Metabolism-related processes are strongly affected in fetal liver as well as in liver and adipose tissues of 3 weeks old HFD-derived offspring in both males and females. Especially lipid and glucose metabolism, which are vital to energy homeostasis in the body are over-represented in the differentially regulated genes. Protein metabolism, which includes protein modifications as well, is affected in the metabolic tissues but also in all preimplantation stages. Here, posttranslational modifications of proteins and chromatin modifications are markedly affected suggesting alterations in epigenetic regulation of gene expression. Indeed, several processes that are part of the DNA/RNA metabolism such as gene expression, RNA processing, histone modifications, and gene silencing are affected in preimplantation embryos and especially in 2-cell embryos. Clearly, start of embryonic transcription during ZGA is of major importance for development and affected by a parental HFD. These DNA/RNA metabolic processes are still affected during organogenesis and in young mice but to a lesser extend with increasing age. A couple of different signaling pathways are affected throughout development. Interestingly, Wnt and MAPK signaling, which are inter alia vital during early development are over-represented in zygotes and also slightly affected in 3 weeks old mice. During organogenesis, insulin signaling and response to hormones such as insulin is affected mainly in males. At the age of 3 weeks, genes involved in the response to hormones such as

insulin, leptin and glucocorticoids are only affected in females. Furthermore, the immune response is over-represented in some of the tissues from HFD- compared to LFD-derived offspring corresponding to a chronic low-grade inflammation present in obesity (*276*).

Consequentially, changes in important pathways and in DNA/RNA metabolism during early embryonic development could actually hint to altered epigenetic regulation in preimplantation embryos originating from parental HFD treatment and influencing basic pathways and processes related to energy metabolism in offspring.

4.4 Limitations and further questions

This study gives a broad and comprehensive overview of the transcriptional changes due to parental HFD treatment over the course of development and therefore important insights into potential mechanisms of intergenerational epigenetic inheritance via the gametes. However, this comprehensiveness is also a disadvantage as it renders a more detailed view challenging and makes it difficult to exactly determine a responsible mechanism. Dysregulation of either specific genes or several genes combined during early embryonic development might cause epigenetic signature changes and therefore the inheritance of an environmentally induced phenotype. Altered expression of metabolically active genes in certain tissues could be cause or consequence of the metabolic phenotype. For example, *Npr3* was reported to be an obesity-causing gene (*210, 211*), therefore its upregulation in adipose tissue could lead to production of more adipose tissue and overall increase body weight. On the other hand, *Lep* mRNA content could be increased as a consequence of more adipose tissue.

Additionally, this study exhibits some technical and biological limitations.

Regarding technical issues, although RNA-Seq is a state-of-the-art technique it is very sensitive to even small differences in the sample preparation process and the bioinformatic analysis. Both steps were performed as accurately as possible in order to prevented batch effects within and between groups. Nevertheless, IVFs and embryo transfers were performed over several different days and weeks in order to reduce daily workload. This introduced a batch effect of two mouse cohorts in the tissue analysis of 3 weeks old mice. This batch effect was clearly visible in the PCA but could be adjusted for by defining it as a known covariate in the analysis. Similarly, a batch effect was unwillingly introduced during library preparation by different "amplification dates" of liver samples from TS22 versus TS20 and TS23. In case of preimplantation embryos, every sample was produced in an independent IVF over different days but library preparation and sequencing were performed in batches. In the analysis, these known batches were also taken into account. Analysis of long transcripts of all developmental stages was performed using the same "pipeline" of preprocessing and differentially expression analysis and additionally adjusting for the appropriate covariates. In the analysis of small RNAs, the "library preparation date" and the "sequencing date" were included as covariates in order to adjust for these batch effects. Additionally, SVA identified two more hidden batches that were also included as covariates. Unfortunately, preprocessing of small RNA sequencing data turned out to be not ideal because 50 bp reads are first mapped to the genome and in the likely case that it maps to more than one region in the genome only the first and best annotation is counted, thereby disregarding all other equally likely possibilities. This way, a lot of information might be lost or a regulated sequence might be even appointed to an

alternative small RNA. Nevertheless, it represents the common method for small RNA-Seq analysis and was therefore used.

A further issue of preimplantation embryos poses their small size and therefore little RNA content as well as the small number of oocytes per female. In order to obtain enough RNA of good quality but at the same time not use too many animals as demanded by the principles of the 3Rs (277), embryos of the same IVF were pooled before RNA extraction. Pooling of embryos was performed manually and is therefore error-prone, although certain quality criteria were established. Moreover, as fertilization occurs autonomously during co-cultivation of sperm and oocytes, the exact time of fertilization is unknown and might vary. Also, although harvest was performed preferably at a certain time after start of the co-cultivation, the exact time might vary a little. Therefore, the exact age of each embryo varies introducing small differences between the samples but also within the pooled samples. Moreover, although great care was taken by harvesting only embryos of good quality, some dead or damaged embryos may have been collected as well. In the following library preparation for long and small RNA-Seq, methods were selected based on minimal RNA input material requirement. Therefore, these methods might be susceptible to other shortcomings such as a higher number of mRNA degradation products and piRNAs instead of miRNAs compared to other available methods (278).

Biological issues arise mainly due to the fact that two groups are being compared that are very similar and the only difference between them is the parental diet. Although offspring of HFD-treated parents shows significantly higher body weight than offspring of LFD-treated parents and this metabolic phenotype is accompanied by differences in gene expression, the significance and magnitude of the gene regulation is not very high. Because analysis takes place during many different developmental stages, it makes it difficult to find small meaningful transcriptomic differences in a rapidly changing transcriptome. This is one likely reason that no gene was detected to be differentially regulated throughout all developmental stages. Another reason is the improbability that one gene alone is responsible for the transmission of the parental metabolic disorder to the offspring.

A major complication presents the sex-specificity of the phenotype in adulthood. While a sex-specific analysis is easily possible in tissues of fetal and young mice, it is complicated in preimplantation embryos. Because preimplantation embryos were pooled for analysis, male and female embryos are collected together within the same sample in an unknown ratio. In order to analyze males and females separately, the sex has to be determined previous to the harvest or RNA-Seq has to be performed on single embryos. However, both of these possibilities might introduce other problems and biases into the analysis. Having said this, little is known about sexual dimorphism of the preimplantation embryo and the impact on

epigenetic inheritance. Although male and female early embryos only differ in their sex chromosome content, studies of bovine preimplantation embryos suggest transcriptional differences of male and female embryos already at the early stages after fertilization and even in the expression of autosomal genes (*279*). Interestingly, known epigenetic regulators such as *Dnmt3a*, *Dnmt3b*, *Hmt1* and *Ilf3* are upregulated in male bovine blastocysts compared to female blastocysts (*280*). In our study, expression of Y-chromosome specific gene *Kdm5d* is relatively similar in all samples, assuming approximately equal distribution of male and female embryos within the pooled samples. In zygotes, samples vary from -4.5% to +14.6% from the average. In 2-cell embryos, samples deviate between -4.1% and +3.8% from the average and between -11.4% and +8.6% in blastocysts. Therefore, the comparison of HFD and LFD preimplantation embryos is unlikely to be biased by the sex. But ultimately, the possibility that sex-specific epigenetic regulation during preimplantation phase is involved in the transmission of the sex-specific phenotype cannot be excluded. Even further, a sex-specific epigenetic regulation would be hidden by this kind of pooled analysis. An indication of a sex-specific epigenetic regulation was presented in a recent study, in which murine blastocysts derived from obese males showed opposite gene regulation dependent on the sex of the embryo (*255*). Nevertheless, candidate epigenetic modifier genes were detected in male and female embryos combined that could induce intergenerational inheritance independent of the sex but lead to a sex-specific phenotype later in life.

As a consequence, further experiments are required in order to validate these results and obtain a clearer picture of the mechanism(s) behind intergenerational epigenetic inheritance. Obviously, a validation of the detected candidate genes by qPCR would be appropriate but requires a lot of RNA material, which is scarce. Performing RNA-Seq on single embryos might be more sensible and elegant in order to validate candidate genes and at the same time check for sex-specific gene expression in preimplantation embryos. Besides, a variety of methods to prepare libraries from very small amounts of RNA is available nowadays.

Since candidate genes such as *Usp16*, *Usp22*, *Usp15*, *Rnf20*, *Lcmt2*, *Nsun2* and *Tet1* act via altering histone modifications or the methylation status of genes, more detailed examination of histones and differentially methylated regions in the genome is necessary to understand the potential impact of their actions. This could be achieved for example by ChIP-Seq and MeDIP-Seq or bisulfite sequencing.

Furthermore, a complete transcriptome analysis of gametes from HFD- versus LFD-treated males and females is imperative in order to compare it to the transcriptome of preimplantation embryos and especially to the zygote. Although preliminary data is available and shows promising differences between HFD- and LFD-derived sperm and oocytes, methods that were used to prepare sequencing libraries and in the subsequent bioinformatic analysis differ

markedly from the methods applied in this study. Therefore, direct comparison of differentially expressed genes would be complicated and results doubtful even with adjusting for the method differences.

Even with the gained knowledge of affected genes, miRNAs and biological processes that are potentially involved in the intergenerational epigenetic inheritance of metabolic disorders, many questions remain unanswered.

Intergenerational inheritance has been proven in many studies with rodent models and suggested in human retrospective and prospective studies, however, evidence for transgenerational inheritance remains scarce (*2*). Experiments in our lab applying IVF and embryo transfer in a HFD mouse model over three generations yielded only inconclusive results so far. Nevertheless, an increasing number of human and rodent studies indicate transgenerational epigenetic inheritance but should still be interpreted with great care. Another relevant question that is investigated in our lab is the reversibility of the inherited metabolic phenotype. Until the age of 3 weeks, F1 mice derived from HFD-treated parents show differences in the transcriptome and in body weight compared to offspring of LFD-treated parents. However, these differences diminish until adulthood on a normal diet and sex-specific metabolic differences between HFD- and LFD-derived offspring are only exhibited under an additional HFD challenge. Therefore, by adjusting their lifestyle through diet and exercise the F1 generation has (theoretically) the choice of adapting their metabolic phenotype independent of the parental diet. But an unhealthy parental diet still renders the offspring more susceptible to develop a metabolic phenotype. Nevertheless, since the inheritance of environmentally-induced phenotypes occurs via an epigenetic mechanism, it should - per definition - be reversible on a molecular level. In order to test this reversibility, transmission of the phenotype has to be investigated in a mouse model with an inactivated candidate gene. For example, a recent study could already show that deletion of the murine tRNA methyltransferase *Dnmt2* abolished the sncRNA-mediated transmission of HFD-induced metabolic disorders to the offspring (*176*). However, more studies investigating the potential mechanisms of intergenerational epigenetic inheritance are required to completely understand this highly complex phenomenon.

The question regarding the situation in human remains open to date. It would be most desirable to understand if and how this fundamental process of inheritance – transmission of environmental experiences additional to the parental genes to the offspring – functions in humans. Although suggested by epidemiological studies, epigenetic inheritance is difficult to investigate in humans due to a variety of confounding factors. Therefore, insights from animal models are so far the best option to draw conclusions about the situation in humans.

4.5 Conclusion

This project aimed to uncover candidate genes and/or small RNA transcripts that might play a role in the epigenetic inheritance of metabolic disorders. Furthermore, potentially involved biological processes and pathways were investigated. By extensively analyzing the transcriptomic differences between offspring of HFD- and LFD-treated parents at various developmental stages, a comprehensive overview depicting the course of transcriptome changes was created.

At each developmental stage, a set of significantly regulated genes was identified that could mostly distinguish HFD offspring from LFD offspring. During embryonic development, the distinction was clearly possible in zygotes but not as clear in 2-cell embryos and blastocysts. Analysis of specific tissues during organogenesis and in 3 weeks old mice revealed sex-specific transcriptomic differences between HFD and LFD offspring. In accordance with the transcriptome differences, phenotypic differences between HFD and LFD offspring were apparent at the age of 3 weeks with increased body weight in HFD males and females as well as during adulthood with increased obesity in both and impaired glucose tolerance in male HFD offspring.

No transcript was differentially regulated at all developmental stages and only very few regulated transcripts were identified overlapping between the stages of early embryogenesis or organogenesis or the different organs at the age of 3 weeks. Furthermore, small RNA transcripts were also not consistently regulated throughout preimplantation phase and regulated miRNAs did only target very few of the regulated long transcripts in the same or later developmental stage. This indicates a high variation of gene expression changes due to parental HFD treatment throughout development meaning that the kind of alteration in gene expression is different at each stage. Moreover, overall parental HFD-induced changes in gene expression (i.e. fold changes) were measurable but relatively small. Nevertheless, although drastic changes overlapping all developmental stages were not found, minor expression changes of certain genes in specific stages could still be causative of the epigenetic inheritance of this metabolic phenotype.

Overall, this approach of screening the F1 generation for transcriptomic differences and therefore alteration in biological processes between HFD and LFD offspring enabled the identification of RNA transcripts that are potentially responsible for the intergenerational epigenetic transmission of HFD-induced metabolic disorders. These candidate genes during early embryonic development include *Tet1*, *Nsun2* and *Drosha*, whereas *Lep*, *Npr3*, *Tst*, *Retsat* and *Ddah* are potential candidate genes for the metabolic phenotype in 3 weeks old mice. Moreover, affected processes during the preimplantation phase include mainly

processes of epigenetic regulation such as gene expression and gene silencing, RNA processing and histone modifications. In liver and adipose tissues on the other hand, lipid, glucose and protein metabolism as well as response to hormones and the immune response were over-represented. Interestingly, different regulated genes mediated the impact on these metabolic processes in each developmental stage and in males and females. Although these insights cannot clearly prove a specific mechanism, they demonstrate that the complete process of intergenerational and transgenerational epigenetic inheritance is considerably more dynamic, versatile and complex than postulated by other studies so far (*63, 171, 173, 253-255, 257*). However, they might lead the way to further investigate the complex phenomenon of intergenerational epigenetic inheritance.

5. REFERENCES

1. M. Irmler, D. Kaspar, M. Hrabě de Angelis, J. Beckers, in *Beyond Our Genes: Pathophysiology of Gene and Environment Interaction and Epigenetic Inheritance,* R. Teperino, Ed. (Springer International Publishing, Cham, 2020), pp. 175-208.

2. D. Kaspar, S. Hastreiter, M. Irmler, M. Hrabe de Angelis, J. Beckers, Nutrition and its role in epigenetic inheritance of obesity and diabetes across generations. *Mammalian genome : official journal of the International Mammalian Genome Society*, (2020).

3. International Diabetes Federation. IDF Diabetes Atlas, 8th edn. Brussels, Belgium: International Diabetes Federation, 2017. http://www.diabetesatlas.org.

4. Diagnosis and classification of diabetes mellitus. *Diabetes care* **33 Suppl 1**, S62-69 (2010).

5. A. T. Hattersley *et al.*, ISPAD Clinical Practice Consensus Guidelines 2018: The diagnosis and management of monogenic diabetes in children and adolescents. *Pediatric diabetes* **19 Suppl 27**, 47-63 (2018).

6. S. E. Kahn, M. E. Cooper, S. Del Prato, Pathophysiology and treatment of type 2 diabetes: perspectives on the past, present, and future. *Lancet (London, England)* **383**, 1068-1083 (2014).

7. E. S. Schellenberg, D. M. Dryden, B. Vandermeer, C. Ha, C. Korownyk, Lifestyle interventions for patients with and at risk for type 2 diabetes: a systematic review and meta-analysis. *Annals of internal medicine* **159**, 543-551 (2013).

8. 2. Classification and Diagnosis of Diabetes: Standards of Medical Care in Diabetes— 2018. **41**, S13-S27 (2018).

9. P. Felig, Pathophysiology of diabetes mellitus. *The Medical clinics of North America* **55**, 821-834 (1971).

10. P. B. Iynedjian, Mammalian glucokinase and its gene. *The Biochemical journal* **293 (Pt 1)**, 1-13 (1993).

11. J. E. Hall, *Guyton and Hall Textbook of Medical Physiology.* (Elsevier Health Sciences, 2015).

12. M. J. Perley, D. M. Kipnis, Plasma insulin responses to oral and intravenous glucose: studies in normal and diabetic sujbjects. *The Journal of clinical investigation* **46**, 1954-1962 (1967).

13. J. Seufert, T. J. Kieffer, J. F. Habener, Leptin inhibits insulin gene transcription and reverses hyperinsulinemia in leptin-deficient ob/ob mice. *Proceedings of the National Academy of Sciences of the United States of America* **96**, 674-679 (1999).

14. M. Z. Strowski, R. M. Parmar, A. D. Blake, J. M. Schaeffer, Somatostatin inhibits insulin and glucagon secretion via two receptors subtypes: an in vitro study of pancreatic islets from somatostatin receptor 2 knockout mice. *Endocrinology* **141**, 111-117 (2000).

15. E. R. Seaquist, G. S. Damberg, I. Tkac, R. Gruetter, The effect of insulin on in vivo cerebral glucose concentrations and rates of glucose transport/metabolism in humans. *Diabetes* **50**, 2203-2209 (2001).

16. D. Accili *et al.*, Early neonatal death in mice homozygous for a null allele of the insulin receptor gene. *Nature genetics* **12**, 106-109 (1996).

17. Y. Lee, M. Y. Wang, X. Q. Du, M. J. Charron, R. H. Unger, Glucagon receptor knockout prevents insulin-deficient type 1 diabetes in mice. *Diabetes* **60**, 391-397 (2011).

18. M. Stumvoll, B. J. Goldstein, T. W. van Haeften, Type 2 diabetes: principles of pathogenesis and therapy. *Lancet (London, England)* **365**, 1333-1346 (2005).

19. Y. Zheng, S. H. Ley, F. B. Hu, Global aetiology and epidemiology of type 2 diabetes mellitus and its complications. *Nature reviews. Endocrinology* **14**, 88-98 (2018).

20. L. Chen, D. J. Magliano, P. Z. Zimmet, The worldwide epidemiology of type 2 diabetes mellitus--present and future perspectives. *Nature reviews. Endocrinology* **8**, 228-236 (2011).

21. A. L. Gloyn, M. I. McCarthy, The genetics of type 2 diabetes. *Best practice & research. Clinical endocrinology & metabolism* **15**, 293-308 (2001).

22. G. Willemsen *et al.*, The Concordance and Heritability of Type 2 Diabetes in 34,166 Twin Pairs From International Twin Registers: The Discordant Twin (DISCOTWIN) Consortium. *Twin research and human genetics : the official journal of the International Society for Twin Studies* **18**, 762-771 (2015).

23. T. Karaderi, A. W. Drong, C. M. Lindgren, Insights into the Genetic Susceptibility to Type 2 Diabetes from Genome-Wide Association Studies of Obesity-Related Traits. *Current diabetes reports* **15**, 83 (2015).

24. B. Maher, Personal genomes: The case of the missing heritability. *Nature* **456**, 18-21 (2008).

25. T. A. Manolio *et al.*, Finding the missing heritability of complex diseases. *Nature* **461**, 747-753 (2009).

26. C. Fuchsberger *et al.*, The genetic architecture of type 2 diabetes. *Nature* **536**, 41-47 (2016).

27. J. V. Neel, Diabetes mellitus: a "thrifty" genotype rendered detrimental by "progress"? *American journal of human genetics* **14**, 353-362 (1962).

28. K. O'Dea, Overview of the thrifty genotype hypothesis. *Asia Pacific journal of clinical nutrition* **4**, 339-340 (1995).

29. F. B. Hu *et al.*, Diet, lifestyle, and the risk of type 2 diabetes mellitus in women. *The New England journal of medicine* **345**, 790-797 (2001).

30. C. N. Hales, D. J. Barker, Type 2 (non-insulin-dependent) diabetes mellitus: the thrifty phenotype hypothesis. *Diabetologia* **35**, 595-601 (1992).

31. M. Garg *et al.*, Glucose metabolic adaptations in the intrauterine growth-restricted adult female rat offspring. *American journal of physiology. Endocrinology and metabolism* **290**, E1218-1226 (2006).

32.   A. C. Ravelli *et al.*, Glucose tolerance in adults after prenatal exposure to famine. *Lancet (London, England)* **351**, 173-177 (1998).

33.   P. Vuguin, E. Raab, B. Liu, N. Barzilai, R. Simmons, Hepatic insulin resistance precedes the development of diabetes in a model of intrauterine growth retardation. *Diabetes* **53**, 2617-2622 (2004).

34.   R. Barres, J. R. Zierath, The role of diet and exercise in the transgenerational epigenetic landscape of T2DM. *Nature reviews. Endocrinology* **12**, 441-451 (2016).

35.   O. Aydin, M. Nieuwdorp, V. Gerdes, The Gut Microbiome as a Target for the Treatment of Type 2 Diabetes. *Current diabetes reports* **18**, 55 (2018).

36.   N. Chevalier, P. Fenichel, Endocrine disruptors: new players in the pathophysiology of type 2 diabetes? *Diabetes & metabolism* **41**, 107-115 (2015).

37.   C. H. Waddington, The Epigenotype. *Endeavour*, 18-20 (1942).

38.   S. Choudhuri, From Waddington's epigenetic landscape to small noncoding RNA: some important milestones in the history of epigenetics research. *Toxicology mechanisms and methods* **21**, 252-274 (2011).

39.   R. M. Rivera, L. B. Bennett, Epigenetics in humans: an overview. *Current opinion in endocrinology, diabetes, and obesity* **17**, 493-499 (2010).

40.   H. Slomko, H. J. Heo, F. H. Einstein, Minireview: Epigenetics of obesity and diabetes in humans. *Endocrinology* **153**, 1025-1030 (2012).

41.   U. Weber-Stadlbauer, Epigenetic and transgenerational mechanisms in infection-mediated neurodevelopmental disorders. *Translational psychiatry* **7**, e1113 (2017).

42.   K. Luger, A. W. Mader, R. K. Richmond, D. F. Sargent, T. J. Richmond, Crystal structure of the nucleosome core particle at 2.8 A resolution. *Nature* **389**, 251-260 (1997).

43.   R. Schneider *et al.*, Histone H3 lysine 4 methylation patterns in higher eukaryotic genes. *Nature cell biology* **6**, 73-77 (2004).

44.   R. J. Sims, 3rd, K. Nishioka, D. Reinberg, Histone lysine methylation: a signature for chromatin function. *Trends in genetics : TIG* **19**, 629-639 (2003).

45.   T. Jenuwein, C. D. Allis, Translating the histone code. *Science (New York, N.Y.)* **293**, 1074-1080 (2001).

46.   A. J. Ruthenburg, H. Li, D. J. Patel, C. D. Allis, Multivalent engagement of chromatin modifications by linked binding modules. *Nature reviews. Molecular cell biology* **8**, 983-994 (2007).

47.   P. Tessarz, T. Kouzarides, Histone core modifications regulating nucleosome structure and dynamics. *Nature reviews. Molecular cell biology* **15**, 703-708 (2014).

48.   P. A. Jones, Functions of DNA methylation: islands, start sites, gene bodies and beyond. *Nature reviews. Genetics* **13**, 484-492 (2012).

49.   R. Holliday, J. E. Pugh, DNA modification mechanisms and gene activity during development. *Science (New York, N.Y.)* **187**, 226-232 (1975).

50. P. A. Jones, G. Liang, Rethinking how DNA methylation patterns are maintained. *Nature reviews. Genetics* **10**, 805-811 (2009).

51. A. V. Probst, E. Dunleavy, G. Almouzni, Epigenetic inheritance during the cell cycle. *Nature reviews. Molecular cell biology* **10**, 192-206 (2009).

52. E. Li, T. H. Bestor, R. Jaenisch, Targeted mutation of the DNA methyltransferase gene results in embryonic lethality. *Cell* **69**, 915-926 (1992).

53. T. Chen, Y. Ueda, J. E. Dodge, Z. Wang, E. Li, Establishment and maintenance of genomic methylation patterns in mouse embryonic stem cells by Dnmt3a and Dnmt3b. *Molecular and cellular biology* **23**, 5594-5605 (2003).

54. G. Liang *et al.*, Cooperativity between DNA methyltransferases in the maintenance methylation of repetitive elements. *Molecular and cellular biology* **22**, 480-491 (2002).

55. X. Wu, Y. Zhang, TET-mediated active DNA demethylation: mechanism, function and beyond. *Nature reviews. Genetics* **18**, 517-534 (2017).

56. L. Ma, V. B. Bajic, Z. Zhang, On the classification of long non-coding RNAs. *RNA biology* **10**, 925-933 (2013).

57. J. S. Mattick, I. V. Makunin, Non-coding RNA. *Human molecular genetics* **15 Spec No 1**, R17-29 (2006).

58. A. Fire *et al.*, Potent and specific genetic interference by double-stranded RNA in Caenorhabditis elegans. *Nature* **391**, 806-811 (1998).

59. D. P. Bartel, MicroRNAs: genomics, biogenesis, mechanism, and function. *Cell* **116**, 281-297 (2004).

60. A. M. Mohr, J. L. Mott, Overview of microRNA biology. *Seminars in liver disease* **35**, 3-11 (2015).

61. Y. W. Iwasaki, M. C. Siomi, H. Siomi, PIWI-Interacting RNA: Its Biogenesis and Functions. *Annual review of biochemistry* **84**, 405-433 (2015).

62. L. M. Vaschetto, miRNA activation is an endogenous gene expression pathway. *RNA biology* **15**, 826-828 (2018).

63. U. Sharma *et al.*, Biogenesis and function of tRNA fragments during sperm maturation and fertilization in mammals. *Science (New York, N.Y.)* **351**, 391-396 (2016).

64. P. A. Jazwiec, D. M. Sloboda, Nutritional adversity, sex and reproduction: 30 years of DOHaD and what have we learned? *The Journal of endocrinology* **242**, T51-t68 (2019).

65. S. F. Gilbert, *Developmental Biology; Chapter 19.* (Sunderland (MA): Sinauer Associates, ed. 6th edition, 2000).

66. W. S. Ward, D. S. Coffey, DNA packaging and organization in mammalian spermatozoa: comparison with somatic cells. *Biology of reproduction* **44**, 569-574 (1991).

67. S. Nonchev, R. Tsanev, Protamine-histone replacement and DNA replication in the male mouse pronucleus. *Molecular reproduction and development* **25**, 72-76 (1990).

68. S. S. Hammoud *et al.*, Distinctive chromatin in human sperm packages genes for embryo development. *Nature* **460**, 473-478 (2009).

69. S. M. Wykes, S. A. Krawetz, The structural organization of sperm chromatin. *The Journal of biological chemistry* **278**, 29471-29477 (2003).

70. J. C. Kiefer, Epigenetics in development. *Developmental dynamics : an official publication of the American Association of Anatomists* **236**, 1144-1156 (2007).

71. I. Cantone, A. G. Fisher, Epigenetic programming and reprogramming during development. *Nature structural & molecular biology* **20**, 282-289 (2013).

72. W. Reik, W. Dean, J. Walter, Epigenetic reprogramming in mammalian development. *Science (New York, N.Y.)* **293**, 1089-1093 (2001).

73. S. A. Smallwood, G. Kelsey, De novo DNA methylation: a germ cell perspective. *Trends in genetics : TIG* **28**, 33-42 (2012).

74. S. Gkountela *et al.*, DNA Demethylation Dynamics in the Human Prenatal Germline. *Cell* **161**, 1425-1436 (2015).

75. D. Monk, Germline-derived DNA methylation and early embryo epigenetic reprogramming: The selected survival of imprints. *The international journal of biochemistry & cell biology* **67**, 128-138 (2015).

76. S. Seisenberger *et al.*, Reprogramming DNA methylation in the mammalian life cycle: building and breaking epigenetic barriers. *Philosophical transactions of the Royal Society of London. Series B, Biological sciences* **368**, 20110330 (2013).

77. M. Saitou, Germ cell specification in mice. *Current opinion in genetics & development* **19**, 386-395 (2009).

78. P. Hajkova *et al.*, Epigenetic reprogramming in mouse primordial germ cells. *Mechanisms of development* **117**, 15-23 (2002).

79. Y. Zeng, T. Chen, DNA Methylation Reprogramming during Mammalian Development. *Genes* **10**, (2019).

80. W. Dean, F. Santos, W. Reik, Epigenetic reprogramming in early mammalian development and following somatic nuclear transfer. *Seminars in cell & developmental biology* **14**, 93-100 (2003).

81. G. Wu, L. Lei, H. R. Scholer, Totipotency in the mouse. *Journal of molecular medicine (Berlin, Germany)* **95**, 687-694 (2017).

82. G. Auclair, S. Guibert, A. Bender, M. Weber, Ontogeny of CpG island methylation and specificity of DNMT3 methyltransferases during embryonic development in the mouse. *Genome biology* **15**, 545 (2014).

83. W. Reik, J. Walter, Genomic imprinting: parental influence on the genome. *Nature reviews. Genetics* **2**, 21-32 (2001).

84. M. A. Surani, S. C. Barton, M. L. Norris, Development of reconstituted mouse eggs suggests imprinting of the genome during gametogenesis. *Nature* **308**, 548-550 (1984).

85. J. McGrath, D. Solter, Completion of mouse embryogenesis requires both the maternal and paternal genomes. *Cell* **37**, 179-183 (1984).

86. T. M. DeChiara, E. J. Robertson, A. Efstratiadis, Parental imprinting of the mouse insulin-like growth factor II gene. *Cell* **64**, 849-859 (1991).

87. M. S. Bartolomei, S. Zemel, S. M. Tilghman, Parental imprinting of the mouse H19 gene. *Nature* **351**, 153-155 (1991).

88. D. P. Barlow, R. Stoger, B. G. Herrmann, K. Saito, N. Schweifer, The mouse insulin-like growth factor type-2 receptor is imprinted and closely linked to the Tme locus. *Nature* **349**, 84-87 (1991).

89. J. Peters, The role of genomic imprinting in biology and disease: an expanding view. *Nature reviews. Genetics* **15**, 517-530 (2014).

90. W. Tadros, H. D. Lipshitz, The maternal-to-zygotic transition: a play in two acts. *Development (Cambridge, England)* **136**, 3033-3042 (2009).

91. M. T. Lee, A. R. Bonneau, A. J. Giraldez, Zygotic genome activation during the maternal-to-zygotic transition. *Annual review of cell and developmental biology* **30**, 581-613 (2014).

92. M. J. Goddard, H. P. Pratt, Control of events during early cleavage of the mouse embryo: an analysis of the '2-cell block'. *Journal of embryology and experimental morphology* **73**, 111-133 (1983).

93. C. M. Warner, L. R. Versteegh, In vivo and in vitro effect of alpha-amanitin on preimplantation mouse embryo RNA polymerase. *Nature* **248**, 678-680 (1974).

94. G. Kaati, L. O. Bygren, S. Edvinsson, Cardiovascular and diabetes mortality determined by nutrition during parents' and grandparents' slow growth period. *European journal of human genetics : EJHG* **10**, 682-688 (2002).

95. S. P. Mourtakos *et al.*, Maternal lifestyle characteristics during pregnancy, and the risk of obesity in the offspring: a study of 5,125 children. *BMC pregnancy and childbirth* **15**, 66 (2015).

96. T. Roseboom, S. de Rooij, R. Painter, The Dutch famine and its long-term consequences for adult health. *Early human development* **82**, 485-491 (2006).

97. C. Li, O. Casanueva, Epigenetic inheritance of proteostasis and ageing. **60**, 191-202 (2016).

98. M. F. Perez, B. Lehner, Intergenerational and transgenerational epigenetic inheritance in animals. *Nature cell biology*, (2019).

99. L. Daxinger, E. Whitelaw, Understanding transgenerational epigenetic inheritance via the gametes in mammals. *Nature reviews. Genetics* **13**, 153-162 (2012).

100. C. Ling, T. Ronn, Epigenetics in Human Obesity and Type 2 Diabetes. *Cell metabolism*, (2019).

101. R. C. Painter, T. J. Roseboom, O. P. Bleker, Prenatal exposure to the Dutch famine and disease in later life: an overview. *Reproductive toxicology (Elmsford, N.Y.)* **20**, 345-352 (2005).

102. A. D. Stein, P. A. Zybert, M. van de Bor, L. H. Lumey, Intrauterine famine exposure and body proportions at birth: the Dutch Hunger Winter. *International journal of epidemiology* **33**, 831-836 (2004).

103. Z. Stein, M. Susser, Fertility, fecundity, famine: food rations in the dutch famine 1944/5 have a causal relation to fertility, and probably to fecundity. *Human biology* **47**, 131-154 (1975).

104. L. H. Lumey, A. D. Stein, H. Kahn, *Food restriction during gestation and impaired fasting glucose or glucose tolerance and type 2 diabetes mellitus in adulthood: Evidence from the DutchHunger Winter Families Study.* (2009), vol. 1, pp. S164.

105. M. V. Veenendaal *et al.*, Transgenerational effects of prenatal exposure to the 1944-45 Dutch famine. *BJOG : an international journal of obstetrics and gynaecology* **120**, 548-553 (2013).

106. B. T. Heijmans *et al.*, Persistent epigenetic differences associated with prenatal exposure to famine in humans. *Proceedings of the National Academy of Sciences of the United States of America* **105**, 17046-17049 (2008).

107. E. W. Tobi *et al.*, DNA methylation signatures link prenatal famine exposure to growth and metabolism. *Nature communications* **5**, 5592 (2014).

108. E. W. Tobi *et al.*, DNA methylation differences after exposure to prenatal famine are common and timing- and sex-specific. *Human molecular genetics* **18**, 4046-4053 (2009).

109. C. Li, L. H. Lumey, Exposure to the Chinese famine of 1959-61 in early life and long-term health conditions: a systematic review and meta-analysis. *International journal of epidemiology* **46**, 1157-1170 (2017).

110. J. Li *et al.*, Prenatal exposure to famine and the development of hyperglycemia and type 2 diabetes in adulthood across consecutive generations: a population-based cohort study of families in Suihua, China. *The American journal of clinical nutrition* **105**, 221-227 (2017).

111. R. Yehuda, J. Schmeidler, E. L. Giller, Jr., L. J. Siever, K. Binder-Brynes, Relationship between posttraumatic stress disorder characteristics of Holocaust survivors and their adult offspring. *The American journal of psychiatry* **155**, 841-843 (1998).

112. R. Yehuda *et al.*, Parental posttraumatic stress disorder as a vulnerability factor for low cortisol trait in offspring of holocaust survivors. *Archives of general psychiatry* **64**, 1040-1048 (2007).

113. A. Lehrner *et al.*, Maternal PTSD associates with greater glucocorticoid sensitivity in offspring of Holocaust survivors. *Psychoneuroendocrinology* **40**, 213-220 (2014).

114. R. Yehuda, A. Bell, L. M. Bierer, J. Schmeidler, Maternal, not paternal, PTSD is related to increased risk for PTSD in offspring of Holocaust survivors. *Journal of psychiatric research* **42**, 1104-1111 (2008).

115. R. Yehuda *et al.*, Influences of maternal and paternal PTSD on epigenetic regulation of the glucocorticoid receptor gene in Holocaust survivor offspring. *The American journal of psychiatry* **171**, 872-880 (2014).

116. D. Mehta *et al.*, DNA methylation from germline cells in veterans with PTSD. *Journal of psychiatric research* **116**, 42-50 (2019).

117. K. Northstone, J. Golding, G. Davey Smith, L. L. Miller, M. Pembrey, Prepubertal start of father's smoking and increased body fat in his sons: further characterisation of paternal transgenerational responses. *European journal of human genetics : EJHG* **22**, 1382-1386 (2014).

118. M. E. Pembrey *et al.*, Sex-specific, male-line transgenerational responses in humans. *European journal of human genetics : EJHG* **14**, 159-166 (2006).

119. L. L. Miller, M. Pembrey, G. Davey Smith, K. Northstone, J. Golding, Is the growth of the fetus of a non-smoking mother influenced by the smoking of either grandmother while pregnant? *PloS one* **9**, e86781 (2014).

120. W. Eriksen, J. M. Sundet, K. Tambs, Paternal age at birth and the risk of obesity in young adulthood: a register-based birth cohort study of Norwegian males. *American journal of human biology : the official journal of the Human Biology Council* **25**, 29-34 (2013).

121. I. Donkin *et al.*, Obesity and Bariatric Surgery Drive Epigenetic Variation of Spermatozoa in Humans. *Cell metabolism* **23**, 369-378 (2016).

122. A. Soubry *et al.*, Newborns of obese parents have altered DNA methylation patterns at imprinted genes. *International journal of obesity (2005)* **39**, 650-657 (2015).

123. J. Denham, Exercise and epigenetic inheritance of disease risk. *Acta physiologica (Oxford, England)* **222**, (2018).

124. R. Barres *et al.*, Acute exercise remodels promoter methylation in human skeletal muscle. *Cell metabolism* **15**, 405-411 (2012).

125. A. Bye *et al.*, Circulating microRNAs and aerobic fitness--the HUNT-Study. *PloS one* **8**, e57496 (2013).

126. S. Nielsen *et al.*, The miRNA plasma signature in response to acute aerobic exercise and endurance training. *PloS one* **9**, e87308 (2014).

127. S. L. Wardle *et al.*, Plasma microRNA levels differ between endurance and strength athletes. *PloS one* **10**, e0122107 (2015).

128. J. Denham, B. J. O'Brien, J. T. Harvey, F. J. Charchar, Genome-wide sperm DNA methylation changes after 3 months of exercise training in humans. *Epigenomics* **7**, 717-731 (2015).

129. L. E. McCullough *et al.*, Associations between prenatal physical activity, birth weight, and DNA methylation at genomically imprinted domains in a multiethnic newborn cohort. *Epigenetics : official journal of the DNA Methylation Society* **10**, 597-606 (2015).

130. T. L. Bale, Epigenetic and transgenerational reprogramming of brain development. *Nature reviews. Neuroscience* **16**, 332-344 (2015).

131. A. Fischer, Epigenetic memory: the Lamarckian brain. *The EMBO journal* **33**, 945-967 (2014).

132. P. A. Dell, F. D. Rose, Transfer of effects from environmentally enriched and impoverished female rats to future offspring. *Physiology & behavior* **39**, 187-190 (1987).

133. J. A. Arai, S. Li, D. M. Hartley, L. A. Feig, Transgenerational rescue of a genetic defect in long-term potentiation and memory formation by juvenile enrichment. *The Journal of neuroscience : the official journal of the Society for Neuroscience* **29**, 1496-1502 (2009).

134. E. Benito *et al.*, RNA-Dependent Intergenerational Inheritance of Enhanced Synaptic Plasticity after Environmental Enrichment. *Cell reports* **23**, 546-554 (2018).

135. D. P. Ryan *et al.*, A paternal methyl donor-rich diet altered cognitive and neural functions in offspring mice. *Molecular psychiatry* **23**, 1345-1355 (2018).

136. C. R. McCoy, N. L. Jackson, J. Day, S. M. Clinton, Genetic predisposition to high anxiety- and depression-like behavior coincides with diminished DNA methylation in the adult rat amygdala. *Behavioural brain research* **320**, 165-178 (2017).

137. C. R. McCoy *et al.*, A paternal methyl donor depleted diet leads to increased anxiety- and depression-like behavior in adult rat offspring. *Bioscience reports* **38**, (2018).

138. G. Winther *et al.*, Grandmaternal high-fat diet primed anxiety-like behaviour in the second-generation female offspring. *Behavioural brain research* **359**, 47-55 (2019).

139. L. N. Vandenberg *et al.*, Urinary, circulating, and tissue biomonitoring studies indicate widespread exposure to bisphenol A. *Environmental health perspectives* **118**, 1055-1070 (2010).

140. S. Salian, T. Doshi, G. Vanage, Perinatal exposure of rats to Bisphenol A affects the fertility of male offspring. *Life sciences* **85**, 742-752 (2009).

141. A. Ziv-Gal, W. Wang, C. Zhou, J. A. Flaws, The effects of in utero bisphenol A exposure on reproductive capacity in several generations of mice. *Toxicology and applied pharmacology* **284**, 354-362 (2015).

142. Z. Drobna *et al.*, Transgenerational Effects of Bisphenol A on Gene Expression and DNA Methylation of Imprinted Genes in Brain. *Endocrinology* **159**, 132-144 (2018).

143. M. D. Anway, A. S. Cupp, M. Uzumcu, M. K. Skinner, Epigenetic transgenerational actions of endocrine disruptors and male fertility. *Science (New York, N.Y.)* **308**, 1466-1469 (2005).

144. C. Guerrero-Bosagna *et al.*, Epigenetic transgenerational inheritance of vinclozolin induced mouse adult onset disease and associated sperm epigenome biomarkers. *Reproductive toxicology (Elmsford, N.Y.)* **34**, 694-707 (2012).

145. L. Stenz, D. S. Schechter, S. R. Serpa, A. Paoloni-Giacobino, Intergenerational Transmission of DNA Methylation Signatures Associated with Early Life Stress. *Current genomics* **19**, 665-675 (2018).

146. I. C. Weaver *et al.*, Epigenetic programming by maternal behavior. *Nature neuroscience* **7**, 847-854 (2004).

147. I. C. Weaver *et al.*, Reversal of maternal programming of stress responses in adult offspring through methyl supplementation: altering epigenetic marking later in life.

The Journal of neuroscience : the official journal of the Society for Neuroscience **25**, 11045-11054 (2005).

148. I. C. Weaver, M. J. Meaney, M. Szyf, Maternal care effects on the hippocampal transcriptome and anxiety-mediated behaviors in the offspring that are reversible in adulthood. *Proceedings of the National Academy of Sciences of the United States of America* **103**, 3480-3485 (2006).

149. T. B. Franklin *et al.*, Epigenetic transmission of the impact of early stress across generations. *Biological psychiatry* **68**, 408-415 (2010).

150. K. Gapp *et al.*, Early life stress in fathers improves behavioural flexibility in their offspring. *Nature communications* **5**, 5466 (2014).

151. K. Gapp *et al.*, Implication of sperm RNAs in transgenerational inheritance of the effects of early trauma in mice. *Nature neuroscience* **17**, 667-669 (2014).

152. K. Gapp *et al.*, Potential of Environmental Enrichment to Prevent Transgenerational Effects of Paternal Trauma. *Neuropsychopharmacology : official publication of the American College of Neuropsychopharmacology* **41**, 2749-2758 (2016).

153. D. M. Dietz *et al.*, Paternal transmission of stress-induced pathologies. *Biological psychiatry* **70**, 408-414 (2011).

154. B. G. Dias, K. J. Ressler, Parental olfactory experience influences behavior and neural structure in subsequent generations. *Nature neuroscience* **17**, 89-96 (2014).

155. H. S. Aoued *et al.*, Reversing Behavioral, Neuroanatomical, and Germline Influences of Intergenerational Stress. *Biological psychiatry* **85**, 248-256 (2019).

156. A. Ost *et al.*, Paternal diet defines offspring chromatin state and intergenerational obesity. *Cell* **159**, 1352-1364 (2014).

157. T. de Castro Barbosa, P. S. Alm, A. Krook, R. Barres, J. R. Zierath, Paternal high-fat diet transgenerationally impacts hepatic immunometabolism. *FASEB J* **33**, 6269-6280 (2019).

158. T. Fullston *et al.*, Paternal obesity initiates metabolic disturbances in two generations of mice with incomplete penetrance to the F2 generation and alters the transcriptional profile of testis and sperm microRNA content. *FASEB journal : official publication of the Federation of American Societies for Experimental Biology* **27**, 4226-4243 (2013).

159. S. F. Ng *et al.*, Chronic high-fat diet in fathers programs beta-cell dysfunction in female rat offspring. *Nature* **467**, 963-966 (2010).

160. G. Sarker *et al.*, Transgenerational transmission of hedonic behaviors and metabolic phenotypes induced by maternal overnutrition. *Translational psychiatry* **8**, 195 (2018).

161. Y. Wei *et al.*, Paternally induced transgenerational inheritance of susceptibility to diabetes in mammals. *Proceedings of the National Academy of Sciences of the United States of America* **111**, 1873-1878 (2014).

162. P. Huypens *et al.*, Epigenetic germline inheritance of diet-induced obesity and insulin resistance. *Nature genetics*, (2016).

163. B. R. Carone *et al.*, Paternally induced transgenerational environmental reprogramming of metabolic gene expression in mammals. *Cell* **143**, 1084-1096 (2010).

164. D. Peleg-Raibstein *et al.*, Enhanced sensitivity to drugs of abuse and palatable foods following maternal overnutrition. *Translational psychiatry* **6**, e911 (2016).

165. E. J. Radford *et al.*, In utero effects. In utero undernourishment perturbs the adult sperm methylome and intergenerational metabolism. *Science* **345**, 1255903 (2014).

166. J. L. A. Ferey *et al.*, A maternal high-fat, high-sucrose diet induces transgenerational cardiac mitochondrial dysfunction independently of maternal mitochondrial inheritance. *American journal of physiology. Heart and circulatory physiology* **316**, H1202-h1210 (2019).

167. C. L. Pankey *et al.*, Intergenerational impact of maternal overnutrition and obesity throughout pregnancy in sheep on metabolic syndrome in grandsons and granddaughters. *Domestic animal endocrinology* **60**, 67-74 (2017).

168. S. S. Sharma, N. M. Jangale, A. M. Harsulkar, M. K. Gokhale, B. N. Joshi, Chronic maternal calcium and 25-hydroxyvitamin D deficiency in Wistar rats programs abnormal hepatic gene expression leading to hepatic steatosis in female offspring. *The Journal of nutritional biochemistry* **43**, 36-46 (2017).

169. Y. Zhu *et al.*, Maternal dietary intakes of refined grains during pregnancy and growth through the first 7 y of life among children born to women with gestational diabetes. *The American journal of clinical nutrition* **106**, 96-104 (2017).

170. T. An *et al.*, Long non-coding RNAs could act as vectors for paternal heredity of high fat diet-induced obesity. *Oncotarget* **8**, 47876-47889 (2017).

171. Q. Chen *et al.*, Sperm tsRNAs contribute to intergenerational inheritance of an acquired metabolic disorder. *Science (New York, N.Y.)* **351**, 397-400 (2016).

172. T. Fullston *et al.*, Paternal obesity induces metabolic and sperm disturbances in male offspring that are exacerbated by their exposure to an "obesogenic" diet. *Physiological reports* **3**, (2015).

173. V. Grandjean *et al.*, RNA-mediated paternal heredity of diet-induced obesity and metabolic disorders. *Scientific reports* **5**, 18193 (2015).

174. J. M. Shea *et al.*, Genetic and Epigenetic Variation, but Not Diet, Shape the Sperm Methylome. *Developmental cell* **35**, 750-758 (2015).

175. M. V. Cannon *et al.*, Maternal nutrition induces pervasive gene expression changes but no detectable DNA methylation differences in the liver of adult offspring. *PloS one* **9**, e90335 (2014).

176. Y. Zhang *et al.*, Dnmt2 mediates intergenerational transmission of paternally acquired metabolic disorders through sperm small non-coding RNAs. *Nature cell biology* **20**, 535-540 (2018).

177. A. Champroux, J. Cocquet, J. Henry-Berger, J. R. Drevet, A. Kocer, A Decade of Exploring the Mammalian Sperm Epigenome: Paternal Epigenetic and Transgenerational Inheritance. *Frontiers in cell and developmental biology* **6**, 50 (2018).

178. Y. Zhang, J. Shi, M. Rassoulzadegan, F. Tuorto, Q. Chen, Sperm RNA code programmes the metabolic health of offspring. *Nature reviews. Endocrinology* **15**, 489-498 (2019).

179. K. Theiler, *The House Mouse: Atlas of Embryonic Development* (Springer Verlag, ed. 1, 1989).

180. J. F. Lambert *et al.*, Quick sex determination of mouse fetuses. *Journal of neuroscience methods* **95**, 127-132 (2000).

181. J. Rainer, F. Sanchez-Cabo, G. Stocker, A. Sturn, Z. Trajanoski, CARMAweb: comprehensive R- and bioconductor-based web service for microarray data analysis. *Nucleic acids research* **34**, W498-503 (2006).

182. M. Martin, CUTADAPT removes adapter sequences from high-throughput sequencing reads. *EMBnet.journal* **17**, (2011).

183. A. Dobin *et al.*, STAR: ultrafast universal RNA-seq aligner. *Bioinformatics (Oxford, England)* **29**, 15-21 (2013).

184. P. Ewels, M. Magnusson, S. Lundin, M. Kaller, MultiQC: summarize analysis results for multiple tools and samples in a single report. *Bioinformatics (Oxford, England)* **32**, 3047-3048 (2016).

185. M. Lawrence *et al.*, Software for computing and annotating genomic ranges. *PLoS computational biology* **9**, e1003118 (2013).

186. P. A. Ewels *et al.*, The nf-core framework for community-curated bioinformatics pipelines. *Nature biotechnology* **38**, 276-278 (2020).

187. R. Consortium, RNAcentral 2021: secondary structure integration, improved sequence search and new member databases. *Nucleic acids research*, (2020).

188. B. Langmead, C. Trapnell, M. Pop, S. L. Salzberg, Ultrafast and memory-efficient alignment of short DNA sequences to the human genome. *Genome biology* **10**, R25 (2009).

189. M. I. Love, W. Huber, S. Anders, Moderated estimation of fold change and dispersion for RNA-seq data with DESeq2. *Genome biology* **15**, 550 (2014).

190. J. T. Leek, svaseq: removing batch effects and other unwanted noise from sequencing data. *Nucleic acids research* **42**, e161 (2014).

191. T. G. O. Consortium, The Gene Ontology Resource: 20 years and still GOing strong. *Nucleic acids research* **47**, D330-d338 (2019).

192. Y. Chen, X. Wang, miRDB: an online database for prediction of functional microRNA targets. *Nucleic acids research* **48**, D127-d131 (2020).

193. R. Burcelin, V. Crivelli, A. Dacosta, A. Roy-Tirelli, B. Thorens, Heterogeneous metabolic adaptation of C57BL/6J mice to high-fat diet. *American journal of physiology. Endocrinology and metabolism* **282**, E834-842 (2002).

194. J. O. Hill, S. K. Fried, M. DiGirolamo, Effects of a high-fat diet on energy intake and expenditure in rats. *Life sciences* **33**, 141-149 (1983).

195. M. R. Jackman, P. S. MacLean, D. H. Bessesen, Energy expenditure in obesity-prone and obesity-resistant rats before and after the introduction of a high-fat diet. *American journal of physiology. Regulatory, integrative and comparative physiology* **299**, R1097-1105 (2010).

196. S. Kim *et al.*, Hepatic gene expression profiles in a long-term high-fat diet-induced obesity mouse model. *Gene* **340**, 99-109 (2004).

197. T. Li *et al.*, Dimethylarginine Dimethylaminohydrolase 1 Protects Against High-Fat Diet-Induced Hepatic Steatosis and Insulin Resistance in Mice. *Antioxidants & redox signaling* **26**, 598-609 (2017).

198. T. I. Krisko, K. B. LeClair, D. E. Cohen, Genetic ablation of phosphatidylcholine transfer protein/StarD2 in ob/ob mice improves glucose tolerance without increasing energy expenditure. *Metabolism: clinical and experimental* **68**, 145-149 (2017).

199. E. F. Scapa *et al.*, Regulation of energy substrate utilization and hepatic insulin sensitivity by phosphatidylcholine transfer protein/StarD2. *FASEB journal : official publication of the Federation of American Societies for Experimental Biology* **22**, 2579-2590 (2008).

200. M. Kanasaki *et al.*, Deficiency in catechol-o-methyltransferase is linked to a disruption of glucose homeostasis in mice. *Scientific reports* **7**, 7927 (2017).

201. C. R. Wooton-Kee *et al.*, Metabolic dysregulation in the Atp7b (-/-) Wilson's disease mouse model. *Proceedings of the National Academy of Sciences of the United States of America* **117**, 2076-2083 (2020).

202. D. J. Orlicky *et al.*, Perilipin-2 promotes obesity and progressive fatty liver disease in mice through mechanistically distinct hepatocyte and extra-hepatocyte actions. *The Journal of physiology* **597**, 1565-1584 (2019).

203. G. Lomberk *et al.*, Krüppel-like factor 11 regulates the expression of metabolic genes via an evolutionarily conserved protein interaction domain functionally disrupted in maturity onset diabetes of the young. *The Journal of biological chemistry* **288**, 17745-17758 (2013).

204. A. Mathison *et al.*, Phenotypic Characterization of Mice Carrying Homozygous Deletion of KLF11, a Gene in Which Mutations Cause Human Neonatal and MODY VII Diabetes. *Endocrinology* **156**, 3581-3595 (2015).

205. H. Soliman *et al.*, Attenuation of obesity-induced insulin resistance in mice with heterozygous deletion of ROCK2. *International journal of obesity (2005)* **40**, 1435-1443 (2016).

206. R. Zhang, T. Hou, H. Cheng, X. Wang, NDUFAB1 protects against obesity and insulin resistance by enhancing mitochondrial metabolism. *FASEB journal : official publication of the Federation of American Societies for Experimental Biology* **33**, 13310-13322 (2019).

207. S. Ghosh Dastidar *et al.*, Glutathione S-transferase P deficiency induces glucose intolerance via JNK-dependent enhancement of hepatic gluconeogenesis. *American journal of physiology. Endocrinology and metabolism* **315**, E1005-e1018 (2018).

208. T. Yamamotoya *et al.*, Trk-fused gene (TFG) regulates pancreatic β cell mass and insulin secretory activity. *Scientific reports* **7**, 13026 (2017).

209.   A. Yadav, M. A. Kataria, V. Saini, A. Yadav, Role of leptin and adiponectin in insulin resistance. *Clinica chimica acta; international journal of clinical chemistry* **417**, 80-84 (2013).

210.   N. M. Morton *et al.*, A stratified transcriptomics analysis of polygenic fat and lean mouse adipose tissues identifies novel candidate obesity genes. *PloS one* **6**, e23944 (2011).

211.   W. Wu *et al.*, Enhancing natriuretic peptide signaling in adipose tissue, but not in muscle, protects against diet-induced obesity and insulin resistance. *Science signaling* **10**, (2017).

212.   J. Cui *et al.*, Adipose-specific deletion of Kif5b exacerbates obesity and insulin resistance in a mouse model of diet-induced obesity. *FASEB journal : official publication of the Federation of American Societies for Experimental Biology* **31**, 2533-2547 (2017).

213.   H. Fan *et al.*, Cold-Inducible Klf9 Regulates Thermogenesis of Brown and Beige Fat. *Diabetes*, (2020).

214.   N. M. Morton *et al.*, Genetic identification of thiosulfate sulfurtransferase as an adipocyte-expressed antidiabetic target in mice selected for leanness. *Nature medicine* **22**, 771-779 (2016).

215.   E. Henriksson *et al.*, SIK2 regulates CRTCs, HDAC4 and glucose uptake in adipocytes. *Journal of cell science* **128**, 472-486 (2015).

216.   A. R. Moise *et al.*, Increased adiposity in the retinol saturase-knockout mouse. *FASEB journal : official publication of the Federation of American Societies for Experimental Biology* **24**, 1261-1270 (2010).

217.   X. Y. Pang, S. Wang, M. J. Jurczak, G. I. Shulman, A. R. Moise, Retinol saturase modulates lipid metabolism and the production of reactive oxygen species. *Archives of biochemistry and biophysics* **633**, 93-102 (2017).

218.   A. Lombardi *et al.*, Absence of Uncoupling Protein-3 at Thermoneutrality Impacts Lipid Handling and Energy Homeostasis in Mice. *Cells* **8**, (2019).

219.   T. Yamauchi *et al.*, Inhibition of RXR and PPARgamma ameliorates diet-induced obesity and type 2 diabetes. *The Journal of clinical investigation* **108**, 1001-1013 (2001).

220.   E. D. Rosen *et al.*, PPAR gamma is required for the differentiation of adipose tissue in vivo and in vitro. *Molecular cell* **4**, 611-617 (1999).

221.   J. Phan, K. Reue, Lipin, a lipodystrophy and obesity gene. *Cell metabolism* **1**, 73-83 (2005).

222.   C. R. González *et al.*, Regulation of lipin1 by nutritional status, adiponectin, sex and pituitary function in rat white adipose tissue. *Physiology & behavior* **105**, 777-783 (2012).

223.   C. X. Xu *et al.*, Aryl hydrocarbon receptor deficiency protects mice from diet-induced adiposity and metabolic disorders through increased energy expenditure. *International journal of obesity (2005)* **39**, 1300-1309 (2015).

224. A. Nabeshima *et al.*, Peroxiredoxin 4 protects against nonalcoholic steatohepatitis and type 2 diabetes in a nongenetic mouse model. *Antioxidants & redox signaling* **19**, 1983-1998 (2013).

225. S. Göddeke *et al.*, CDH13 abundance interferes with adipocyte differentiation and is a novel biomarker for adipose tissue health. *International journal of obesity (2005)* **42**, 1039-1050 (2018).

226. P. Deng *et al.*, Cysteine dioxygenase type 1 promotes adipogenesis via interaction with peroxisome proliferator-activated receptor gamma. *Biochemical and biophysical research communications* **458**, 123-127 (2015).

227. D. A. Wardhana *et al.*, Family with sequence similarity 13, member A modulates adipocyte insulin signaling and preserves systemic metabolic homeostasis. *Proceedings of the National Academy of Sciences of the United States of America* **115**, 1529-1534 (2018).

228. R. Salomon-Kent *et al.*, New Face for Chromatin-Related Mesenchymal Modulator: n-CHD9 Localizes to Nucleoli and Interacts With Ribosomal Genes. *Journal of cellular physiology* **230**, 2270-2280 (2015).

229. J. Park *et al.*, SIK2 is critical in the regulation of lipid homeostasis and adipogenesis in vivo. *Diabetes* **63**, 3659-3673 (2014).

230. J. Y. Li, B. X. Chai, W. Zhang, H. Wang, M. W. Mulholland, Expression of ankyrin repeat and suppressor of cytokine signaling box protein 4 (Asb-4) in proopiomelanocortin neurons of the arcuate nucleus of mice produces a hyperphagic, lean phenotype. *Endocrinology* **151**, 134-142 (2010).

231. B. T. Kile *et al.*, Functional analysis of Asb-1 using genetic modification in mice. *Molecular and cellular biology* **21**, 6189-6197 (2001).

232. G. Marcelin, S. M. Liu, G. J. Schwartz, S. C. Chua, Jr., Identification of a loss-of-function mutation in Ube2l6 associated with obesity resistance. *Diabetes* **62**, 2784-2795 (2013).

233. A. Gray *et al.*, Global Igfbp1 deletion does not affect prostate cancer development in a c-Myc transgenic mouse model. *The Journal of endocrinology* **211**, 297-304 (2011).

234. S. Bhaskaran *et al.*, Loss of mitochondrial protease ClpP protects mice from diet-induced obesity and insulin resistance. *EMBO reports* **19**, (2018).

235. C. Becker *et al.*, CLPP deficiency protects against metabolic syndrome but hinders adaptive thermogenesis. *EMBO reports* **19**, (2018).

236. J. V. James, J. Varghese, A. T. McKie, S. Vaulont, M. Jacob, Enhanced insulin signaling and its downstream effects in iron-overloaded primary hepatocytes from hepcidin knock-out mice. *Biochimica et biophysica acta. Molecular cell research* **1867**, 118621 (2020).

237. D. Simaite *et al.*, Recessive mutations in PCBD1 cause a new type of early-onset diabetes. *Diabetes* **63**, 3557-3564 (2014).

238. J. H. Bayle *et al.*, Hyperphenylalaninemia and impaired glucose tolerance in mice lacking the bifunctional DCoH gene. *The Journal of biological chemistry* **277**, 28884-28891 (2002).

239. J. Y. Huang *et al.*, Neutrophil Elastase Regulates Emergency Myelopoiesis Preceding Systemic Inflammation in Diet-induced Obesity. *The Journal of biological chemistry* **292**, 4770-4776 (2017).

240. Y. W. Teng, J. M. Ellis, R. A. Coleman, S. H. Zeisel, Mouse betaine-homocysteine S-methyltransferase deficiency reduces body fat via increasing energy expenditure and impairing lipid synthesis and enhancing glucose oxidation in white adipose tissue. *The Journal of biological chemistry* **287**, 16187-16198 (2012).

241. X. Shen *et al.*, Long non-coding RNA Bhmt-AS attenuates hepatic gluconeogenesis via modulation of Bhmt expression. *Biochemical and biophysical research communications* **516**, 215-221 (2019).

242. H. W. Kang, J. Wei, D. E. Cohen, PC-TP/StARD2: Of membranes and metabolism. *Trends Endocrinol Metab* **21**, 449-456 (2010).

243. N. M. Pollak, M. Hoffman, I. J. Goldberg, K. Drosatos, Krüppel-like factors: Crippling and un-crippling metabolic pathways. *JACC. Basic to translational science* **3**, 132-156 (2018).

244. K. S. Bell-Anderson *et al.*, Loss of Krüppel-like factor 3 (KLF3/BKLF) leads to upregulation of the insulin-sensitizing factor adipolin (FAM132A/CTRP12/C1qdc2). *Diabetes* **62**, 2728-2737 (2013).

245. N. Sue *et al.*, Targeted disruption of the basic Krüppel-like factor gene (Klf3) reveals a role in adipogenesis. *Molecular and cellular biology* **28**, 3967-3978 (2008).

246. D. Zou *et al.*, A critical role of RBM8a in proliferation and differentiation of embryonic neural progenitors. *Neural development* **10**, 18 (2015).

247. Y. Lee *et al.*, The nuclear RNase III Drosha initiates microRNA processing. *Nature* **425**, 415-419 (2003).

248. F. Tuorto *et al.*, RNA cytosine methylation by Dnmt2 and NSun2 promotes tRNA stability and protein synthesis. *Nature structural & molecular biology* **19**, 900-905 (2012).

249. S. Ito *et al.*, Role of Tet proteins in 5mC to 5hmC conversion, ES-cell self-renewal and inner cell mass specification. *Nature* **466**, 1129-1133 (2010).

250. M. Tahiliani *et al.*, Conversion of 5-methylcytosine to 5-hydroxymethylcytosine in mammalian DNA by MLL partner TET1. *Science (New York, N.Y.)* **324**, 930-935 (2009).

251. G. H. Eom *et al.*, Histone methyltransferase SETD3 regulates muscle differentiation. *The Journal of biological chemistry* **286**, 34733-34742 (2011).

252. J. A. King *et al.*, Distinct requirements for the Sprouty domain for functional activity of Spred proteins. *The Biochemical journal* **388**, 445-454 (2005).

253. T. de Castro Barbosa *et al.*, High-fat diet reprograms the epigenome of rat spermatozoa and transgenerationally affects metabolism of the offspring. *Molecular metabolism* **5**, 184-197 (2016).

254. T. Fullston, E. M. Ohlsson-Teague, C. G. Print, L. Y. Sandeman, M. Lane, Sperm microRNA Content Is Altered in a Mouse Model of Male Obesity, but the Same Suite of microRNAs Are Not Altered in Offspring's Sperm. *PloS one* **11**, e0166076 (2016).

255. K. Hedegger *et al.*, Sex-specific programming effects of parental obesity in pre-implantation embryonic development. *International journal of obesity (2005)* **44**, 1185-1190 (2020).

256. J. F. Landrier, A. Derghal, L. Mounien, MicroRNAs in Obesity and Related Metabolic Disorders. *Cells* **8**, (2019).

257. L. Wang *et al.*, A MicroRNA Linking Human Positive Selection and Metabolic Disorders. *Cell*, (2020).

258. H. Li *et al.*, A novel microRNA targeting HDAC5 regulates osteoblast differentiation in mice and contributes to primary osteoporosis in humans. *The Journal of clinical investigation* **119**, 3666-3677 (2009).

259. C. Pheiffer, S. Dias, P. Rheeder, S. Adam, Decreased Expression of Circulating miR-20a-5p in South African Women with Gestational Diabetes Mellitus. *Molecular diagnosis & therapy* **22**, 345-352 (2018).

260. Q. Zhang *et al.*, Maternal chromium restriction induces insulin resistance in adult mice offspring through miRNA. *International journal of molecular medicine* **41**, 1547-1559 (2018).

261. R. T. Sussman *et al.*, The epigenetic modifier ubiquitin-specific protease 22 (USP22) regulates embryonic stem cell differentiation via transcriptional repression of sex-determining region Y-box 2 (SOX2). *The Journal of biological chemistry* **288**, 24234-24246 (2013).

262. S. Y. Cai, R. W. Babbitt, V. T. Marchesi, A mutant deubiquitinating enzyme (Ubp-M) associates with mitotic chromosomes and blocks cell division. *Proceedings of the National Academy of Sciences of the United States of America* **96**, 2828-2833 (1999).

263. S. Shinoda *et al.*, Mammalian NSUN2 introduces 5-methylcytidines into mitochondrial tRNAs. *Nucleic acids research* **47**, 8734-8745 (2019).

264. R. Tupler, G. Perini, M. R. Green, Expressing the human genome. *Nature* **409**, 832-833 (2001).

265. J. H. Lee *et al.*, Ring finger protein20 regulates hepatic lipid metabolism through protein kinase A-dependent sterol regulatory element binding protein1c degradation. *Hepatology (Baltimore, Md.)* **60**, 844-857 (2014).

266. P. Ren *et al.*, RNF20 promotes the polyubiquitination and proteasome-dependent degradation of AP-2α protein. *Acta biochimica et biophysica Sinica* **46**, 136-140 (2014).

267. A. K. Wade *et al.*, LIM-domain transcription complexes interact with ring-finger ubiquitin ligases and thereby impact islet β-cell function. *The Journal of biological chemistry* **294**, 11728-11740 (2019).

268. K. Iqbal, S. G. Jin, G. P. Pfeifer, P. E. Szabó, Reprogramming of the paternal genome upon fertilization involves genome-wide oxidation of 5-methylcytosine. *Proceedings of*

the National Academy of Sciences of the United States of America **108**, 3642-3647 (2011).

269. L. J. Yao *et al.*, Novel role for SGK3 in glucose homeostasis revealed in SGK3/Akt2 double-null mice. *Molecular endocrinology (Baltimore, Md.)* **25**, 2106-2118 (2011).

270. S. Bernaudo *et al.*, Cyclin G2 inhibits epithelial-to-mesenchymal transition by disrupting Wnt/β-catenin signaling. *Oncogene* **35**, 4816-4827 (2016).

271. M. Hashimoto *et al.*, Nepro is localized in the nucleolus and essential for preimplantation development in mice. *Development, growth & differentiation* **57**, 529-538 (2015).

272. K. Lee *et al.*, Receptor heterodimerization as a novel mechanism for the regulation of Wnt/β-catenin signaling. *Journal of cell science* **127**, 4857-4869 (2014).

273. K. C. Shin *et al.*, Macrophage VLDLR mediates obesity-induced insulin resistance with adipose tissue inflammation. *Nature communications* **8**, 1087 (2017).

274. J. R. Goudriaan *et al.*, Protection from obesity in mice lacking the VLDL receptor. *Arteriosclerosis, thrombosis, and vascular biology* **21**, 1488-1493 (2001).

275. Y. He *et al.*, High fat diet significantly changed the global gene expression profile involved in hepatic drug metabolism and pharmacokinetic system in mice. *Nutrition & metabolism* **17**, 37 (2020).

276. R. Medzhitov, Origin and physiological roles of inflammation. *Nature* **454**, 428-435 (2008).

277. B. R. Russell WMS, *The principles of humane experimental technique.* (1959).

278. A. M. L. Coenen-Stass *et al.*, Evaluation of methodologies for microRNA biomarker detection by next generation sequencing. *RNA biology* **15**, 1133-1145 (2018).

279. P. Bermejo-Alvarez, D. Rizos, P. Lonergan, A. Gutierrez-Adan, Transcriptional sexual dimorphism during preimplantation embryo development and its consequences for developmental competence and adult health and disease. *Reproduction (Cambridge, England)* **141**, 563-570 (2011).

280. P. Bermejo-Alvarez, D. Rizos, D. Rath, P. Lonergan, A. Gutierrez-Adan, Epigenetic differences between male and female bovine blastocysts produced in vitro. *Physiological genomics* **32**, 264-272 (2008).

V. DANKSAGUNG

Herzlich bedanken möchte ich mich auch bei meinen Mitstreitern Nirav, Marina, Selina, Anna, Raffaele und Max für die schöne gemeinsame Zeit, für unsere mehr oder weniger wissenschaftlichen Diskussionen und die gute Laune, auch wenn wieder einmal das Experiment nicht geklappt hat. Unsere unterhaltsamen Kaffeepausen und das gemeinsame Feierabendbier bzw. der Feierabend-Lillet werden mir immer in schöner Erinnerung bleiben!

Nicht zuletzt möchte ich meinen Freunden, meiner Familie und besonders meinen Eltern danken, die immer an mich geglaubt haben, mich unterstützt haben und jederzeit für mich da waren.

Abschließend ein großer Dank an Philipp für deine interessierten Fragen, das Korrekturlesen sowie die hilfreichen Verbesserungsvorschläge und Ideen. Danke für die unermüdliche Unterstützung vor allem im Endspurt mit Felix und dafür, dass du mich immer wieder aufgebaut hast, wenn es gerade mal nicht so gut lief.

VIELEN DANK EUCH ALLEN!

VI. AFFIRMATION

Ich erkläre hiermit an Eides statt, dass ich die vorliegende Arbeit selbstständig, ohne unzulässige fremde Hilfe und ausschließlich mit den angegebenen Quellen und Hilfsmitteln angefertigt habe.

Die verwendeten Literaturquellen sind im Literaturverzeichnis (References) vollständig zitiert.

Diese Arbeit hat in dieser oder ähnlicher Form noch keiner anderen Prüfungsbehörde vorgelegen.

_____

Karlsfeld, den 21.12.2020   Daniela Kaspar

VII. PUBLICATIONS, TALKS AND POSTERS

Publications

<u>Daniela Kaspar</u>, Karolina Worf, Martin Irmler, Marc Horlacher, Susan Marschall, Nikola Müller, Annalisa Marsico, Fabian Theis, Martin Hrabĕ de Angelis, Johannes Beckers

Complex and dynamic changes in the transcriptome are associated with inter-generational inheritance of acquired metabolic disorders

Manuscript in preparation

Peter Huypens, Steffen Sass, Moya Wu, <u>Daniela Dyckhoff</u>, Mathias Tschöp, Fabian Theis, Susan Marschall, Martin Hrabĕ de Angelis, Johannes Beckers

Epigenetic germline inheritance of diet-induced obesity and insulin resistance

Nature Genetics, 2016. 48(5): p. 497-9.

<u>Daniela Kaspar</u>, Sieglinde Hastreiter, Martin Irmler, Martin Hrabĕ de Angelis, Johannes Beckers

Nutrition and its role in epigenetic inheritance of obesity and diabetes across generations

Mammalian Genome, 2020

Martin Irmler, <u>Daniela Kaspar</u>, Martin Hrabĕ de Angelis, Johannes Beckers

The (not so) Controversial Role of DNA Methylation in Epigenetic Inheritance Across Generations

*in **Beyond Our Genes: Pathophysiology of Gene and Environment Interaction and Epigenetic Inheritance.**, R. Teperino, Editor. 2020, Springer International Publishing: Cham. p. 175-208*

Oral presentations

<u>Daniela Kaspar</u>, Peter Huypens, Martin Irmler, Susan Marschall, Martin Hrabĕ de Angelis, Johannes Beckers

Development of epigenomic signatures during intergenerational inheritance of diet-induced obesity and type 2 diabetes

Munich Epigenetics Spotlight Meeting, 2016

Daniela Kaspar, Johannes Beckers

Ontogenesis of epigenomic signatures

ICEMED final joint meeting, 2017

Daniela Kaspar, Peter Huypens, Martin Irmler, Susan Marschall, Martin Hrabě de Angelis, Johannes Beckers

Development of epigenomic signatures during intergenerational inheritance of diet-induced obesity and type 2 diabetes

HDC seminar, 2018

Daniela Kaspar, Karolina Worf, Martin Irmler, Fabian Theis, Martin Hrabě de Angelis, Johannes Beckers

Multiple pathways associate with epigenetic inheritance of diet-induced obesity

AMPro Summer School, 2019

Poster presentations

Daniela Dyckhoff, Peter Huypens, Susan Marschall, Martin Hrabě de Angelis, Johannes Beckers

Development of epigenomic signatures during inheritance of diet-induced obesity and type 2 diabetes

DZD Research School, 2015

Daniela Dyckhoff, Peter Huypens, Susan Marschall, Martin Hrabě de Angelis, Johannes Beckers

Development of epigenomic signatures during inheritance of diet-induced obesity and type 2 diabetes

DZD Research School, 2016

Daniela Kaspar, Peter Huypens, Susan Marschall, Martin Irmler, Martin Hrabě de Angelis, Johannes Beckers

Development of epigenomic signatures during inheritance of diet-induced obesity and type 2 diabetes

DZD Research School, 2017

Daniela Kaspar, Peter Huypens, Susan Marschall, Martin Irmler, Martin Hrabě de Angelis, Johannes Beckers

Development of epigenomic signatures during inheritance of diet-induced obesity and type 2 diabetes

Symposium on Insulin receptor and Insulin Action, 2017

Daniela Kaspar, Peter Huypens, Susan Marschall, Martin Irmler, Martin Hrabě de Angelis, Johannes Beckers

Development of epigenomic signatures during inheritance of diet-induced obesity and type 2 diabetes

Conference: "Chromatin and epigenetics: from mechanism to function", 2017

Daniela Kaspar, Peter Huypens, Susan Marschall, Martin Irmler, Martin Hrabě de Angelis, Johannes Beckers

Development of epigenomic signatures during inheritance of diet-induced obesity and type 2 diabetes

Conference of Gesellschaft für Genetik, 2017; poster prize awarded

Daniela Kaspar, Karolina Worf, Fabian Theis, Martin Hrabě de Angelis, Johannes Beckers

Multiple pathways associate with epigenetic inheritance of diet-induced obesity

Keystone Symposium "Drivers of Type 2 Diabetes – From Genes to Environment", 2018